

Characterization of Human Background Rhythms with functional Magnetic Resonance Imaging

Dissertation

zur Erlangung des akademischen Grades
doctor rerum naturalium (Dr. rer. nat.)

im Fach Biologie
eingereicht an der
Mathematisch-Naturwissenschaftlichen Fakultät I
der Humboldt-Universität zu Berlin

von
Diplom Physiker Matthias Walter Moosmann
geboren am 24.8.1973 in Bühl/Baden

Präsident der Humboldt-Universität zu Berlin
Prof. Dr. Christoph Marksches

Dekan der Mathematisch-Naturwissenschaftlichen Fakultät I
Prof. Dr. Christian Limberg

Gutachter: 1. Prof. Dr. Andreas V. M. Herz
 2. Prof. Dr. Arno Villringer
 3. Prof. Dr. Vince D. Calhoun

Tag der mündlichen Prüfung: 7. Februar 2007

Danksagung

An dieser Stelle möchte ich mich ganz herzlich fuer die breite Unterstützung und Hilfe während meiner gesamten Dissertation bedanken.

An erster Stelle danke ich Herrn Professor Arno Villringer für die fachlich exzellente und zugleich freundschaftliche Betreuung. Seine sympatische Art strahlt auf die gesamte von ihm geleitete Arbeitsgruppe aus und trägt zu einem Arbeitsklima bei, in dem gerne wissenschaftliche Arbeit betrieben wird.

Herrn Professor Andreas V. M. Herz danke ich für die Annahme dieser Arbeit als Promotion. Für die regelmässigen Diskussionen, die mir sehr geholfen haben einen roten Faden in meinem Dissertationsprojekt zu finden und meine wissenschaftliche Arbeitsweise zu schaerfen, möchte ich ihm ausdrücklich danken.

Mein besonderer Dank gilt Dr. Petra Ritter. Als Medizinerin-Physiker-Team, haben wir gemeinsam begonnen, Hintergrundaktivitäten des Gehirns zu studieren und dabei die Methodik der simultanen EEG-fMRI Aufzeichnungen entwickelt. Ohne unseren beiden unterschiedlichen Sichtweisen und Stärken wäre ein solch komplexes Projekt sicher nicht zu bewältigen gewesen. Über die fachliche Zusammenarbeit hinaus, möchte ich ihr aber vor allem für die enge Freundschaft während unserer gemeinsamen Zeit am Berlin Neuroimaging Center danken.

Dr. Jens Steinbrink hat mir sehr dabei geholfen die vorliegende Arbeit endlich formal anzugehen und mich darin sowohl fachlich unterstützt als auch persönlich motiviert. Seine Betreuung hat wesentlich dazu beigetragen, dass die vorliegende Arbeit konzeptionell eine runde Sache wurde. Auch möchte ich ihm für die methodischen Ratschläge und die Korrektur der Dissertationsschrift danken.

Im Zusammenhang mit den methodischen Arbeiten zum EEG-fMRI Setup danke ich Robert Becker, Vinzenz Schönfelder und Dr. Kimitaka Anami.

Bei Dr. Benjamin Blankertz, Dr. Andreas Ziehe und Prof. Dr. Klaus Robert Müller vom Fraunhofer-Institut für Rechnerarchitektur und Softwaretechnik bedanke ich mich für die fachlichen Diskussionen um die Methodik der blinden Quellentrennung.

Meinem langjährigen Zimmernachbarn Dr. Birol Taskin danke ich für fruchtbare Diskussionen und die nette Zeit.

Viele meiner ehemaligen Arbeitskollegen kann ich an dieser Stelle nicht namentlich nennen, da dies den Rahmen sprengen würde. Daher ein kollektives Dankeschön an alle Mitglieder des Berlin Neuroimaging Center für die interessante und nette Zeit unterm Dach der Neurologischen Klinik.

Meinen Kollegen in Bergen, Tom Eichele und Dr. Karsten Specht, möchte ich für das Korrekturlesen und den ein oder anderen Tritt, diese Arbeit endlich fertigzustellen, herzlichst danken.

Besonderer Dank gilt auch meiner Familie für die liebevolle Unterstützung, bei allem was ich mir vorgenommen habe.

Schliesslich gilt mein grösster Dank Alexandra Schulmeister. Sie ist der Sonnenschein in meinem Leben.

Zusammenfassung

Diese Dissertation zeigt, dass Hintergrundrhythmen mit Hilfe der gleichzeitigen Messung von EEG und fMRI Signalen untersucht werden können. Die Methodik dieses Ansatzes wurde durch den Einsatz einer speziellen fMRI Sequenz weiterentwickelt, und die Signalqualität durch visuell evozierte Potentiale überprüft.

Der prominente okzipitale Alpha-Rhythmus und die vergleichsweise schwächeren rolandischen Rhythmen konnten in der elektromagnetisch störenden Umgebung des Magnetresonanztomografen, auch und gerade während der funktionellen Messsequenzen identifiziert werden.

Durch den Einsatz der in dieser Arbeit vorgestellten Nachverarbeitungsmethoden kann die simultane Aufnahme von EEG und fMRI Signalen wertvolle Informationen über die neuronale Grundlage von Hirnrhythmen und ihrer hemodynamischer Korrelate liefern.

Die hier vorgestellten Daten bekräftigen die Hypothese, dass die Amplitude der Hintergrundrhythmen mit spezifischen Deaktivierungen in sensorischen Hirnarealen einhergehen. Eine erhöhte Amplitude aller untersuchter Rhythmen war mit einem negativen BOLD Signal in sensorischen kortikalen Arealen verknüpft, was auf einen erniedrigten Energieverbrauch in Arealen mit höherer Synchronizität schließen lässt.

Der posteriore Alpha Rhythmus, ist invers mit dem hemodynamischen Signal in primären visuellen Arealen gekoppelt, während hämodynamische Korrelate der rolandischen Alpha und Beta Rhythmen in somatomotorischen Arealen lokalisiert wurden. Für den rolandischen Alpha und Beta Rhythmus wurden unterschiedliche regionale Netzwerke gefunden. Der rolandische Beta Rhythmus ist mit dem Motornetzwerk, während der rolandische Alpha Rhythmus mit einem somatosensorischen bzw. Assoziationsnetzwerk assoziiert ist, was eine fundamentale Eigenschaft des Somatomotorischen Systems zu sein scheint. Die rolandischen Rhythmen könnten dadurch somatomotorische Areale während der Erhaltung oder Planung von Bewegungsabläufen funktional koppeln [Brovelli, et al., 2004]. Desweiteren wurde gezeigt, dass thalamische und cinguläre Strukturen mögliche Generatoren oder Modulatoren der hier untersuchten Hintergrundrhythmen sind.

Die experimentellen Daten der hier vorgestellten Studien legen nahe, dass eine inverse Beziehung der Stärke eines Hintergrundrhythmus mit regional kortikalem Metabolismus und gleichzeitig eine „antagonistische“, positive Beziehung mit thalamischen oder cingulären Strukturen ein generelles organisatorisches Prinzip des Gehirns zu sein scheint. Der Begriff der Grundaktivität des Gehirns [Gusnard, et al., 2001] müsste daher in verschiedene Netzwerke der Grundaktivität unterteilt werden, die elektrophysiologisch durch Hintergrundrhythmen definiert wären.

Selbstständigkeitserklärung

Hiermit erkläre ich, die Dissertation selbstständig und nur unter Verwendung der angegebenen Hilfen und Hilfsmittel angefertigt habe.

I hereby declare to have prepared this thesis independently, using only the materials and methods described in this work.

Table of Contents

1	Introduction	1
1.1	<i>Introduction to EEG.....</i>	<i>1</i>
1.1.1	Physiological Basis of the EEG	2
1.2	<i>Human Brain Rhythms.....</i>	<i>3</i>
1.2.1	The Posterior Alpha Rhythm.....	3
1.2.2	The Rolandic Alpha and Rolandic Beta Rhythm.....	4
1.2.3	Other EEG Rhythms.....	5
1.2.4	Origin of EEG Rhythms	6
1.3	<i>Introduction to fMRI.....</i>	<i>7</i>
1.3.1	The Physical Basis of the MR signal.....	7
1.3.2	The Blood Flow Response.....	8
1.3.3	The BOLD Contrast	9
1.4	<i>Physiological Relationship of EEG and fMRI Signals.....</i>	<i>10</i>
1.5	<i>Are Brain Rhythms metabolically active?</i>	<i>11</i>
1.6	<i>Approaches of EEG-fMRI integration.....</i>	<i>12</i>
1.7	<i>EEG recordings in MR environment</i>	<i>13</i>
1.7.1	Patient Safety during EEG-fMRI measurements.....	13
1.7.2	MRI influences on the EEG system	14
1.7.3	How does the EEG system influence the MRI system	16
2	Aims of this Study	17
2.1	<i>Establishing & Quality Insurance of the EEG in the fMRI.....</i>	<i>17</i>
2.2	<i>Studies on the human Posterior Alpha Rhythm.....</i>	<i>17</i>
2.3	<i>Studies on the Human Rolandic Rhythms.....</i>	<i>17</i>
3	General Materials & Methods	19
3.1	<i>EEG Recording.....</i>	<i>19</i>
3.1.1	EEG Equipment used	19
3.2	<i>EEG Data Analysis.....</i>	<i>20</i>
3.2.1	Filter for Gradient- and HF-Artifacts	20

3.2.2	Time Resolved Frequency Analysis.....	22
3.2.3	Blind Source Separation.....	25
3.3	<i>FMRI recording</i>	26
3.4	<i>FMRI data analysis</i>	27
3.4.1	Preprocessing	27
3.4.2	Statistical Parametric Mapping.....	29
4	Improvements & Quality Insurance of the EEG in the fMRI	33
4.1	<i>Visual evoked potentials recovered from fMRI scan periods</i>	33
4.1.1	Data acquisition.....	33
4.1.2	Paradigm and Experimental Design.....	33
4.1.3	FMRI-artifact detection and correction.....	35
4.1.4	Visual Evoked Potential analysis.....	35
4.1.5	Evaluation of artifact removal algorithm via spectral analysis	37
4.1.6	fMRI data analysis.....	37
4.1.7	Results: Recovered Visual Evoked Potentials	37
4.1.8	Results: Frequency analysis of recovered VEPs.....	40
4.1.9	Results of the fMRI data set.....	41
4.2	<i>Stepping Stone Sampling: A MR sequence for improved EEG signal quality</i>	42
4.2.1	Stepping Stone Principle.....	42
4.2.2	Recordings with Stepping Stone Principle	44
5	Studies on the Posterior Alpha Rhythm	47
5.1	<i>Subjects</i>	47
5.2	<i>MRI data acquisition</i>	47
5.3	<i>EEG recording</i>	48
5.4	<i>Paradigm and Study Design</i>	49
5.5	<i>Data Analysis</i>	49
5.5.1	FMRI-artifact correction.....	49
5.5.2	Estimation of the alpha power	49
5.5.3	Functional MRI-Analysis.....	49
5.6	<i>Results</i>	51
6	Studies on the Rolandic Alpha & Beta Rhythm	57
6.1	<i>Subjects</i>	57
6.2	<i>Simultaneous EEG-fMRI recordings</i>	57

6.3	<i>Experimental task</i>	58
6.4	<i>Analysis of EEG Data obtained under the motor-task condition</i>	58
6.4.1	Identification of rolandic alpha and beta rhythms	59
6.4.2	Left and Right rolandic alpha and beta rhythms during motor-task	60
6.4.3	Blind source separation	60
6.4.4	Overview of EEG-rhythms used for fMRI cross-correlation	61
6.5	<i>Analysis of fMRI Data</i>	62
6.5.1	Bimanual movement task	62
6.5.2	Rest condition	62
6.6	<i>Results</i>	63
6.6.1	Results - Motor-task	63
6.6.2	Results - Rest condition.....	73
7	Discussion	75
7.1	<i>Quality Insurance of the EEG-fMRI setup</i>	75
7.1.1	VEP as measure of EEG signal quality.....	76
7.1.2	'Stepping Stone Sequence' phase shifts.....	77
7.1.3	Cardioballistic artifacts.....	77
7.1.4	Spectral analysis and implications for EEG-fMRI recordings	78
7.2	<i>Simultaneous EEG-fMRI measurements of spontaneous rhythms</i>	78
7.2.1	Inverse relation between posterior alpha activity and fMRI-signal in the occipital cortex	80
7.2.2	There is distinct laterality of the fMRI response to right versus left rolandic rhythms:.....	82
7.2.3	During motor-task: Maximum inverse fMRI responses to rolandic alpha and beta rhythms are located in precentral and postcentral areas respectively.	82
7.2.4	During rest: different networks for rolandic alpha and beta rhythms with topographies similar to those reported by invasive cortical recordings.....	84
7.2.5	Non-linear analyses	84
7.3	<i>Functional Implications</i>	85
7.3.1	Where rhythms idle, cortex deactivates?	85
7.3.2	Thalamus as generator of the posterior alpha rhythm.....	87
7.3.3	Motor-task versus rest: Different dynamics - different networks	89
7.3.4	Functional significance of rolandic rhythms.....	90
7.3.5	Implications on the term baseline in fMRI	93
8	Conclusion	95
9	Outlook	97

10	References.....	101
11	Curriculum Vitae	113
12	Publications in Peer Reviewed Journals	115

1 Introduction

The background rhythms in the human electroencephalogram (EEG) are known since the early days of electrophysiological recordings in the 19th century. Despite being the most prevalent features of the scalp EEG in healthy subjects, and showing alterations in a variety of neuropsychiatric conditions, the generators have not been localized and the function is a matter of ongoing research. This is potentially due to the inherent limitations in the imaging methods that have so far been used to investigate these rhythms. Such as the EEG has a poor spatial resolution. Through the recent advent of the possibility to simultaneously measure the human EEG together with its spatially highly resolved neurovascular counterpart, i.e. the hemodynamic signal in functional magnetic resonance image (fMRI) a better localization and thus a better understanding could be gained.

The present work mainly aims at characterizing human background rhythms within the framework of this newly developed multimodal neuroimaging method. The following introductory section explains the necessary physiological and technical details of EEG and fMRI, and is followed by the aims of this thesis.

1.1 Introduction to EEG

Electroencephalography (EEG) is one of the oldest physiological methods to study brain activity non-invasively. The presence of fluctuating electric fields originating from the brain was first observed by Richard Caton in the late 19th century when he studied a monkey [Caton, 1875]. He could demonstrate that stimulating one eye of the monkey with light led to changes in the electrical activity occurring in the opposite side of the posterior scalp surface. However, Caton's work was not widely recognized (since he published his work only in medical journals), and it was not until 1929 that Hans Berger first demonstrated scalp recordings of electrical activity in humans [Berger, 1929]. In his initial experiments, Berger placed two large pad electrodes soaked in saline over the forehead and the back of the head and discovered regular rhythmic waves at a frequency of around 10 Hz. He labelled these events "waves of the first order" or "alpha-waves". One aim of the present work is to find brain areas that generate or modulate this very phenomenon (see chapter 5).

EEG has become a routinely used way of assessing brain activity non-invasively, and it is a valuable tool to both researchers and clinicians. EEG recordings feature many virtues as a direct measure of brain function that can be used in several applications. The limitation

having a poor spatial resolution can be overcome by combining it with fMRI as done in this study and described later.

1.1.1 Physiological Basis of the EEG

As demonstrated in animal studies, the cortical origin of EEG activity is primarily located in the pyramidal neurons in the gray matter of the cerebral cortex [Purves, et al., 2001]. Pyramidal cells are oriented perpendicular to the cortical surface, and they generate post-synaptic potentials (PSPs) (see Figure 1) [Kandel, et al., 2000].

It is generally agreed that ongoing EEG activity originates from summated PSPs in the dendrites of cortical neurons, and becomes measurable on the scalp only when larger patches of cortical tissue are synchronously active [Davidson, et al., 2000]. It should be noted that EEG is thus not a direct product of action potentials (AP), and in contrast to the all-or-none principle of APs, PSPs are graded potentials which are characterized by either a hyperpolarization or a depolarization of the cell membrane that may eventually lead to an AP.

An incoming excitatory signal at the synapse gives rise from resting membrane potential (RMP) to a postsynaptic potential (PSP) resulting from positively charged ions flowing into the cell. Thus, a negative charge in the extracellular space in the vicinity of the synapse is given. Although current circuits are induced by PSPs, only the extracellular currents flowing from the source to the sink can be detected in EEG recordings. The electrodes measure the field potentials by registering the nearby located negativity or positivity of the tissue relative to a reference electrode as a positive deflection, because the potential at the site of the active electrode is decreased in relation to the reference electrode. The situation is reversed when a current flows toward the surface electrode, which results in the registration of a negative deflection [Kandel, et al., 2000].

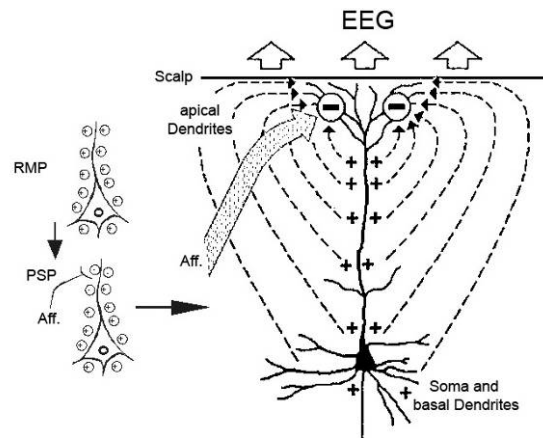


Figure 1: Formation of a neuronal dipole. Considering the electrical activity of a single pyramidal cell activated by an afferent pathway. The incoming excitatory signal at the synapse gives rise from resting membrane potential (RMP) to a postsynaptic potential (PSP) resulting from positively charged ions flowing into the cell. Thus, a negative charge in the extracellular space in the vicinity of the synapse is given. The inward current at the synapse flows down the dendrite and ultimately moves outward across the cell membrane at sites distant from the synapse. The resulting dipole induces currents which also reach the scalp surface. The resulting voltage differences on the scalp can be recorded as the electroencephalogram (EEG).

The EEG reflects the activity of many cortical neurons, because the maximal dipole moment of one single neuron is far too low to produce a measurable signal on the scalp. The spatial distribution of EEG signals is distorted, because the conducting layers of tissue and bone act like resistors and capacitors in an electric circuit. Due to filtering and attenuation, the amplitude of EEG potentials (microvolts) is much smaller than that in a single neuron (millivolt) [Kandel, et al., 2000]. As a consequence, large clusters of neighbouring neurons with simultaneous activity are required to generate a detectable EEG signal.

1.2 Human Brain Rhythms

Since the discovery of the alpha waves by Berger in 1929 other human brain rhythms were discovered which will be described in the following sections. This thesis focuses on the posterior alpha rhythm, and the rolandic (or pericentral) rhythms in the alpha and beta-band.

1.2.1 The Posterior Alpha Rhythm

The posterior alpha rhythm is an electrical oscillation that is most predominant in subjects that are in a state of relaxed wakefulness with their eyes closed. The alpha rhythm is one of the strongest electrical events in the healthy brain with an amplitude of up to $\pm 100 \mu\text{V}$ [Dustman, et al., 1999]. The amplitude is highly variable over time and depends on

features such as the level of vigilance or attention. Spontaneous amplitude fluctuations of the alpha rhythm will be used in chapter 5 to draw inferences on the generators of this phenomenon. The posterior alpha rhythm has been associated with a function in the visual system. This is based on its occipital location and its modulation by visual input. The amplitude of the oscillation can be strongly attenuated ('blocked') upon eye opening and during mental operations [Berger, 1933; Zschocke and Hansen, 2002]. The frequency of the alpha rhythm is centered around 10 Hz with individual differences in peak frequency ranging from around 8 to 12Hz [Zschocke and Hansen, 2002]. There are also changes of the peak frequency with age, such that the individual alpha frequency increases until the age of around 25 and then decreases again [Dustman, et al., 1999]. A study on healthy 100 year-olds showed that their mean alpha frequency was decreased to 8.6 Hz [Hubbard, et al., 1976]. The frequency of the alpha rhythm is substantially slowed down during a large array of neurological conditions, and is therefore an important marker in clinical EEG [Levin and Lüders, 2000; Llinas, et al., 1999; Niedermeyer, 1997].

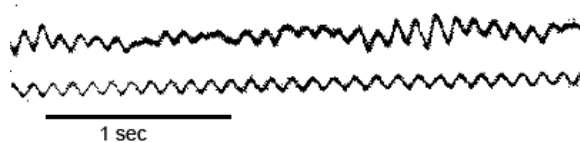


Figure 2: Posterior Alpha rhythm spindles as recorded by Hans Berger in 1929.

1.2.2 The Rolandic Alpha and Rolandic Beta Rhythm

Functionally connected to the sensorimotor system are two brain rhythms [Salmelin and Hari, 1994b]. One of them has a peak frequency in the alpha band (around 10 Hz), and has been termed 'mu' or 'rolandic alpha rhythm' [Gastaut, 1952], the other has a peak frequency in the beta band (around 20 Hz), and is usually referred to as 'central' or 'rolandic beta rhythm' [Pfurtscheller, 1981; Pfurtscheller, 1992; Salmelin and Hari, 1994a]. A functional relationship of these rhythms to the sensorimotor system is strongly suggested by their pericentral (pre- and post-central gyrus) location ("rolandic rhythms") and their modulation by movements and somatosensory input [Arroyo, et al., 1993; Jasper and Penfield, 1949; Manganotti, et al., 1998; Pfurtscheller, et al., 1998; Salenius, et al., 1997]. It is further supported by the dependence of motor cortex excitability on the strength of these rhythms, i. e. facilitation of motor response during beta desynchronization after somatosensory stimulation [Deletis, et al., 1992] and decreased motor cortex excitability during beta-rebound [Chen, et al., 1999; Manganotti, et al., 1998]. Due to its spectral

similarity and its smaller amplitude compared to the posterior alpha rhythm the rolandic rhythms were thought to be prevalent only in a subsample (~15%) of subjects [Jasper and Andrews, 1938b; Maddochs, et al., 1951; Schutz and Muller, 1951]. Modern data analysis techniques revealed a similar prevalence of the rolandic rhythms as the alpha rhythm [Schoppenhorst, et al., 1980]. It is further assumed that the two spectral components have functional more distinct determinations. Magnetoencephalographic (MEG) studies on the human brain suggest that the alpha component is bound to the somatosensory whereas the beta component is connected to the precentral motor system [Salmelin, et al., 1995]. The hypothesis of distinct functional assignments of the rolandic rhythms shall be examined in this thesis by means of the combined approach of EEG and fMRI.

1.2.3 Other EEG Rhythms

Besides posterior alpha and the rolandic rhythms there is variety of other oscillatory phenomena which have been described in the human scalp EEG. Though these rhythms are not examined in this thesis they shall be shortly introduced.

Walter [Walter, 1936] introduced the term delta rhythm to designate the human EEG spectrum below the alpha range. However, he found himself a need to introduce a special designation for the 4-7 Hz band and used the letter theta because he presumed the origin of these waves in the thalamus. Delta activity is prevalent in deep sleep, during anaesthesia and prior and after certain types of epileptic seizures. During drowsiness theta activity with amplitudes usually greater than 20 μ V takes place. Theta has been also associated with working memory and action monitoring [Luu, et al., 2004; Onton, et al., 2005]. It has also been reported to occur during deep meditation [Kubota, et al., 2001]. Beta (15-30 Hz) is the brain wave usually recorded in awake and behaving subjects, active thinking, active attention, focus on the outside world or solving concrete problems [Zschocke and Hansen, 2002]. Synchronous activity within the gamma frequency band of 30-90 Hz appears to be involved in higher mental activity, including perception and consciousness. It may be involved in binding sensory inputs into the object we perceive [Eckhorn, et al., 1988; Gray, et al., 1989]. Recordings of neurons in cat visual cortex show that synchronisation in the gamma band links parts of the cortex excited by the same object. For instance the colour, shape and the location of an object are processed in different parts of the visual cortex, and these features seem to be united by synchronisation in the gamma band.

1.2.4 Origin of EEG Rhythms

The EEG rhythms previously discussed are oscillations of post-synaptic potentials with their electrical origin lying in the cortex [Davidson, et al., 2000; Kandel, et al., 2000; Manshanden, et al., 2002]. The knowledge about the origin of these rhythms comes so far from lesion or animal studies. This thesis shows how the the origin and functionality of EEG rhythms can be studied non-invasively in man. From the early days it was speculated that the thalamus is involved in coordinating human brain rhythms such as alpha [Berger, 1933; Berger, 1936]. Due to In relaxed wakefulness thalamo-cortical afferences lead to rhythmical oscillations in the cortex that are then recorded through the EEG. Lesion studies showed that a pronounced disorganisation or even complete suppression of EEG alpha activity follows a thalamic stroke or thalamic arteriovenous malformations [Lukashevich and Sazonova, 1996; Ohmoto, et al., 1978; Terao, et al., 1993]. On the other hand, thalamic lesions have been reported to have a minimal [Yazawa, et al., 2001] or inconsistent [Toumskoy and Maiorchik, 1969] influence on spontaneous alpha rhythms.



Figure 3: Rhythmic spindle activity in the EEG signal compared to an intracellular recording of a cortical neuron [Zschocke and Hansen, 2002]

Cortical oscillations cannot emerge intrinsically. In the animal model it was shown that deafferented cortex structures that remained vascularized showed no rhythmical activity [Creutzfeldt and Struck, 1962]. At least rhythmical potentials can be evoked by electrical stimulation when arrangements of cortical areas of one hemisphere remain intact even if they are deafferented from subcortical structures [Petsche and Sterc, 1968]. However, under normal conditions cortical potentials are based on afferent inputs by the thalamus and the formatio reticularis that influences the thalamus. Lateral parts of the thalamus are supposed to produce rhythmical activities that are conducted to cortical areas via thalamo-cortical fiber tracks [Andersen, et al., 1968]. In the dog it was demonstrated that alpha rhythm of the same peak frequency, bandwidth and reactivity can be recorded from the visual cortex as well as from the visual thalamus (laterate geniculate body, pulvinar nuclei) [Lopes da Silva, et al., 1973].

1.3 Introduction to fMRI

Magnetic resonance imaging (MRI) is based upon the phenomenon of nuclear magnetic resonance. Applied to protons it produces images of the human body with excellent soft tissue contrast. In the brain this allows for distinguishing between gray and white matter and for detection of brain defects such as tumors.

Functional magnetic resonance imaging (fMRI) extends the use of MRI to enable studies of dynamic physiological processes. This can be used for spatially localizing dynamic processes in the brain, such as neuronal activity.

1.3.1 The Physical Basis of the MR signal

Hydrogen nuclei in water are the by far most abundant in the human body. As spin-1/2 particles they bear a magnetic moment and thus split in two energy levels in a static magnetic field B_0 . The Boltzmann statistics describes the proportion of spins aligned parallel and anti-parallel to the static magnetic field at a given temperature. The magnetic spins can be excited to the higher energy level by a radio frequency pulse (HF) that matches the energy difference of the energy levels. This is the Larmor frequency

$$\omega_L = g B_0,$$

whereas g is the gyromagnetic ratio of hydrogen.

The HF excitation pulses and magnetic field gradients superimposed on the B_0 field can be applied according to a variety of different timing and amplitude parameters. Adjustments to these parameters permit to obtain images that distinguish various properties of the brain, including structure (anatomical imaging), flow (perfusion imaging), or neural activity (functional imaging).

When turning off the source of the electromagnetic wave the excited magnetic spins start to relax to the magnetization given by the Boltzmann statistics. The relaxation back to the original state can be described as changes in two dimensions, longitudinal re-growth and transverse relaxation. Two exponential processes with time constants (T_1 and T_2) describe the relaxation back to the low-energy state. The T_1 constant measures the relaxation in the direction of the B_0 magnetic field. The T_2 constant measures the transverse relaxation of the dipole in the plane that is perpendicular to the B_0 field. These changes in the local magnetic field can be recorded in the coil that transmitted the HF pulse as an induced

voltage. The Bloch equations form the mathematical basis for the quantitative description of these mechanisms (see e. g. [Huettel, et al., 2004] for details).

The transverse relaxation, also called spin dephasing or spin-spin interactions, is of special significance for fMRI. Any spin flip of a nucleus changes the local field at nearby the nuclei. These exchanges are called spin-spin interactions. In an ideal homogeneous magnetic field, the transverse relaxation follows an exponentially signal decay with a time constant called T2. However, in physiological tissue the transverse relaxation is more rapid because of local field inhomogeneities including those caused by the tissue itself. When inhomogeneities are present, this faster decay constant is called T2*. In the brain, the size of these inhomogeneities depends upon the physiological state and in particular the composition of the local blood supply. This physiological state depends, in turn, on the neural activity (as seen in chapter 1.3.2).

As seen above the Larmor frequency is dependant on the magnetic field strength B_0 . This can be used for spatially coding of the MR signal. Additional magnetic gradients superimposed on the static magnetic field B_0 produce different magnetic field strengths throughout the observed object. The MR signal from different loci can thus be identified and depicted as an image ([Mansfield and Grannell, 1973] or [Huettel, et al., 2004] for an overview).

1.3.2 The Blood Flow Response

fMRI is an indirect measure of brain activity and is based upon the temporal and spatial coupling of neuronal activity, metabolic activity and blood flow parameters (such as blood flow and volume) in the cortex [Villringer and Dirnagl, 1995]. The mechanism that describes the coupling of neuronal activity and metabolic demand is called neurovascular coupling and can roughly be summarized by two empirically supported assumptions [Heeger and Ress, 2002]:

- The regional blood flow is coupled to the metabolic demand
- The metabolic demand is mainly defined by synaptic activity, and therefore blood flow and synaptic activity are coupled.

As indicated in Figure 4 a neuronal activation leads to changes in blood flow and metabolism which can be detected via fMRI. The neurovascular coupling that transfers neuronal to hemodynamic changes is complex and not yet fully understood [Buxton, et al.,

2004; Logothetis and Pfeuffer, 2004]. However, the main effect of a neuronal activation can be described as a hemodynamic overcompensation and thus to a local raise of the concentration of oxygenated hemoglobine [oxy-Hb].



Figure 4: Signal cascade in functional magnetic resonance imaging (fMRI): An external stimulation leads to a neuronal activation in distinct brain areas which alters the metabolism, blood flow and blood volume in that area. These parameters affect the concentration of [deoxy-Hb] and [oxy-Hb] which determines the BOLD fMRI signal.

1.3.3 The BOLD Contrast

Brain ‘activity’ cannot be detected with conventional MRI imaging techniques. In order to study brain function, a contrast agent that changes the MRI signal intensity of activated regions is required. Initially, such contrast agents were injected, until in 1992 three research groups independently found [Frahm, et al., 1992; Kwong, et al., 1992; Ogawa, et al., 1992] that blood itself changes its magnetic susceptibility during brain activation. This contrast mechanism depends on the blood oxygenation level, the so called Blood Oxygen Level Dependent (BOLD) contrast. The contrast depends on the magnetic properties of haemoglobin, the molecule carrying the oxygen necessary for aerobic cellular metabolism in the brain. Deoxygenated hemoglobin ([deoxy-Hb]) is a paramagnetic molecule, whereas oxygenated haemoglobin ([oxy-Hb]) is diamagnetic. The presence of [deoxy-Hb] in a blood vessel causes dephasing of the local magnetization, leading to a reduction in the transverse relaxation time $T2^*$. $T2^*$ is a net property of the material being scanned, which specifies the signal decay and so produces the contrast in a MRI scan that is setup to be sensitive to $T2^*$. Conversely, [oxy-Hb] is diamagnetic and hence does not produce the same dephasing. This means that changes in oxygenation of the blood can be observed as signal changes in $T2^*$ -weighted images.

The mechanism that defines the relationship of [deoxy-Hb] and [oxy-Hb] in a certain area of the brain tissue during neuronal activation is called neurovascular coupling. The proportion of [deoxy-Hb] and [oxy-Hb] that defines the BOLD contrast depends on the change of the three parameters cerebral oxygen extraction rate, cerebral blood flow and cerebral blood volume.

1.4 Physiological Relationship of EEG and fMRI Signals

In the early days of combining EEG and fMRI signals scepticism arose whether it is possible to find meaningful results by combining signals with vascular and electrophysiological origins [Horwitz and Poeppel, 2002; Nunez and Silberstein, 2000]. EEG signals reflect the signal cascade of postsynaptic activity, local field potential and finally voltage fluctuations on the skull whereas fMRI signal measures a complicate and not fully understood mixture of cerebral oxygen extraction rate, cerebral blood flow and cerebral blood volume. Significant advances regarding this relationship have been made by simultaneous recordings of intracortical neural signals and fMRI signal [Logothetis, et al., 2001]. This work showed a better correlation of the BOLD signal with local field potential (LFP, which represent the synchronized synaptic inputs of a given neural popoulation) than with multi-unit activity (MUA, which represents spiking activity) in the visual cortex of monkeys. Since it is well known that the EEG reflects the LFP that is spatially and temporally filtered by the skull the relationship between EEG and hemodynamic signals (e. g. fMRI) was supposed be linear as well. Further studies show significant linear correlations of fMRI BOLD and evoked potentials from median nerve stimulations in humans [Arthurs and Boniface, 2003] and studies on evoked field potentials and cerebral blood flow in animals [Brinker, et al., 1999; Ngai, et al., 1999; Ogawa, et al., 2000]. However an optical imaging study in the rat showed by presenting stimulus intensities of a large dynamic range that pronounced non-linearities of hemodynamic responses and electrophysiological measures of neuronal activity can occur [Devor, et al., 2005].

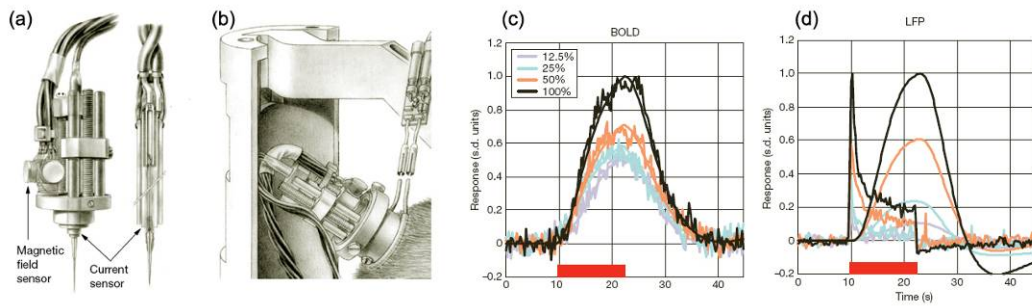


Figure 5: Logothetis and colleagues showed the direct linear relationship of local field potentials with the BOLD signal. Intracortical neural signals and the BOLD signal were recorded simultaneously in the awake monkey (a, b). By varying stimulus contrasts he showed direct correlation of the measured (c) with the predicted (d) BOLD signal. The measured LFP amplitude predicted the BOLD response in (d) [Logothetis, et al., 2001].

1.5 Are Brain Rhythms metabolically active?

An important prerequisite to study brain rhythms with fMRI is that they are metabolically active or at least covary with the BOLD signal which is an indicator of metabolic or blood flow changes. That means for instance that fluctuations of the quality or quantity of brain rhythms lead to changes in metabolic demand that can be measured by means of BOLD fMRI. It was discussed very early that human posterior alpha rhythm could reflect an idling and energy conserving state of the visual system [Adrian and Matthews, 1934]. Theoretical simulations of synchronisation and of ongoing metabolic demand showed that in nearly every domain of the manipulated parameters the mean activity and synchronization were tightly coupled [Chawla, et al., 1999]. Recently it was theoretically shown that, activation can cause an acceleration of temporal dynamics leading to increased energy dissipation and a shift in the EEG spectral profile to higher frequencies [Kilner, et al., 2005]. Additionally, there is evidence for interactions between the neuronal background activity and the amplitude of the visual evoked response on the neuronal as well as on the metabolic level. Electrophysiological studies investigating the relationship between pre-stimulus EEG power and evoked responses indicated positive correlation in the visual cortex of human beings [Brandt, et al., 1991] and cats [Arieli, et al., 1996]. Negative correlations have been found between the amplitudes of motor evoked responses and spectral alpha content [Rossini, et al., 1991], as well as between alpha and theta band EEG activity and auditory evoked responses (AER) in human beings [Rahn and Basar, 1993]. Inhomogeneous energy consumptions during rest in different brain areas observed in PET studies could be also related to the metabolic demand of background activities [Raichle, et al., 2001]. These

studies indicate that brain rhythms have a significant impact on blood flow or metabolism and should therefore be accessible to neuroimaging methods such as fMRI.

1.6 Approaches of EEG-fMRI integration

There are generally three different approaches of EEG-fMRI data integration (see Figure 6):

Studies employing *integration* through constraints take spatial information from focal fMRI activations to enable a constraint dipole or distributed estimate of EEG or MEG sources [Dale, et al., 2000; Krakow, et al., 2001; Phillips, et al., 2002; Thees, et al., 2003].

Integration through *prediction* uses measures of EEG signals to predict the fMRI responses. The ensuing region-specific hemodynamic correlates can then be characterized with high spatial resolution by the fMRI methodology. Combined EEG-fMRI analyses by prediction were first employed to localize sources of interictal epileptic activity [Krakow, et al., 2001; Krakow, et al., 1999; Seeck, et al., 1998; Symms, et al., 1999; Warach, et al., 1996]. In these measurements, fMRI signal was correlated by EEG-recorded epileptic spikes. The studies about human background rhythms in this work use the approach of integration through prediction.

Fusion refers to the use of a common forward or generative model that can explain both the ERP and fMRI data. Advances to this approach have been made by Dynamic Causal Modelling, an approach based on a hierarchical Bayesian framework [Friston, 2005], Parallel Factor Analysis [Martinez-Montes, et al., 2004; Valdes-Sosa, 2004], and Joint Independent Components Analysis (ICA) [Calhoun, et al., 2005; Eichele, et al., 2006].

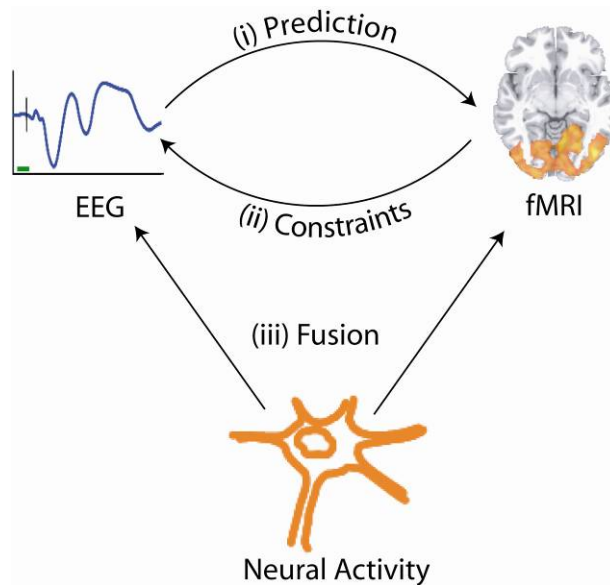


Figure 6: Different approaches to EEG-fMRI integration: Integration through prediction (i), through constraints (ii) or by fusion (iii) [Kilner, et al., 2005].

1.7 EEG recordings in MR environment

Simultaneous EEG-fMRI measurements are a technically demanding set-up since the apparatus for both measures strongly interfere with each other. From the first attempts of EEG recordings in a MR environment [Ives, et al., 1993] several concerns arose when measuring EEG in a MR environment:

- (i) Patient Safety
- (ii) MR-related artifacts in the EEG signal and
- (iii) Signal distortions of the MR signal due to the EEG set-up.

1.7.1 Patient Safety during EEG-fMRI measurements

MR imaging may induce significant currents in EEG electrodes and wires by (i) the static magnetic field, (ii) fast switching gradient fields, needed for spatial coding of the MR image, or (iii) radio frequency (RF) pulses emitted by the MR coils. These currents may heat up the EEG electrodes and wires and could harm the patient or subject. To minimize safety hazards of that manner conductive loops of electrode cables should be minimized and current-limiting resistors should be introduced [Krakow, et al., 2000]. Radio frequency induced electromotive forces were identified as the most important potential hazard [Lemieux, et al., 1997] but latest developments of MR compatible amplifiers, MR

compatible electrode cables and the use of sintered silver/silver-chloride (Ag/AgCl) ring electrodes eliminated EEG related patient hazards.

1.7.2 MRI influences on the EEG system

1.7.2.1 Cardio-ballistic Artifact

An EEG measured in the static magnetic field of a MR scanner shows an artifact occurring with the frequency of about one Hertz, the so called pulse or cardio-ballistic artifact [Ives, et al., 1993]. It is generally thought that the cardio-ballistic artifact arises mainly from arterial pulse-associated movements of the electrodes in the B_0 -field [Anami, et al., 2003] and possibly to a lesser degree from electromotive force of blood ions [Bonmassar, et al., 2002]. The pulsatile movements of the subjects' skin are picked up by the electrodes and wires. Following Faraday's Law [Faraday, 1832]. This leads to an additional inductive voltage U_{Pulse} that is recorded by the EEG. The cardio-ballistic artifact can be dramatically minimized by immobilizing the patients head (e.g. by large vacuum cushions), and tightly fixing the electrodes to an electrode cap and by immobilising the wiring between electrode cap and EEG amplifier [Anami, et al., 2002; Benar, et al., 2002]. If avoiding cardio-ballistic artifacts fails e. g. when measuring at higher magnetic field strengths they can be corrected by adaptive artifact filtering methods [Allen, et al., 1998; Bonmassar, et al., 2002; Muri, et al., 1998].

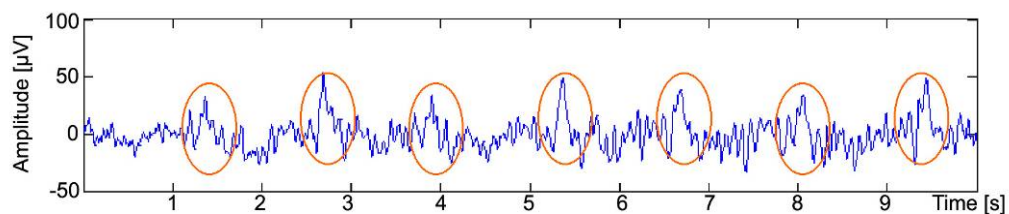


Figure 7: EEG signal recorded in the static magnetic field of a MR scanner showing the cardio-ballistic artifact (indicated by the circles).

1.7.2.2 Gradient- and HF-Artifacts

The largest influence of the MR-environment on the EEG system results from switching MR gradients and high frequency (HF) pulses (see Figure 8 and Figure 9). fMRI is normally performed using echo-planar sequences (EPI) to measure the BOLD contrast. The MR gradients of this imaging technique are particularly high. Both HF pulses as well as MR-gradients are registered in the EEG by inducing voltages in electrode cables so that the recorded EEG is obscured completely. For this reason earlier EEG/fMRI studies have used

interleaved EEG-fMRI recordings evaluating only artifact free EEG periods. With suitable amplifiers it is possible to record as well low voltage physiological EEG as high voltage artificial artifacts. Further it is possible to filter these artifact by appropriate techniques [Allen, et al., 2000]. Typical filter algorithms are based on estimating an artifact template in the frequency or time domain, which is subtracted from the contaminated EEG-signal.

Further advances to minimize MR-imaging related artifacts were made by Anami et al. [Anami, et al., 2003] who modified the imaging sequence to reduce gradient specific artifacts in the EEG system by synchronizing the internal clocks of the EEG and fMRI system (see chapter 4.2 for details).

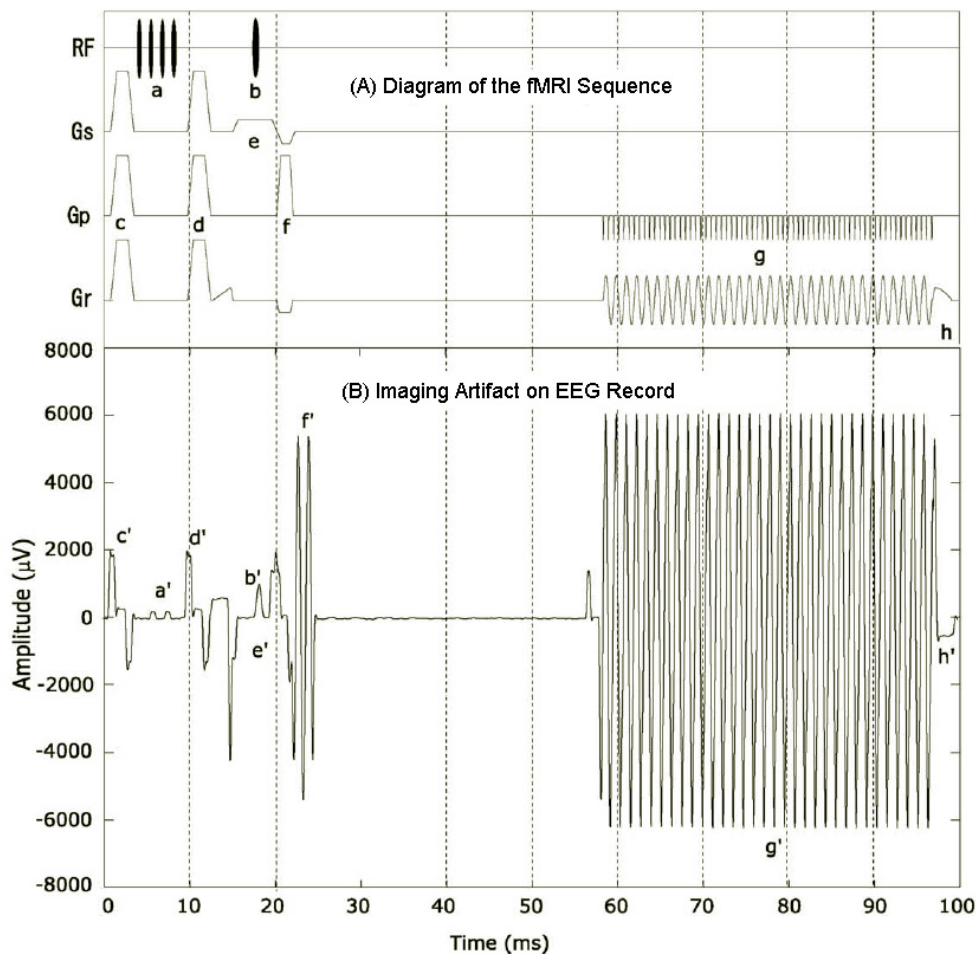


Figure 8: This figure shows how MR gradient switching and HF pulses induce artifacts in the EEG signal (figure from [Anami, et al., 2003]). (A) shows the timings of the radio frequency emission (RF), the gradient pulses (Gs, Gp, Gr) in the fMRI sequence. The artifact corresponding to each MR component (fat suppression pulses [a]; slice selection RF [b]; spoilers [c, d, h]; slice selection gradient [e]; dephasing and rephrasing gradient [f]; readout gradient [g]) can be identified in B and is denoted by the same letter with a prime. The artifact signal is roughly characterized as the first derivative of the gradient switching diagram.

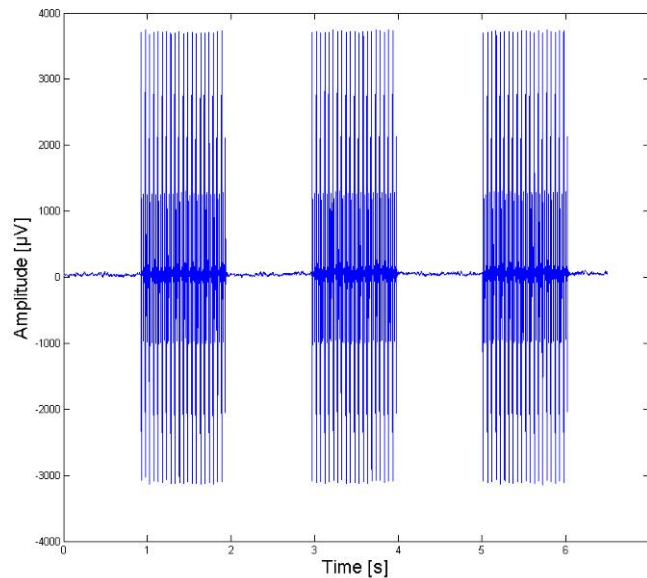


Figure 9: MR-imaging artifact in an EEG signal at our site. MR imaging artifact occurs here every 2 seconds for about 2 seconds and is ~ 100 times larger as the physiological EEG in between. With appropriate filter algorithms the distorted EEG signal can be reconstructed (see chapter 3.2.1).

1.7.3 How does the EEG system influence the MRI system

The quality of MR images can be disturbed by the EEG system as well. In fMRI, EPI sequences are highly sensitive for susceptibility changes which can be induced by the EEG electrodes. However, local signal dropouts are reported to be minor and limited to subcutaneous fat with appropriate electrodes [Krakow, et al., 2000; Lazeyras, et al., 2001]. In a 3 T environment it has been shown that the signal to noise ratio of MR images gets significantly reduced by using 128 electrodes whereas the use of 64 electrodes provides a good trade-off between spatial EEG resolution and MR signal drop-out [Scarff, et al., 2004]. Further sources of imaging artifacts can be electromagnetic noise due to the EEG digitizing circuit, preventable with appropriate shielding of the EEG amplifier [Krakow, et al., 2000].

2 Aims of this Study

2.1 Establishing & Quality Insurance of the EEG in the fMRI

Simultaneous EEG and fMRI may allow functional imaging of the brain at a high temporal *and* spatial resolution. However, artifacts generated in the EEG-signal during MR-acquisition distort the EEG signal. Thus it should be tested whether the signal quality of MR-artifact filtered EEG is good enough to perform *continuous*, simultaneous EEG-fMRI measurements as done later in chapter 5 and 0. We therefore wanted to test whether:

- Visual Evoked Potentials can be recovered sufficiently from fMRI scan periods.
- The EEG signal quality can be further improved using a specialized fMRI sequence.

2.2 Studies on the human Posterior Alpha Rhythm

Functional neuroimaging studies typically are designed to detect brain activity that occurs transiently after the application of external or internal stimuli. However, intrinsic brain signals like human background rhythms do not follow such a “stimulus on/off“-pattern. Here the prototypical human EEG-rhythm, the posterior alpha rhythm (see paragraph 1.2.1 for details) shall be examined by means of simultaneous EEG-fMRI measurements.

Specifically, the following questions were addressed:

- Is simultaneous recording of the posterior alpha rhythm and fMRI-BOLD signal feasible?
- Are there changes in the fMRI signal that are reproducibly associated with amplitude changes in the alpha rhythm?
- Is the sign of a putative correlation of posterior alpha amplitude and fMRI-BOLD signal positive or negative indicating an activation or deactivation?

2.3 Studies on the Human Rolandic Rhythms

As a follow up study of the work on the posterior alpha rhythm (see paragraph 5) we focused on the more subtle background rolandic rhythms namely rolandic alpha and rolandic beta rhythm. Specifically, the following issues were addressed:

- Is it possible to identify these subtle rhythms despite the artifact prone MR environment?
- How are these rhythms correlated with the fMRI-BOLD signal, especially in primary cortical areas? Specifically, is increased rhythm “strength” associated with a negative BOLD signal in the associated cortical areas as it has been shown for the posterior alpha rhythm in the primary visual cortex ?
- It has been suggested that the alpha and beta component of the rolandic rhythms are distinctively localized in the somatosensory and motor cortex, respectively [Salmelin, et al., 1995]. Can simultaneous EEG-fMRI measurements reveal these assumptions?
- Besides their potential inverse relationship to some cortical areas, is it possible to identify areas of increased activity with these rhythms?

3 General Materials & Methods

3.1 EEG Recording

EEG is recorded by a set of electrodes on the scalp that detect electrical activity arising from neuronal activity, and signals recorded by scalp electrodes are called field potentials. Neuronal activity can be measured on the scalp, because electrical currents produced by synaptic activity are passively conducted through the tissues of the brain, skull, and scalp. The spreading currents reach the scalp surface, on which the neuronal signals are recorded as an electroencephalogram (EEG) (see section 1.1.1 on page 2 for details).

EEGs are usually recorded using the standardized international 10-20 system [Jasper and Andrews, 1938a] system for placement of scalp electrodes. This system defines the electrode locations with respect to fractions of the distance from a reference location (Cz), which is determined as the intersection of the lines between nasion and inion, and the left and right pre-auricular point.

3.1.1 EEG Equipment used

In this study a 32-channel MR compatible EEG amplifier (Brainamp MRplus, Brainproducts, Munich, Germany) was used. This amplifier has been designed for usage in MRI scanners and is therefore non-magnetic, shielded and battery-operated. Neurophysiological signals are amplified in the detector head, converted to digital signals, and transmitted to a computer via optical fibers.

The amplifier has a sampling rate of 5000 Hz, and is capable of acquiring signals with a limiting (aliasing) frequency up to 250 Hz or 1000 Hz (analog hardware low pass filters). The dynamic range is comparably high (16mV, 16 bit) to record small physiological EEG signals as well as large signal distortions due to MR recordings. A specially adapted EEG cap with 29 electrodes (Easi-Cap, FMS, Munich), arranged according to the 10–20 system, referenced against Cz, was used. Sintered Ag-AgCl electrodes with iron-free copper leads twisted pair wise are sewed into the flexible material of the cap to reduce cardio-callistic and other motion-related artifacts.

Electrode to skin impedance for all electrodes was maintained at levels lower than 10 k Ω by conditioning the subject's scalp with an abrasive and conductive paste (AbraLyt 2000; FMS, Herrsching-Breitbrunn, Germany). To avoid movement-related EEG artifacts, the

subject's head was immobilized in the head-coil by a vacuum cushion, and sandbags were used to fixate the electrode leads.

The EEG setup with the Brainamp amplifier and the MR-compatible electrode cap is shown in Figure 10.



Figure 10: A volunteer is prepared for a simultaneous EEG-fMRI measurement wearing the MR-compatible EEG cap which is connected to the EEG amplifier. A 64-channel setup is shown.

In the experiment ‘Posterior Alpha Rhythm with interleaved EEG-fMRI recordings’ in paragraph 5 an older EEG amplifier was used (EMR digital, Schwarzer, Munich, Germany). The EMR amplifier is also MR compatible and battery operated and has a sampling rate of 1000 Hz. The lower sampling frequency and low dynamic range of the amplifier did not provide the possibility to filter MR artifacts sufficiently, so only undistorted EEG intervals were used.

3.2 EEG Data Analysis

3.2.1 Filter for Gradient- and HF-Artifacts

Several techniques for filtering MR imaging artifact have been reported so far. Simply applying low-pass filtering is unlikely to be effective as the electromotive forces induced by the gradient fields contain energy in the EEG frequency band (classically: 0.5–70 Hz). Kreger and coworkers described a method for reducing imaging artifact in ECG signals based on adaptive noise cancellation (ANC) [Kreger and Giordano, 1992]. The x, y, and z gradient waveforms derived from the scanner were processed with a filter, which matched the ECG filter and these formed the reference signals for the ANC algorithm. No

quantitative results were given and its applicability to EEG during fMRI is unknown. Laudon et al. used an external loop placed over ECG electrodes to record the induced electromotive forces and then subtracted this electronically from the ECG signal [Laudon, et al., 1998], reducing the artifact to 20%. However, this is impractical for multichannel EEG recordings.

Felblinger et al. described a method for reducing the artifact induced by gradient fields, which appears to be effective for ECG recordings with gradient slew rates of 10 mT/ms [Felblinger, et al., 1999]. This method determines the impulse response of the ECG recording system for gradient fields applied individually in the x, y, and z planes during a period of low-amplitude ECG (the ventricular diastole) with the assumption that the signals recorded were entirely induced artifact. These responses were then used to filter the x, y, and z gradient waveforms derived from the scanner during imaging and the sum of the filter outputs subtracted from the ECG. However, no quantitative results were given and the extension of this method to EEG signals recorded during fMRI may be inappropriate as the gradient slew rates in fMRI are an order of magnitude higher and EEG signals are an order of magnitude lower than ECG.

Sijbers et al. have reported a method for reducing imaging artifact by the subtraction from the EEG spectrum of a weighted average gradient artifact spectrum, followed by inverse Fourier transform [Sijbers, et al., 1999]. This method was evaluated in EEG recorded from rats with gradient fields comparable to typical human fMRI. Although this method increased the signal-to-artifact ratio by four to eight times, this is unlikely to be sufficient for EEG/fMRI in humans, for which the electrode loop areas, and hence induced artifact amplitude, are typically orders of magnitude larger. Hoffmann et al. proposed filtering with a spectral template in the Fourier domain to reduce MR imaging artifacts [Hoffmann, et al., 2000]. Recently a method based on optimal basis functions identified via PCA (principal component analysis) was proposed [Niazy, et al., 2005].

In this work we employed a method proposed by Allen [Allen, et al., 2000] that assumes that imaging artifact waveforms recorded from subjects during periodic fMRI have very low intervolum variability, and hence subtraction of the image artifact waveform averaged over a number of volume acquisitions is effective [Josephs, et al., 1997]. This approach has also been used successfully to remove pulse artifact from EEG/fMRI recordings [Allen, et al., 1998] and would avoid the complication of recording the impulse response for each

gradient and could deal with artifact persisting after the cessation of gradients. For this method to be effective, the EEG recording system must have a large dynamic range to record both the EEG with appropriate resolution and the image artifact without saturation. With the ‘Brainamp MRplus’ amplifier (see chapter 3.1.1) this prerequisite is fulfilled.

In detail, the artifact reduction algorithm applied in this study contains the following steps:

1.) Epochs including a MR scan period (A_n is an epoch comprising one scan period) are segmented based on the onset of MR artifacts. Epochs are baseline corrected using a time window of 20-5 msec before MR acquisition onset. In the experiment ‘VEP during MR acquisition’ a further correction step was done. To correct for small temporal shifts between artifacts due to a limited sampling frequency of 5 kHz, epochs are interpolated up to 50 kHz (cubic spline method, MATLAB; The MathWorks Inc., Natick, MA) and subsequently aligned by maximizing cross correlation. After phase correction, epochs are downsampled to the original sampling frequency of 5 kHz.

2.) In equation 1, an individual (per epoch) artifact template B_n (n = epoch index) is created for each epoch A_n by calculating a weighted average $w^{|n-i|}$ of all epochs (k = number of epochs) with the parameter w providing an exponential decay, resulting in stronger weights for nearby artifacts and thus accounting for possible changes of the artifact over time. Because physiological signatures of the EEG that were of interest in this study are not time locked to the beginning of each epoch, the average of these signals tend toward zero and only the artifacts remain.

$$B_n = \frac{\sum_{i=1}^k w^{|n-i|} A_i}{\sum_{i=1}^k w^{|n-i|}} \quad (\text{Equation 1})$$

3.) In equation 2 individual templates B_n are subtracted from respective artifact periods A_n to give C_n , the artifact-corrected epoch.

$$C_n = A_n - B_n \quad (\text{Equation 2})$$

3.2.2 Time Resolved Frequency Analysis

Since this work deals with human background rhythms that occur at different frequencies and fluctuate in their strength, a method for estimating the power of a frequency at any time point of the experiment is needed.

The Fast Fourier Transformation (FFT) is an algorithm that decomposes stationary signals and processes (i.e. the properties are statistically invariant over time) into its frequency components. However, FFT provides no local information in time of a signal since the representation functions (sines and cosines) are not localized in time. Despite being relatively stationary with respect to the center frequency, background rhythms display continuous modulation of their amplitude, i.e. they are nonstationary in this respect. Therefore a time-resolved estimate of the strength of EEG frequencies is needed.

The windowed fourier transformation (WFT) or Gabor Analysis [Gabor, 1946] is an extension of the FFT that is capable of assessing time series that contain nonstationary power at different frequencies in a signal. A Fourier transformation is performed on a sliding segment of a fixed length T . The segments can be windowed with an arbitrary function such as a boxcar or a Gaussian window (Kaiser 1994). As discussed by Kaiser (1994), the WFT represents an inaccurate and inefficient method of time–frequency localization, as it imposes a scale or “response interval” T into the analysis. The inaccuracy arises from the aliasing of high- and low-frequency components that do not fall within the frequency range of the window. The inefficiency comes from the number of frequencies, which must be analyzed at each time step, regardless of the window size or the dominant frequencies present.

In the last decades, the advent of wavelet analysis bypasses this problem of the WFT [Daubechies, 1990]. Wavelet Analysis refers to the representation of a signal in terms of a certain waveform with a finite length known as the mother wavelet $\Psi_0(t)$. The waveform is scaled and translated to match the input signal. For time-frequency analysis the so-called Morlet wavelet consisting of a plane wave modulated by a Gaussian is used (see Figure 11 [Torrence and Compo, 1998]):

$$\Psi_0(t) = \pi^{-1/4} e^{-t^2/2} e^{i\omega_0 t} \quad (\text{Equation 3})$$

with ω_0 the frequency of the unscaled mother wavelet.

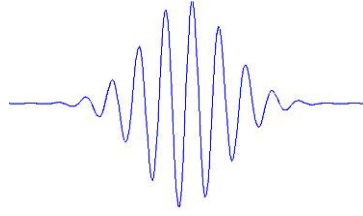


Figure 11: Real part of a Morlet wavelet.

The continuous wavelet transform of a discrete signal $f(t)$ is defined as the convolution of $f(t)$ with a scaled and translated version of $\Psi_0(t)$:

$$W_n(s) = \sum_{t'=0}^{T-1} f(t') \Psi^* \left[\frac{(t'-t)\delta t}{s} \right] \quad (\text{Equation 4})$$

where the (*) indicates the complex conjugate. By varying the wavelet scale s and translating along the localized time index n , one can construct a picture showing both the amplitude of any feature versus the scale and how this amplitude varies with time.

The calculation is usually done in Fourier space since this is considerably faster:

$$W_n(s) = \sum_{k=0}^{N-1} \hat{f}(k) \hat{\Psi}^*(s\omega_k) e^{i\omega_k t \delta t} \quad (\text{Equation 5})$$

To ensure that the wavelet transforms (Equation 4) at each scale s are directly comparable to each other and to the transforms of other time series, the wavelet function at each scale s is normalized to have unit energy:

$$\hat{\Psi}(s\omega_k) = \left(\frac{2\pi s}{\delta t} \right)^{1/2} \hat{\Psi}_0(s\omega_k) \quad (\text{Equation 6})$$

Since the wavelet function $\Psi_0(t)$ is complex the resulting wavelet transformation consists also of a real and imaginary part. As a measure of the strength of a certain frequency we used therefore the ‘Wavelet Power Spectrum’ $|W_n(s)|^2$.

In this work Morlet wavelets of the type ‘cmor1-5’ (Wavelet Toolbox, Matlab 6.5, The MathWorks, Natick, USA) were used. An example of a time-frequency analysis of an EEG signal is shown in Figure 12.

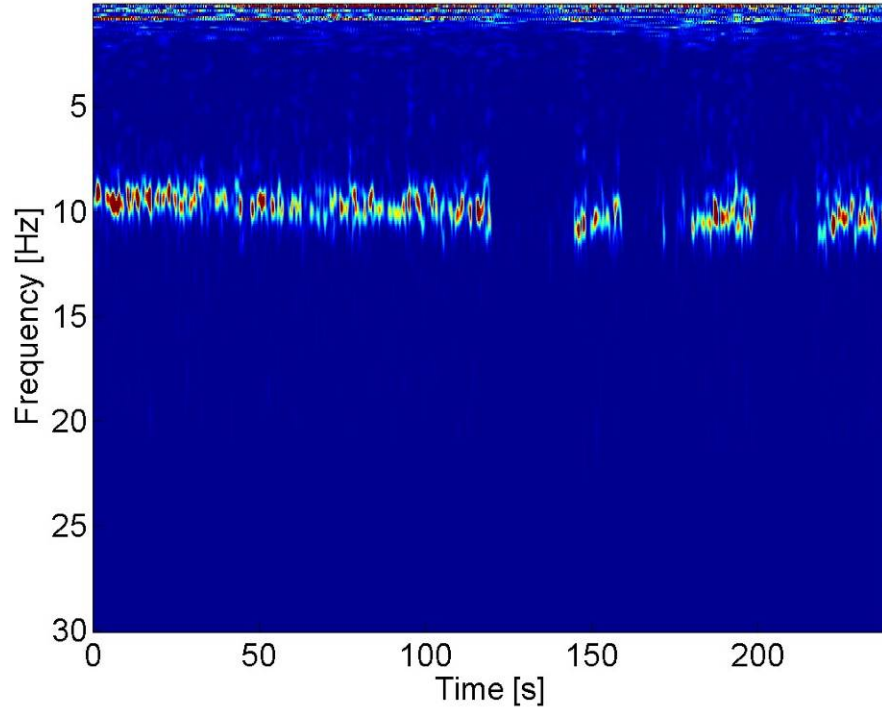


Figure 12: EEG Spectrogram Sample: Example of the squared wavelet spectrogram done with the Morlet Wavelet in Figure 11. The calculation is done on an EEG signal of 240 s length taken from a healthy adult. The subject had its eyes closed for 120 s and then opened its eyes for 20 s. After 20 s it opens its eyes again and so on. The modulation of the alpha rhythm in the frequency band around 10 Hz can be clearly seen.

3.2.3 Blind Source Separation

Blind source separation algorithms were originally developed to recover independent source signals after they are linearly mixed [Bell and Sejnowski, 1995]. Applying blind source separating algorithm to EEG data one assumes that EEG data recorded at multiple scalp sensors are linear sums of temporally or spatially independent components arising from spatially fixed, distinct or overlapping brain networks [Makeig, et al., 1997].

After the principle of superposition one can assume that the recorded EEG signal is a linear mixture of the underlying neuronal activations \vec{q} :

$$\vec{x} = \mathbf{A} \vec{q} \quad (\text{Equation 7})$$

One can further assume that the underlying sources are mutually independent. Since one is interested in the sources \vec{q} one has to blindly estimate the inverse \mathbf{C} of the mixing matrix \mathbf{A} only driven by the known mixed measurement \vec{x} . Ways to achieve the unmixing of the components stress the latter assumption in minimizing a cost function that enforces

statistical independence of the sources. This involves an explicit or implicit calculation of higher-order moments which can be difficult and in the case of scarce data or outliers error prone.

There are different attempts to find the unmixing matrix \mathbf{C} and hence the underlying sources \vec{q} . Principal component Analysis (PCA) assumes uncorellatedness of the sources and therefore minimizes the second-order moments between them, whereas independent component analysis (ICA) uses the stronger criterium by minimizing as well the mutual fourth-order moments [Bell and Sejnowski, 1995; Makeig, et al., 1997].

Since EEG signals have a significant temporal structure e. g. a pronounced autocorrelation the blind source separating method could draw advantage from this prior knowledge. In this study we used a method minimizing mutual time delayed second-order correlations, called TDSep (temporal decorrelation source separation; (Ziehe et al. 2000); <http://wwwold.first.fhg.de/~ziehe/download.html>). Since the autocorrelation of an EEG signal is typically about 30 ms the maximal time delay was set to 30 ms (six discrete steps at a temporal resolution of 200 Hz).

3.3 FMRI recording

All MRI measurements were performed on a 1.5 T whole body scanner (Magnetom Vision, Siemens, Erlangen, Germany) using a standard head coil. Functional imaging was performed using a T2*-weighted BOLD sensitive gradient echo planar imaging sequence. In order to minimize susceptibility distortions due to local static magnetic field inhomogeneities, an automatic shimming procedure was applied. The MRI parameters for different experiments done in this study varied and are given in Table 1.

For each subject, an additional anatomical volume data set was acquired using a T1-weighted 3D-MPRAGE sequence (TR 94 ms, TE 4 ms, flip angle 12°, voxel size 1 × 1 × 1 mm).

Table 1: Experimental Parameters of the studies in this work

Experiment	VEP during fMRI	Posterior α -Rhythm „Rest“ Interleaved	Posterior α -Rhythm „Rest“ Continuous	Rolandic α/β -Rhythm „Motor Task“	Rolandic α/β -Rhythm „Rest“
Numer of Subjects	5	6	14	15	15
Average Age and SD	27y \pm 2.5y	26y \pm 3y	25y \pm 3.5y	26y \pm 4y	26y \pm 4y
Number of fMRI scans	120	750	750	200	480
Number of fMRI slices	20	6	20	20	20
Matrix [voxel]	64x64	64x64	64x64	64x64	64x64
In plane resolution	(3.3 mm) ²	(3.0 mm) ²	(3.0 mm) ²	(3.3 mm) ²	(3.3 mm) ²
Slice resolution	5 mm	6 mm	6 mm	6 mm	6 mm
Gap between slices	0.5 mm	1.5 mm	0.6 mm	1.5 mm	1.5 mm
fMRI repetition Time (TR)	4.2 s	4.0 s	2.0 s	2.1 s	2.1 s
fMRI acquisition Time (TA)	2.1 s	0.65 s	1.65 s	2.5 s	2.2 s
Echo Time (TE)	60 ms	60 ms	60 ms	60 ms	60 ms
Flip Angle	90 degree	90 degree	90 degree	90 degree	90 degree
w (see chapter 3.2.1)	0.9	n. a.	1.0	1.0	1.0
Smoothing kernel applied	6.6x6.6x10	6x6x12 mm ³	6x6x12 mm ³	6.6x6.6x12	6.6x6.6x12
Low-pass Filter	4 s	4 s	4 s	AR(1)*	AR(1)*
High-pass Filter	512 s	512 s	512 s	512 s	512 s

* Pre-whitening through an autoregressive model [Friston, et al., 2002]

3.4 FMRI data analysis

FMRI data analysis were performed using the SPM99 and SPM2 packages [Friston, et al., 1995c].

3.4.1 Preprocessing

3.4.1.1 Realignment

Since the motion subjects cannot be entirely avoided by immobilization, realignment is performed as preprocessing step. The first image of the fMRI image series is used as a reference to which all subsequent scans are realigned using a least squares approach and a rigid body spatial transformation [Friston, et al., 1995a]. The realignment parameters are stored in a separate file for each image scan and will be used in the normalization step (see paragraph 3.4.1.2) for reorienting and normalizing the image slices.

3.4.1.2 Normalization

Functional neuroimaging studies involve a number of participants, all of which will have slightly differently shaped brains. All are likely to have the same gross anatomy, although minor differences will be apparent due to differences in, for example, skull shape and size. Normalization procedure spatially transforms the MR images of different subjects into a standard space to allow for group comparisons of functional activations. SPM2 uses the standard brain from the Montreal Neurological Institute (MNI) as template for normalization. The MNI defined a standard brain by using a large series of MRI scans on normal controls [Brett, et al., 2002; Collins, 1994].

The normalization procedure uses a two step least squares approach to minimize variation from the template to the actual subjects head. First affine transformations and in a second step non-linear deformations are applied, whereby the non-linear deformations are defined by a linear combination of three dimensional discrete cosine basis functions [Ashburner and Friston, 1999].

During normalization, fMRI scans are resliced considering the parameters of the realignment and normalization procedure to an isotropic voxel size.

3.4.1.3 Spatial Smoothing

This step applies a spatial Gaussian smoothing filter to the data. The primary reason for smoothing is to increase signal to noise ratio of fMRI activations. Smoothing increases signal to noise by the matched filter theorem. This theorem states that the filter that will give optimum resolution of signal from noise is a filter that is matched to the signal [Tanaka and Iinuma, 1975]. In the case of smoothing with SPM2, the filter is a Gaussian kernel. Therefore, if we are anticipating a signal in our images that has a Gaussian shape, and is of full width on half of the maximum (FWHM) of a certain size, then this signal will best be detected after we have smoothed our images with a Gaussian filter with that very FWHM size. This is of particular relevance when comparing activations across subjects. The anatomical variability between subjects will mean that the signal across subjects may be expected to be rather widely distributed over the cortical surface.

A Further reason to apply spatial smoothing is to ensure that the image data have the characteristics of a Random Gaussian Field in order to ensure the validity of the assumptions underlying the statistical computations in SPM2 (see chapter 3.4.2)

The dimensions of the smoothing kernels used in this study are given in Table 1.

3.4.2 Statistical Parametric Mapping

In the framework of the General Linear Model (GLM) one assumes that any given event \vec{s} transforms linearly to a hemodynamic response by convolution with a response kernel known as the hemodynamic response function (hrf) [Boynton, et al., 1996]:

$$\vec{x} = hrf \otimes \vec{s} \quad (\text{Equation 8})$$

Note that an event \vec{s} can be external stimulation, or, as in the context of this work, the modulation of an intrinsic brain signal such as a human background rhythm.

The shape of the transfer function was characterized as a summation of 2 gamma function [Boynton, et al., 1996] with a peak latency of about 5 seconds (see Figure 13):

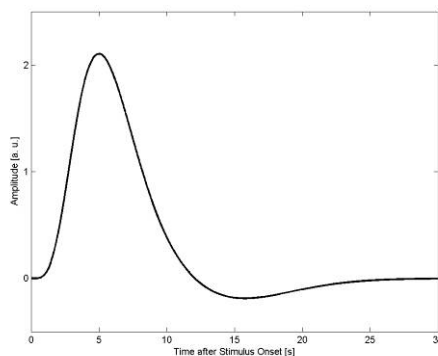


Figure 13: The hemodynamic response function (hrf) is assumed as the point-spread function of a single neuronal event. It models the latency and the blur of the hemodynamic response to a neuronal event.

One further assumes that the mean corrected fMRI data \vec{y} in a given voxel consists of the hemodynamic response \vec{x} and a normally distributed residual noise process $\vec{\epsilon}$:

$$\vec{y} = \beta \vec{x} + \vec{\epsilon} \quad \text{with } \vec{y}, \vec{x}, \vec{\epsilon} \in \mathbf{R}^n \quad (\text{Equation 9})$$

Where n is the number of fMRI scans. Through the assumption that the noise process is normally distributed, meaning white noise $[N(0, \sigma^2)]$ one can calculate the contribution β of a stimulus response to the fMRI BOLD signal \vec{y} via least squares estimates. If the errors are white, then the least squares estimates are also the maximum likelihood estimates and are themselves normally distributed [Scheffe, 1959]. This is a prerequisite

for false positive correction in the framework of the Gaussian random field theory [Worsley, et al., 1996].

In order to decide whether the modeled event \bar{s} leads to a significant activation somewhere in the brain we have to perform a statistical test for every measured voxel, with the null hypothesis that there is no change for that given event:

$$t = \frac{\beta}{\sqrt{\sum_{n=1}^N |\varepsilon_n|^2}} \quad (\text{Equation 10})$$

This voxel-by-voxel test results in a spatial distribution of t -values, so-called t -maps. By assuming a student's t distribution we can decide whether the null hypothesis can be rejected at a certain significance level α in a given voxel.

Since t -tests are performed for every voxel in the volume one deals with a severe multiple comparisons problem. Note that the number of t -tests calculated is typically around 30000 per subject in a fMRI study. The simplest, but most conservative way to correct for multiple comparisons is to adjust the significance level by dividing it by the number of performed tests, the so-called Bonferroni correction. The Bonferroni correction has been shown to be overly conservative [Perneger, 1998]. FMRI data are usually spatially correlated, meaning that data in one voxel shares similar signal, and statistical properties with neighbouring voxels. The degree of spatial correlation can be used to estimate the number of independent voxel clusters, so-called resolution elements or resels. By calculating the Euler characteristics for a given resolution element in the framework of Gaussian random field theory, one can correct thresholds for significance tests in fMRI [Brett, 1999; Friston, et al., 1994; Worsley, et al., 1992; Worsley, et al., 1996]. This procedure is called family-wise-error correction (FWE).

Usually several subjects are examined in a fMRI study in order to make inferences on the overall population. The calculation of a group statistics is done by random effects analysis (rfx). After calculating the β -weights for every single subject (Equation 9), the resulting β -maps enter a second level t -test with the null hypothesis that the mean is zero.

To display results of statistical calculation, t -value maps are thresholded at a certain significance level, e.g. $\alpha < 0.05$, and projected on a higher resolved MR-scan to show anatomical relations of the activated brain areas. Typically they are projected on a high

resolved MR image of Louis Colin provided by the MNI. Colin was scanned 27 times, and the scans were coregistered and averaged to create a very high detail MRI dataset of one brain. This average was the matched to the MNI space.

4 Improvements & Quality Insurance of the EEG in the fMRI

4.1 Visual evoked potentials recovered from fMRI scan periods

Artifacts generated in the EEG-signal during MR-acquisition pose a major technical and analytical challenge (see chapter 1.7.2). Due to these artifacts an interleaved modus has often been used for EEG-fMRI experiments, i.e. only the EEG signals recorded between MRI-scan periods were assessed (see ‘interleaved EEG-fMRI measurements’ in chapter 5 for an example in this work). An obvious disadvantage of this approach is the loss of a portion of the EEG information which might be relevant for the specific scientific question.

Here we recorded continuous, simultaneous EEG-fMRI measurements and tested whether visual evoked potentials (VEPs) can be reconstructed reliably from periods during MR-scanning and in between successive scans [Becker, et al., 2005].

4.1.1 Data acquisition

Simultaneous recording of the EEG while imaging fMRI was performed with the equipment described in paragraph 3.1 and 3.3 respectively. The fMRI parameters are given in Table 1 on page 27.

4.1.2 Paradigm and Experimental Design

Five healthy subjects (all female, mean age 27 y, SD 2.5 y, range 23-30 y) with normal or corrected to normal vision participated in the study. Written informed consent was obtained. Subjects were instructed to fixate the fixation cross of the stimulus and to avoid any movements or excessive eye blinks during the whole experiment. Lying in the bore of the scanner subjects watched the visual stimulus via a mirror above their heads, reflecting the image from a screen attached to the head coil. The stimulus was projected onto the acrylic screen through a collimating lens by a conventional video projector, which was placed about 4 m from the isocenter of the MR-scanner. A black-and-white circular checkerboard (field size adjusted to magnification factors of the retino-cortical representation) with a central fixation cross was presented and contrast reversed once during an acquisition period (when the large MRI-artifact superimposes itself onto the EEG-signal) and once during the non-acquisition period, each lasting 2.1 s (see Figure 14).

The stimulus sequence was programmed using software Presentation, V.0.71 (Neurobehavioral Systems, Albany, USA). The MRI scanner triggered the stimulus computer. Two constraints were given for the stimulus timing: (1) one stimulus was to be presented during scan and inter-scan interval, respectively, (2) stimulation was to start at least 1000 ms (length of the average-VEP) before the next switch between scan/inter-scan period so as to assign each VEP clearly to either a scan or an inter-scan period. Within these constraints interstimulus intervals (ISIs) were variable and randomized. For each subject 120 scans were recorded, comprising 120 trials within the artifact period and 120 trials within the non-artifact period.

A slightly modified version of the above mentioned design was optimized for distinct BOLD-response modulation and used in one subject to examine paradigm correlated functional MR-images. The only difference was the insertion of resting periods after each 10 s of stimulation lasting for 10 s, during which no visual stimuli were presented, to allow for a sufficient modulation of the BOLD response.

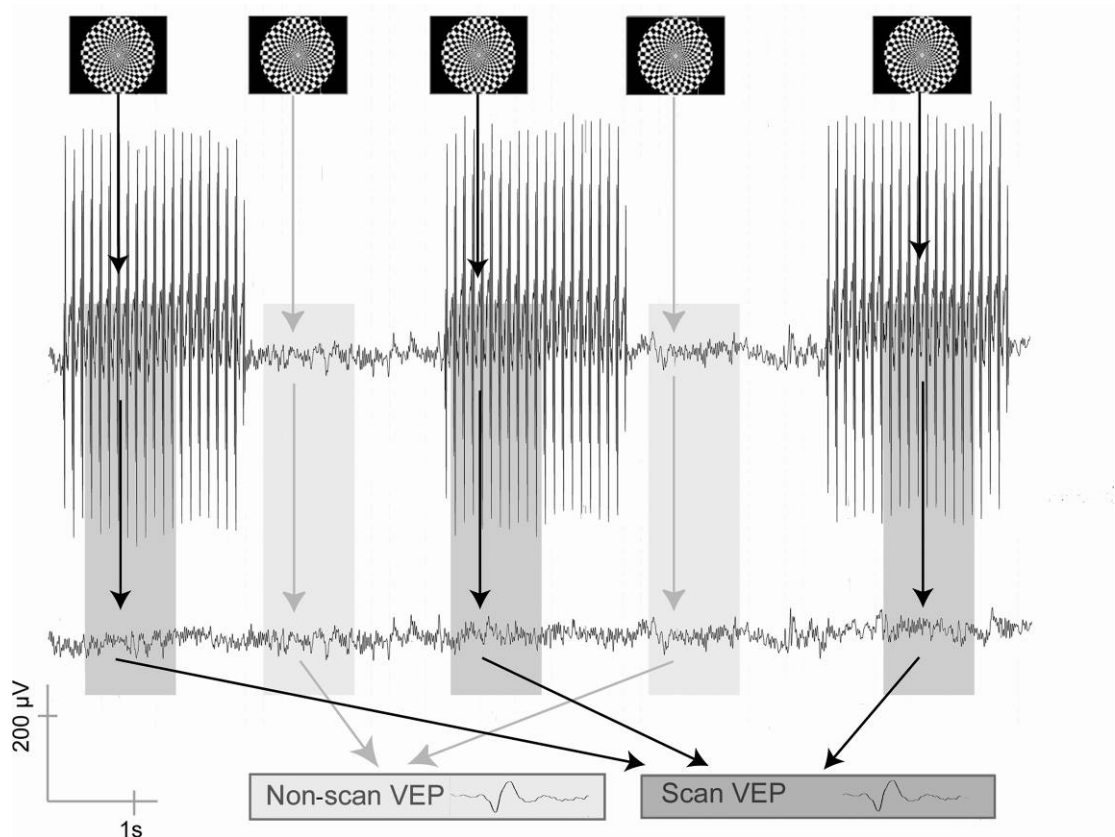


Figure 14: Experimental design for EEG signal quality control in an EEG-fMRI recording: checkerboard-stimuli were presented once in each scan and non-scan interval. After artifact correction VEPs were calculated by respective averaging of scan and non-scan epochs.

4.1.3 FMRI-artifact detection and correction

Using Vision Analyzer Software (Brain Products Inc., Munich, Germany) the onsets of fMRI-artifact periods in the EEG signal were identified by the immediate occurrence of high-amplitude artifacts. Since MR-artifact patterns are supposedly constant in time and add linearly to the EEG signal, the signal was corrected by subtracting weighted moving averages of (scan-wise) artifact epochs, as described in chapter 3.2.1.

4.1.4 Visual Evoked Potential analysis

Analysis was performed using Matlab V.6.1 (The MathWorks Inc., Natick, USA). After MR-artifact correction a band pass filter of 0.53 Hz - 70 Hz (Butterworth, zero phase distortion) was applied. Data from stimulus epochs were segmented and baseline corrected. VEPs were calculated by respective averaging of scan and inter-scan single-trial responses (no epochs were discarded after visual inspection for movement artifacts) from electrode O2 (N = 120 each) (Figure 14). In one subject, four VEPs, each comprising 120 trials, were

acquired without concurrent MR acquisition to obtain a reference measure of physiological VEP-variance.

Even though no prominent ballistocardiograms were visible in the EEG, the effect of ballistocardiogram-correction was determined in one single subject. For ballistocardiogram removal an algorithm provided by Brain Analyzer software (Brain Products, Munich, Germany) was employed, which is based on electrocardiogram-guided artifact identification and subsequent template subtraction similar to the MR-artifact correction procedure described above. Since no improvement was achieved ballistocardiogram removal was not performed in subsequent data analysis (Figure 15).

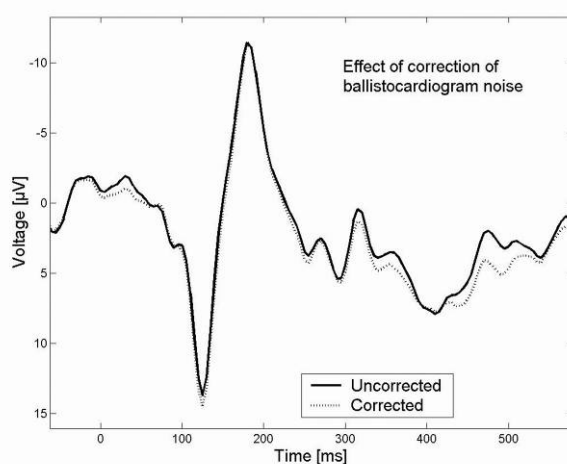


Figure 15: VEPs are highly concordant before and after ballistocardiogram correction (data of one representative subject shown).

To reveal intra-individual differences in the structural VEP-features (P2/N3 complex), latencies and amplitudes of the P2 and the N3 components were calculated and compared. Amplitudes and latencies of all 5 subjects were examined for significant differences between the two conditions by application of the Wilcoxon-signed-rank test (for paired samples). Also a correlation analysis between scan and inter-scan P2/N3 complexes of each subject was performed (highlighted interval, Figure 16 on page 38). Furthermore, signal-to-noise ratios of the VEP in both conditions were estimated. Noise power was defined as the average squared difference between VEP and single trial response. Signal power was defined as the difference of the across-trial average squared amplitude (whole power) and noise power. The ratio was determined by dividing signal power by noise power.

4.1.5 Evaluation of artifact removal algorithm via spectral analysis

In order to assess quality of artifact removal we performed a spectral analysis of the artifact free raw EEG data and the corrected EEG signal (both bandpass filtered and downsampled to 200 Hz). We estimated percentage differences in the spectral density of 5 frequency bands: [0.6-4.3 Hz], [4.3-8 Hz], [8-12.2 Hz], [12.2-25 Hz], [25-44 Hz] by applying the same formula as [Allen, et al., 2000]:

$$\text{Percentage Difference} = 100 \cdot \left| \frac{P_{NS} - P_S}{P_{NS}} \right|.$$

Where P_{NS} is the power spectral density of non-scan periods and P_S is the power spectral density of scan periods.

This was done for channel O2 in each subject and the median of these values (across subjects) was calculated.

Additionally, we analyzed the noise cancellation effect inherent in averaging for scan and non-scan trials by calculating spectral densities as a function of the number of averaged trials (Figure 18). This was done for the physiologically relevant low-frequency range of 1-45 Hz as well as for the high frequency range 50-2500 Hz. The above mentioned signal-to-noise ratio should also indicate the success of artifact removal since residual artifact components would systematically worsen this ratio.

4.1.6 fMRI data analysis

Analysis of the fMRI data set consisted of preprocessing and calculation of statistical parametric maps using SPM2. Preprocessing included realignment, normalization of the anatomical and functional data to the Montreal Neurological Institute standard brain and spatial smoothing of the functional images with a three-dimensional Gaussian filter with a FWHM of double voxel size. See chapter 3.4 for details of fMRI data analysis procedures.

4.1.7 Results: Recovered Visual Evoked Potentials

Typically configured, reproducible VEPs in the form of a P2/N3 complex were found in all subjects and all runs. Single subject results and the grand average are given in Figure 16. The temporal characteristics of the peak responses (P2, N3) were consistent across subjects and also peak-to-peak amplitudes were of similar size (see Table 2). No significant differences were revealed by the (two-tailed) paired Wilcoxon-signed-rank-test [Glantz,

1997], neither for P2/N3 latencies nor for P2/N3 peak-to-peak amplitudes of the two conditions ‘scan phase’ versus ‘non-scan phase’ ($\alpha > 0.05$ n. s.). Power of this test was calculated by estimating the power of the analogous t-test (matched pairs), discounting 5% [Glantz, 1997]. This provides a statistical power of 0.9 for an assumed “true” difference of latencies of > 4 ms for the P2 latency and a P2-N3 amplitude difference of > 5 μ V between groups. Standard deviations at each time point as well as explicitly calculated signal-to-noise-ratios were similar for both conditions (Table 2). Blinks or movement artifacts did not compromise the averaged VEP, thus all trials were included into the VEP average.

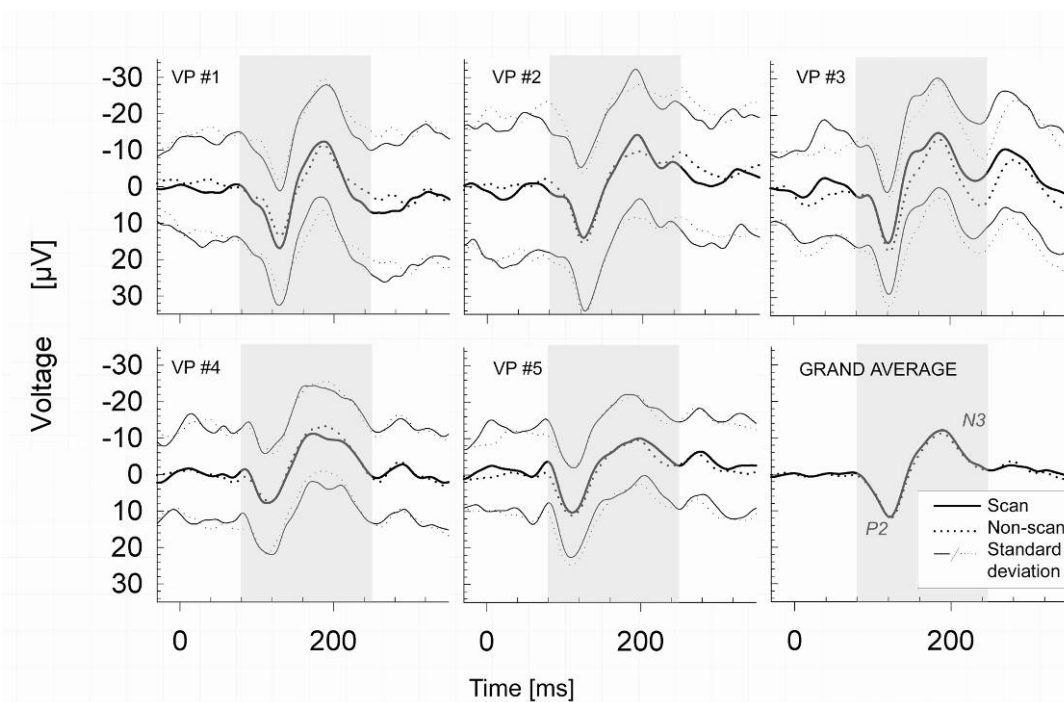


Figure 16: Single subject averages for all 5 subjects and grand average of all subjects (bottom right) for scan (solid line) and non-scan (dashed line) periods. Highlighted periods were included in correlation analysis.

Table 2: Peak-to-peak amplitudes, latencies, standard deviations and correlation coefficients of the P2/N3 complex for all subjects and conditions as well as signal-to-noise ratios (including a reference subject recorded outside the scanner).

		MR-Scan	Non-scan
Subject #1	Latency P2	129 ms	130 ms
	Latency N3	187 ms	186 ms
	Amplitude P2N3	30 μ V	25 μ V
	Mean of SD	15 μ V	16 μ V
	CC P2N3		0.99
	SNR	0.07	0.04
Subject #2	Latency P2	124 ms	124 ms
	Latency N3	193 ms	194 ms
	Amplitude P2N3	29 μ V	26 μ V
	Mean of SD	13 μ V	13 μ V
	CC P2N3		0.98
	SNR	0.06	0.05
Subject #3	Latency P2	121 ms	122 ms
	Latency N3	185 ms	186 ms
	Amplitude P2N3	31 μ V	32 μ V
	Mean of SD	17 μ V	20 μ V
	CC P2N3		0.98
	SNR	0.07	0.08
Subject #4	Latency P2	113 ms	117 ms
	Latency N3	173 ms	189 ms
	Amplitude P2N3	19 μ V	21 μ V
	Mean of SD	14 μ V	15 μ V
	CC P2N3		0.99
	SNR	0.04	0.06
Subject #5	Latency P2	111 ms	111 ms
	Latency N3	198 ms	196 ms
	Amplitude P2N3	21 μ V	21 μ V
	Mean of SD	11 μ V	11 μ V
	CC P2N3		0.99
	SNR	0.09	0.06
Reference	Mean Latency P2	107 +/- 1 ms	
	Mean Latency N3	183 +/- 11 ms	
	Mean amplitude P2N3	22 +/- 1 μ V	
	Mean of SD	13 +/- 1 μ V	
	Mean CC P2N3	0.988 +/- 0.003	
	SNR	0.07 +/- 0.01	
Mean	Latency P2	122 ms	123 ms
	Latency N3	189 ms	188 ms
	Amplitude P2N3	24 μ V	23 μ V
	CC P2N3		0.99
	SNR	0.07	0.06

SD = Mean standard deviation of single-trial electrical activity from VEP (averaged over P2N3 interval)

A robust correlation of 0.98-0.99 was found between both groups of VEPs in all subjects (within the interval of P2/N3 components), comparable to the correlations found between the MR-artifact unafflicted VEPs in the reference subject (Table 2). Differences between scan and non-scan periods seem to lie within the natural variance given by the standard deviation of the reference subject (see Figure 17).

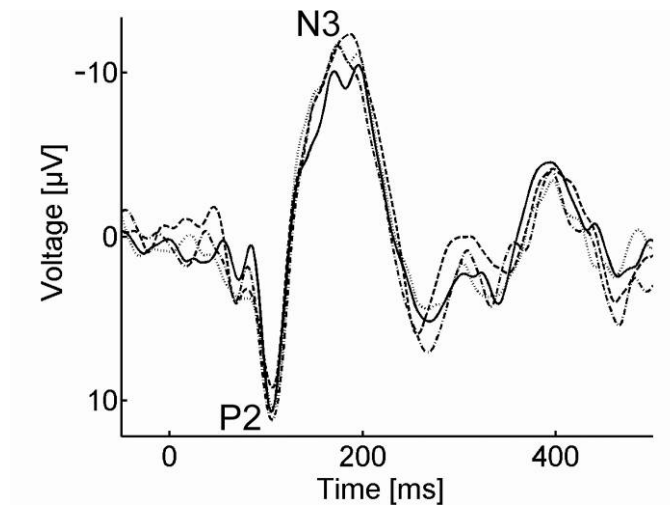


Figure 17: Four VEPs (each averaged over 120 trials) recorded outside the scanner from one single subject during one session under identical environmental conditions.

4.1.8 Results: Frequency analysis of recovered VEPs

Using Fast Fourier Transformation, power spectral densities were calculated for artifact distorted, artifact corrected and MR-artifact free data. For the artifact distorted raw data strong high frequency components were observed. These components and their harmonics completely dominate the frequency spectrum. However, artifacts might also distort lower frequency bands. The results of this work however, show that artifact corrected data have a frequency spectrum similar to the spectrum of the artifact-free non-scan (B0) data. Median percentage differences were as follows: 0.6-4.3 Hz: 8 %, 4.3-8 Hz: 8 %, 8-12.2 Hz: 9 %, 12.2-25 Hz: 8 % and 25-44 Hz: 7 %. In the absence of low-pass filtering residual artifacts remain in the frequency range above 100 Hz. These residual components are one order of magnitude smaller than in the uncorrected data. Spectral power densities in this high frequency range are depicted in Figure 18 (top right) for artifact-corrected, unfiltered data from scan periods. For the physiologically relevant frequency range of 1-45 Hz, power spectra are shown for non-scan as well as scan periods in Figure 18 (left). In this figure the effect of noise cancellation for non-phase locked components is visualized, spectra are depicted as a function of the averaged trial number. For small numbers of averaged trials as well as for the final VEP-average, spectra of scan and non-scan conditions are similar. This indicates that no significant MR-artifact residuals are present after artifact correction in this frequency range. In contrast strong artifact residuals are present in the high frequency range in scan but not in non-scan data (non-scan data not shown).

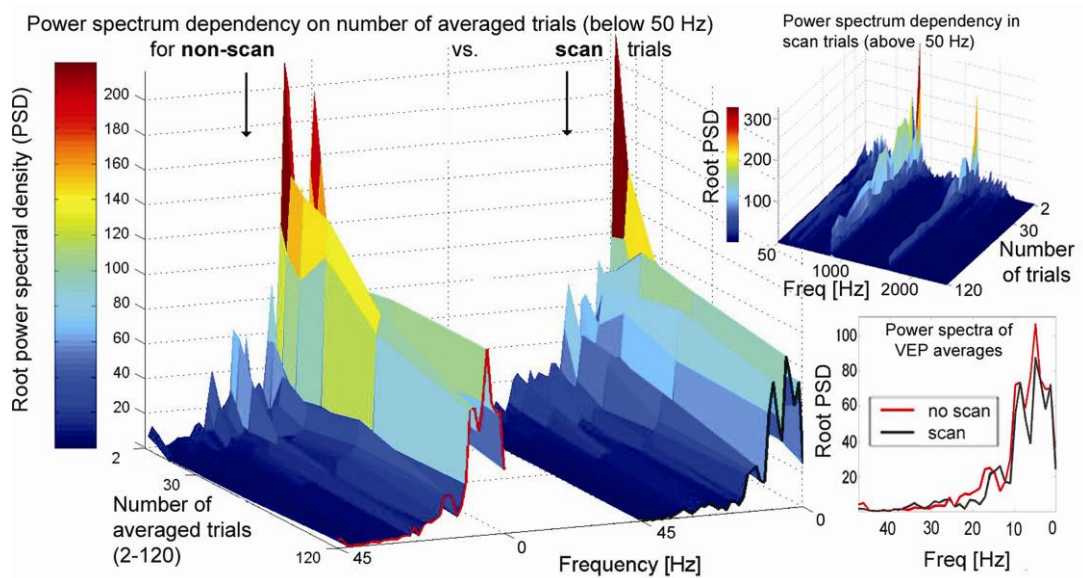


Figure 18: Power spectrum dependency on the number of averaged trials for the physiologically relevant frequency range 1-45 Hz for non-scan and scan trials (left side). High frequency range 50-2500 Hz for scan-trials for one representative subject (top right). For a better comparability power spectra for final VEPs (N=120) are depicted at bottom right.

4.1.9 Results of the fMRI data set

As expected, fMRI data (subject #5, Figure 19) show that visual areas of the occipital cortex are activated, primarily V1 and V2. The electrophysiological response of subject #5 matches the pattern found in the other subjects with the standard paradigm.

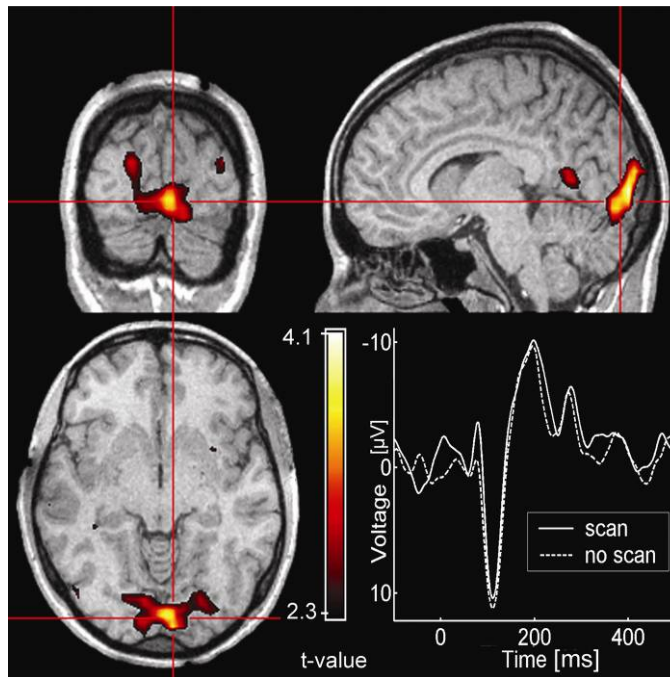


Figure 19: Statistical analysis of fMRI data in subject #5 shows activations ($p < 0.01$) in occipital visual areas, primarily in V1 and V2. The respective scan- and non-scan VEPs of subject #5 are depicted in the lower right corner.

4.2 Stepping Stone Sampling: A MR sequence for improved EEG signal quality

As showed in chapter 4.1 visual evoked potentials can be sufficiently recovered from EEG recordings that were distorted by MR-gradient and high-frequency artifacts. However, with commercially available MR sequences artifacts remain in the data and have to be smoothed out by low pass filtering. This impedes the application of the simultaneous EEG-fMRI methodology to high frequency phenomena as gamma oscillations.

4.2.1 Stepping Stone Principle

To circumvent these restrictions we applied a technique introduced by Anami and coworkers [Anami, et al., 2003]. The quality improvement of the EEG signal using this technique is based on two properties:

1) Synchronisation: The recording clock of the EEG and the internal clock of the MR system are phase locked in this setup. This implies that jittering effects of the recorded MR gradient artifacts are excluded.

The EEG amplifier used in this work offers the possibility to get synchronized with an external clock of 5000 Hz via a ‘phased locked loop’ mechanism. Therefore the internal

clock of the MR system (4 MHz) was downsampled with a self-built device. The downsampling was started via a trigger signal timed to the first fMRI slice acquired in a recording session.

2) ‘Stepping Stone Sampling’: The timing of the echo planar sequence was modified in a way that EEG sampling will be performed exclusively in the period in which the MR artifact resides around the baseline level. Figure 20A shows the modified HF and gradient timing. The artifact recorded by the EEG can be described as the first derivative of the gradient diagram [Anami, et al., 2003] and is depicted in Figure 20B. The round dots depict the sampling points of the EEG sampling with 1000 Hz.

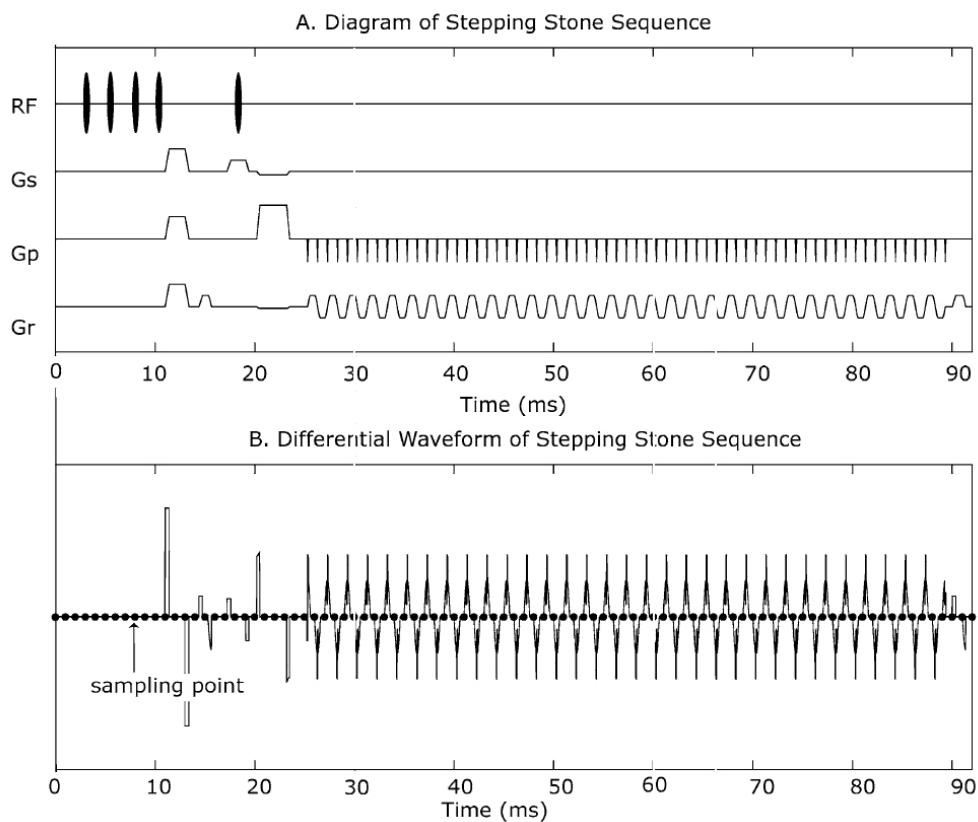


Figure 20: Schematic of the Stepping Stone Sequence [Anami, et al., 2003]. A). Diagram of the series of RF and gradient pulses: RF pulses (RF); Gradient pulses (Gs, Gp, Gr). B) An example of predicted imaging artifact waveform made by sum of the differential waveforms of the gradient pulses. Digitally sampled dots for EEG signal (1000 Hz digitization rate) are superimposed on the artifact waveform. Every sampling point avoids artifact spikes.

The ‘Stepping Stone’ sequence bases on the standard EPI BOLD sequence provided by Siemens (‘ep2d_fid_60b2080_62_64.ekc’, Siemens, Erlangen, Germany). It was shown that the shifts in the timing of the sequence did not result in a loss of BOLD sensitivity [Anami, et al., 2003].

4.2.2 Recordings with Stepping Stone Principle

Two Subjects were recorded in three sessions each with the ‘Stepping Stone’ sequence and compared to one session for each subject recorded with the standard EPI BOLD sequence provided by Siemens (Siemens, Erlangen, Germany).

The adapted sequence was designed for a sampling rate of 1000 Hz. Since the EEG amplifier used in this work (see paragraph 3.1.1 on page 19) records with 5000 Hz only every fifth data point was supposed to match the stepping stone criterium. Figure 21 shows an EEG recording while fMRI scanning with the standard sequence and the ‘Stepping Stone’ sequence (every fifth data point is shown to match the ‘Stepping Stone’ criterium). In the recording with the standard sequence residual artifacts remain whereas the artifact correction of the recording with the ‘Stepping Stone’ sequence provides a clearly visible signal quality improvement.

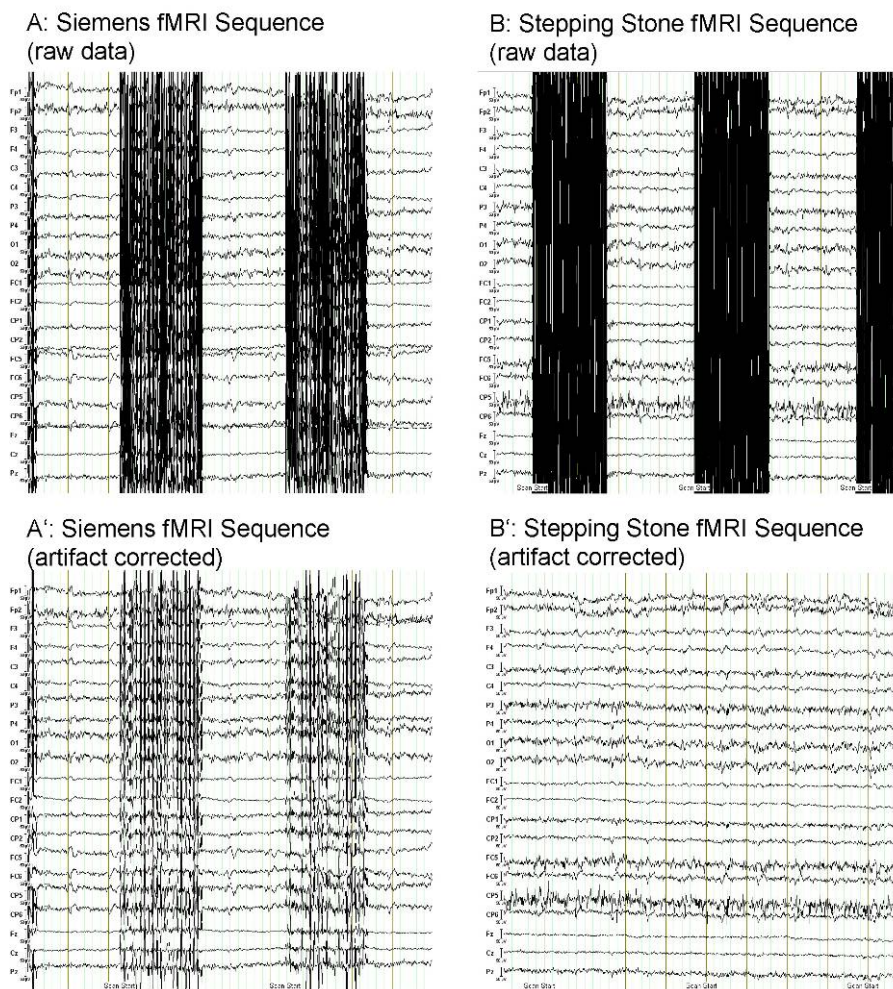


Figure 21: Comparison of the EEG signal quality for EEG recordings during fMRI measurement with a standard EPI sequence (A) and the ‘Stepping Stone’ sequence (B). EEG

signal for all recorded channels is shown. After applying artifact correction as described in paragraph 3.2.1 the residual artifact for the ‘Stepping Stone’ sequence recording is visibly smaller (A, B’).

As a first quantitative measure for the signal quality the variance of the EEG signal was calculated for every recorded channel and exemplarily depicted for session 1 of subject 1 in Figure 22. The per-channel-variance is shown for all five tracks that can form a 1000 Hz signal out of the recorded 5000 Hz EEG signal. The ‘Stepping Stone’ condition is only matched in track 1 (1:5:end, in Matlab nomenclature) as expressed in low variance in all electrodes.

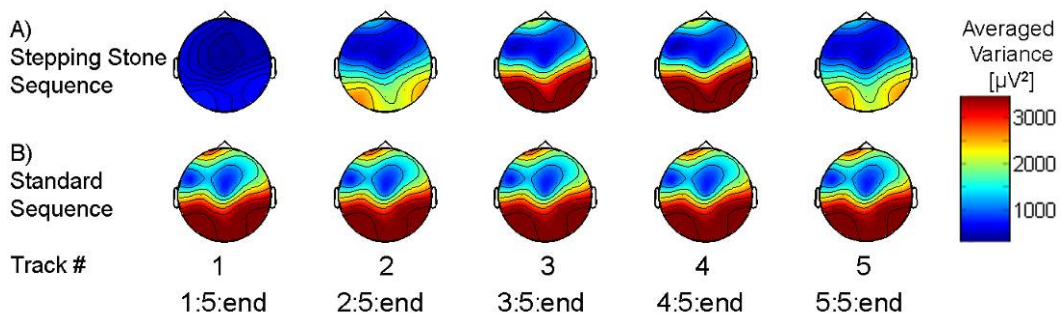


Figure 22: The electrode channel variance was used as a measure for the signal quality of the EEG signal after artifact correction. The variance is shown for all five tracks that can form a 1000 Hz signal out of the recorded 5000 Hz EEG signal (columns). The ‘Stepping Stone’ sequence (A) compared to the standard sequence (B). The ‘Stepping Stone’ condition is only matched in track 1 (1:5: end, in Matlab nomenclature) as expressed in low variance in all electrodes.

A further data reduction step was applied to compare the signal quality of all measurements. Figure 23 shows the mean of the variance of all channels (recording 1 reflects the averaged variance of row A in Figure 22 and recording 7 reflects the average of row B respectively). Subject 1 is shown in row 1, 2, 3 and 7, subject 2 in 4, 5, 6 and 8. It shows that the ‘Stepping Stone’ condition is not always matched in the first track as shown in recording 1. In recording 2 the minimal residual variance is given for the second track. However residual variance is always lower when the ‘Stepping stone’ sequence is used.

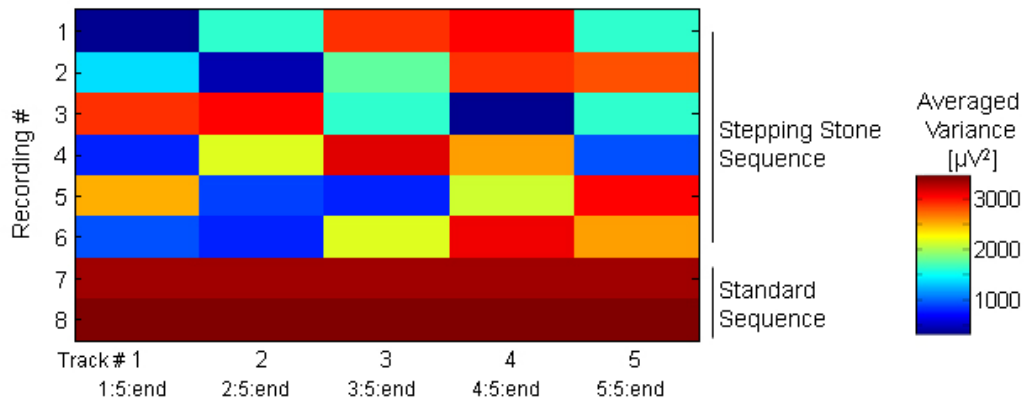


Figure 23: Mean of the variance in all channels. The ‘Stepping Stone’ condition is not always matched in track 1 as seen in recording 1. However residual variance is always lower using the ‘Stepping Stone’ sequence compared to the standard sequence.

5 Studies on the Posterior Alpha Rhythm

In this study [Moosmann, et al., 2003] two methodologically different approaches were used to investigate the human posterior alpha rhythm: (1) interleaved EEG-fMRI measurements, (2) continuous EEG-fMRI measurements. In order to acquire a sufficient number of periods of undisturbed EEG signal, the interleaved EEG-fMRI measurements allowed for only a partial coverage of the brain by fMRI due to the need to minimize the fMRI scan time. Facing this limitation, the MR-adapted EEG-technology was advanced to enable continuous EEG recordings during fMRI and thereby to cover the whole brain by fMRI. Since the study corresponded to a continuous parametric design, continuous EEG-acquisition additionally allowed for a more precise estimation of the putative hemodynamic response for further cross-correlation analysis with the simultaneously acquired BOLD signal. Figure 24 gives an overview of the methodological approach used in this study.

5.1 Subjects

Six volunteers (mean age 26 years, SD 3 years) participated in the interleaved EEG-fMRI study, fourteen volunteers (mean age 25 years, SD 3.5 years) in the continuous EEG-fMRI study. All subjects were apparently healthy and without any history of neurological or psychiatric disease. Written informed consent was obtained from each subject prior to the investigation.

5.2 MRI data acquisition

MRI measurements were performed on a 1.5 T whole body scanner (Magnetom Vision, Siemens, Erlangen, Germany). Subjects' heads were immobilised with a vacuum pad to reduce movement artifacts. Functional imaging was performed using a T2*-weighted BOLD sensitive gradient echo planar imaging sequence.

20 image slices were oriented transversely parallel to the anterior-posterior commissure such that they included the whole brain (bilateral thalami and the primary and secondary visual cortices in the 'interleaved alpha rhythm' study where only 6 fMRI slices were recorded).

Paragraph 3.3 on page 26 and Table 1 on page 27 describe the details and parameters of the MRI data acquisition.

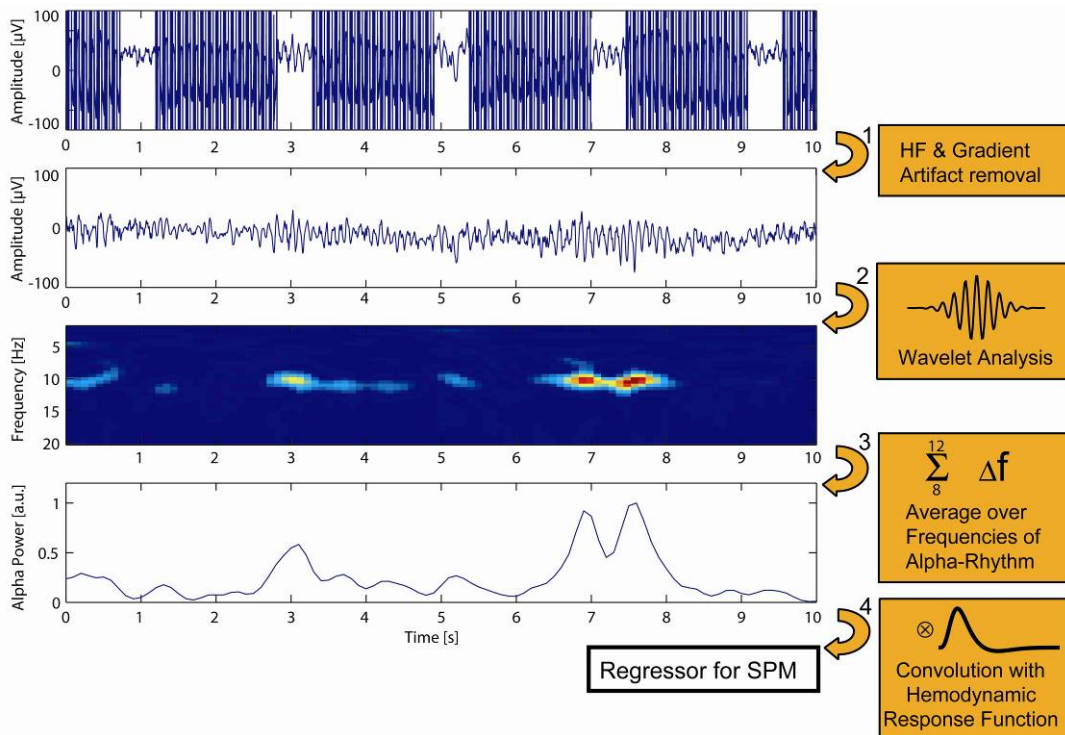


Figure 24: Schematic representation of the different steps (indicated by arrows) in the data analysis: (1) Application of a filter algorithm for MR artifact correction. (2) Time-frequency decomposition by wavelet analysis. (3) Estimation of the alpha power by averaging alpha band band frequencies. (4) Convolution with the hemodynamic response function to estimate a predictor for the BOLD signal.

5.3 EEG recording

In the interleaved EEG-fMRI study, the EEG was recorded by a MR-compatible EEG-device (EMR digital, Schwarzer, Munich, Germany; band pass filter 0.53–70 Hz, sampling rate 1 kHz) on positions O1 and O2 according to the International 10-20 System, referenced to the right ear. To avoid saturation of the EEG-amplifier due to charging effects during MR-scan times and therewith associated relaxation artifacts after the MR-scan, the amplifier was turned off in these periods for 650 ms.

In the continuous EEG-fMRI study, a MR-compatible 32-channel-amplifier (BrainAmp, Brainproducts Inc., Munich, Germany; sampling rate 5 kHz) and an EEG-cap with 29 electrodes (Easy-Cap, FMS, Munich) arranged according to the International 10-20 System, referenced against Cz, were used. Additionally, an electrooculogram (EOG) and an electrocardiogram (ECG) were recorded.

5.4 Paradigm and Study Design

The EEG-fMRI recordings were acquired from subjects while awake and with eyes closed to allow for spontaneous oscillations of alpha activity. Subjects were lying quietly in the dark bore of the MR-scanner. No stimuli were presented. The EEG was visually inspected to control for vigilance changes. Measurements that showed “anteriorization” of alpha activity or cessation of posterior alpha activity (both are signs of a beginning drop in vigilance) for periods exceeding one minute were excluded from further analysis.

5.5 Data Analysis

5.5.1 FMRI-artifact correction

High-frequency (HF) pulse and MR-gradients during MR-scans superimpose the physiological EEG-signal and occur as high- and multi-frequency artifacts (see paragraph 1.7). Since MR-artifacts have a constant pattern, it was possible to correct the EEG-signal by subtracting weighted averages of these artifacts (see chapter 3.2.1 for details)

5.5.2 Estimation of the alpha power

Interleaved EEG-fMRI: To estimate the strength of alpha activity at every sampled time point we applied the algorithm shown in Figure 24. The EEG signal was decomposed by wavelet analysis with the Morlet wavelet base (see chapter 3.2.2). The wavelet scales corresponded to Fourier frequencies from 2 to 60 Hz in steps of 0.5 Hz. The resulting wavelet spectrum was squared to obtain a power spectrum and averaged over the alpha frequency range of 8-12 Hz. The averaged alpha power of electrodes O1 and O2 was defined as a measure of alpha activity. For the 600 ms periods during which EEG-recordings were not available due to MR-artifacts, alpha power was linearly interpolated in the time domain.

Continuous EEG-fMRI: The same procedure as in the interleaved EEG-fMRI study was applied; however, periods containing MR-artifacts were corrected. Thus, no interpolation was necessary. The alpha power of electrode O2 was used as a measure of alpha activity.

5.5.3 Functional MRI-Analysis

Analysis of functional imaging data consisted of pre-processing and calculation of statistical parametric maps using SPM99 (Wellcome Department of Cognitive Neurology,

London, UK). Pre-processing included realignment, normalization of the anatomical and functional data to the Montreal Neurological Institute (MNI) standard brain, and spatial smoothing of the functional images with a three-dimensional Gaussian filter with a FWHM of double voxel size. The first ten functional volumes were excluded to avoid magnetic saturation effects. The normalization procedure was performed by co-registration of the anatomical data set to the canonical T1 template provided by SPM99. The resulting transformation parameters were used for subsequent normalization of the functional images. Low-pass (Gauss, 4 s) and high-pass (512 s) frequency filters were applied to the voxel time series.

Interleaved EEG-fMRI: Statistical parametric maps were calculated by multiple regression analysis as described in chapter 3.4.2 using seven regressors. A first regressor for the fMRI-BOLD signal was calculated by convolving alpha power with the hemodynamic response function taken from SPM99 with standard parameters. Additionally, the six realignment parameters were included in the model to account for residual variance. T-contrast images for the alpha predictor were computed for each subject as well as for all subjects in a fixed effects group analysis. A threshold of $p < 0.05$ was applied, corrected for multiple comparisons (Euler characteristics on random Gaussian fields) with an extent threshold of 5 contiguous voxels. As a control, the same analysis was performed for the 24-28 Hz frequency band.

Continuous EEG-fMRI: A model for the BOLD signal was estimated using the alpha predictor and realignment parameters as described above. Additionally, the first derivative of the alpha predictor was included into the model to allow for an improved fit of the data in the case of a mismatch between the expected (6 s) and the actual peak latency of the hemodynamic response. First, t-contrast images for the alpha predictor were computed for each subject. Second, the group effects were computed by a random effects analysis (one sample t-test, $p < 0.001$, uncorrected for multiple comparisons, extent threshold 5 contiguous voxels) allowing to draw inferences from the observed effects and to apply them to the general population. To investigate whether the correlation patterns are specific for the alpha band and to control for effects which occur in a wide frequency range (e.g. movement artifacts), the same analysis procedure was performed for the 3-6-Hz, 24-28-Hz, 34-38-Hz and 54-58-Hz band. Frequency bands were chosen such that first harmonics of one band were avoided in the others.

5.6 Results

Fixed effects group analysis based on six subjects showed a significant inverse relationship between the alpha predictor and BOLD signal in the occipital Brodmann areas (BAs) 18 and 19 (Figure 25). Statistical analysis of individual subjects (fixed effects analyses; $p < 0.001$; uncorrected for multiple comparisons) showed in five of the six subjects very similar occipital correlation patterns as in the group analysis (Figure 26). In five subjects, further activation sites were noted in the prefrontal cortex, but there was little overlap between subjects. Areas of the anterior cingulate gyrus (BA 32) were significantly correlated to alpha power in two subjects.

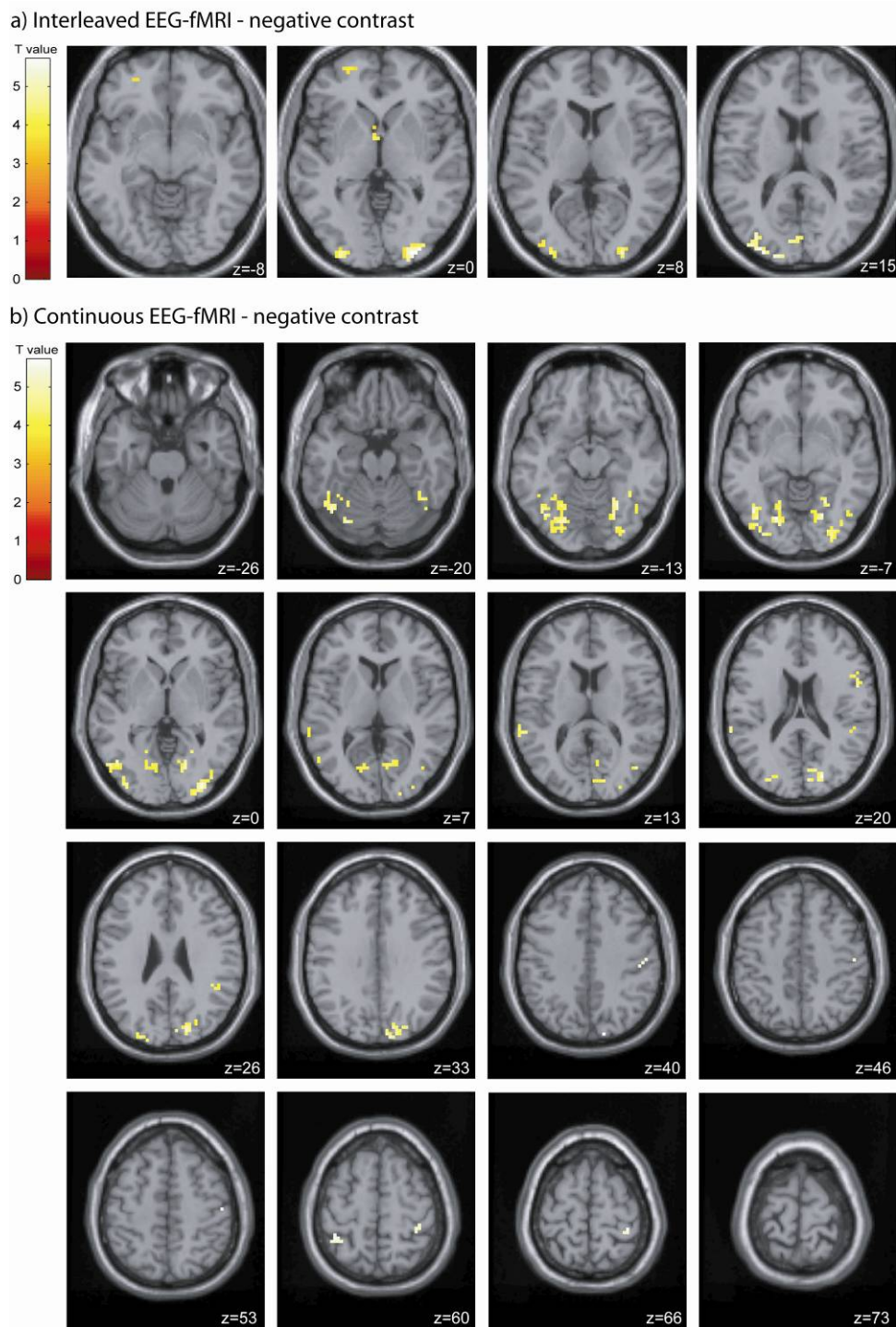


Figure 25: Results of negative correlation analysis between the alpha-predictor and BOLD signal. a) Interleaved EEG-fMRI study. Group analysis of 6 subjects, $p < 0.05$ corrected for multiple comparisons. b) Random effects analysis of 14 subjects, statistical maps of all 16 slices at $p < 0.001$ uncorrected.

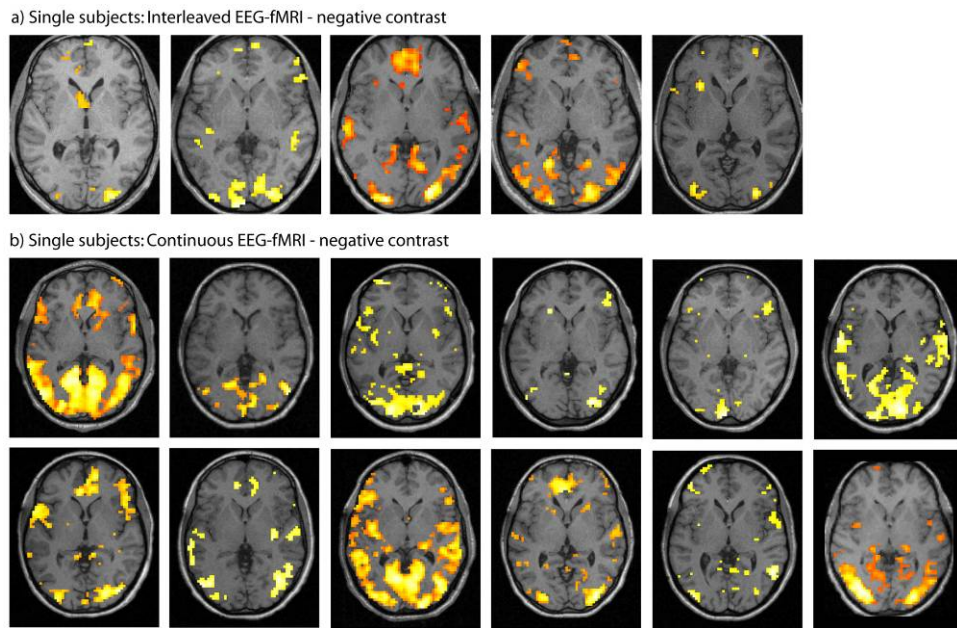


Figure 26: Single subject results of one slice ($z=0$) for negative correlation analysis between alpha-predictor and BOLD signal. a) Interleaved EEG-fMRI study, $p < 0.001$ uncorrected. b) Continuous EEG-fMRI study, $p < 0.001$ uncorrected

In the group analysis, a positive correlation was noted in the thalamus and adjacent areas with a maximum at the left dorsomedial thalamic nucleus. Additional significant positive correlations were found in the right ventrolateral thalamus, left caudal thalamus, areas adjacent to the left thalamus (pertaining possibly to the posterior cingulum and globus pallidus) as well as in the cisterna ambiens (Figure 27a). In single subjects analysis positive correlations similar to those of the group analysis were found in three subjects.

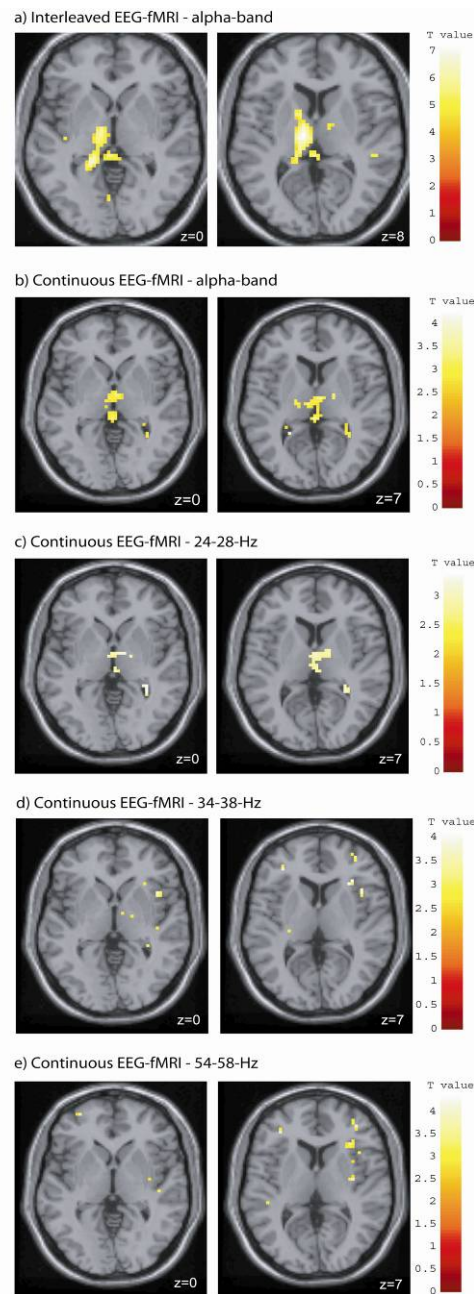


Figure 27: Results of the positive correlation analysis between alpha predictor and BOLD signal.

a) Interleaved EEG-fMRI study. Group analysis based on examinations in 6 subjects, $p < 0.05$ corrected for multiple comparisons. b-e) Continuous EEG-fMRI. Random effects analysis of 14 subjects, $p < 0.001$, uncorrected for frequency bands 9-12 Hz (b), 24-28 Hz (c), 34-38 Hz (d), 54-58 Hz (e).

To test whether these correlations were specific to the alpha band, we performed a fixed-effects group analysis for the 24-28 Hz frequency band. No significant negative correlations were found; however, positive correlations were seen in similar brain areas as for the alpha band (see Figure 27b).

Continuous EEG-fMRI: Results of the random effects analysis based on 14 subjects for the negatively contrasted alpha-predictor are shown in Figure 25b. A significant inverse relationship between alpha predictor and BOLD signal was found predominantly in the occipital cortex in Brodmann's areas 18 and 19. These negative correlations in the occipital cortex have also been found in the single subject analyses in 12 of the 14 subjects (Figure 26b).

In the (random effects) group analysis, additional sites of negative correlation were found in parietal and temporal cortical areas. Three clusters were located in the bilateral somatosensory postcentral gyrus. In six individual subjects, single subject statistics showed additional clusters of correlation in Brodmann's area 32 of the limbic association cortex, which was not significant in the random effects group statistics.

Random effects analysis of all 14 subjects for the positive contrasted alpha predictor did not show any significant correlations at the applied threshold of $p < 0.001$ (uncorrected for multiple comparisons). A lower threshold of $p < 0.05$ yielded positive correlations in the ventrolateral, dorsomedial and caudal thalamus and the inner ventricular system bilaterally (Figure 27c).

For the 3-6 Hz band no significant correlations were found. The 24-28 Hz band showed a negative correlation pattern entirely different from that of the alpha band with predominance in frontoparietal cortical areas. A color-coded SPM "glass-brain" image of significant voxels for the alpha and the 24-28 Hz bands is shown in Figure 28. Positive correlations for the 24-28-Hz band were similar as in the alpha band at the lower threshold of $p < 0.05$ (Figure 27c). The 34-38-Hz band and the 54-58-Hz band yielded positive-correlation patterns different from that of the alpha band (Figure 27d/e).

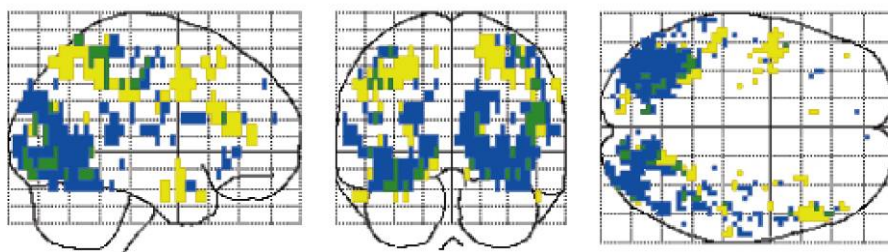


Figure 28: Glass brain image of significant voxels of the alpha band (blue), the 24-28 Hz-band (yellow) and the overlap of both (green) for negative correlations. Continuous EEG-fMRI study, random effects analysis of 14 subjects, $p < 0.001$, uncorrected.

6 Studies on the Rolandic Alpha & Beta Rhythm

The rolandic alpha and beta rhythm have, compared to the posterior alpha rhythm, relatively low amplitudes and are thus more difficult to recognize in the EEG signal (see paragraph 1.2.2 for details). To reveal the functional correlates of the subtle rolandic rhythms more elaborated analysis methods were needed, compared to the study on the posterior alpha rhythm, which shall shortly be described here and in more detail in the following sections.

Additionally to a resting condition session (as it was solely recorded in the study on the posterior alpha rhythm. See paragraph 5.4) a further session was recorded where the subjects had to perform a hand movement task. It is known that the rolandic rhythms are strongly modulated by hand movement (see paragraph 1.2.2 for details). A blind source separation algorithm (see paragraph 3.2.3 for details) was applied to filter the rolandic rhythms from other signals in the EEG before crosscorrelation with the fMRI signal was performed (analog as in the study on the posterior alpha rhythm). The individually estimated filter was then applied to the EEG signal recorded in the ‘resting condition’.

6.1 Subjects

Sixteen healthy subjects (mean age 26 y, SD 4 y) with no history of neurological or psychiatric disorder were included in the study. All subjects gave written informed consent prior to the investigation. The experiments were performed in compliance with the relevant laws and institutional guidelines and were approved by the local ethics committee.

6.2 Simultaneous EEG-fMRI recordings

Simultaneous EEG-fMRI recordings were performed with a 1.5-T scanner (Magnetom Vision, Siemens, Erlangen, Germany) and a 32-channel MR-compatible EEG (Brain Products, Munich, Germany). Functional imaging was performed using a T2*-weighted BOLD sensitive gradient echo planar imaging sequence (see chapter 3.3 and Table 1 on page 27 for details). For EEG recordings, a customized 32-channel EEG-cap was used including six electromyography (EMG) electrodes for bipolar recordings from chin and bilateral hand muscles, three electrooculogram (EOG) electrodes for vertical and horizontal EOG and two electrocardiogram (ECG) electrodes. An MR-compatible amplifier described as used (see chapter 3.1). EEG was recorded from 21 electrode positions (International 10-20 system) referenced to a point between Cz and Fz. EEGs

were MR-artifact corrected as described in chapter 1.7.2.2 and subsequently a 70 Hz low pass filter was applied.

6.3 Experimental task

Every subject underwent two experiments.

(1) Simultaneous EEG-fMRI recordings (TR = 2.2 s, 480 scans, 17.6 minutes) were acquired during rest while subjects were awake with eyes open, lying quietly in the dimly lit bore of the MR-scanner. No stimuli were presented.

(2) Subsequently, simultaneous EEG-fMRI (TR = 2.5 s, 200 scans, 8.3 minutes) was acquired when subjects performed a motor task to modulate rolandic rhythms: This task consisted of self-paced effortless synchronous opening and closing of the hands at a frequency of about 1 Hz (trained before the experiment) for 20 seconds alternating with rest periods of equal duration. In previous studies, it has been shown that such grip tasks induce robust activation in fMRI [Jancke, et al., 1998]. The task blocks were acoustically cued by “start” and “stop” commands presented via MR compatible headsets. The subjects were instructed to keep their eyes open during the entire experiment in order to suppress the posterior alpha rhythm strength. As it is known that rolandic rhythms are enhanced by complex visual input [Brechet and Lecasble, 1965; Jasper and Andrews, 1938b; Koshino and Niedermeyer, 1975], the subjects were instructed to fixate a fixation cross that was embedded in a colored picture (N=9) or watch a video (N=5) [Lelord, 1957] during the experiment. EEG obtained from this experiment were submitted to a blind source separation algorithm (TDSEP, see chapter 3.2.3) in order to define spatial filters for the separation of rolandic alpha and beta rhythmic components from other EEG signatures. These filters were applied on the EEG obtained under motor task as well as under rest condition.

6.4 Analysis of EEG Data obtained under the motor-task condition

Analysis steps for both experiments, motor- task and rest condition, are illustrated in Figure 29.

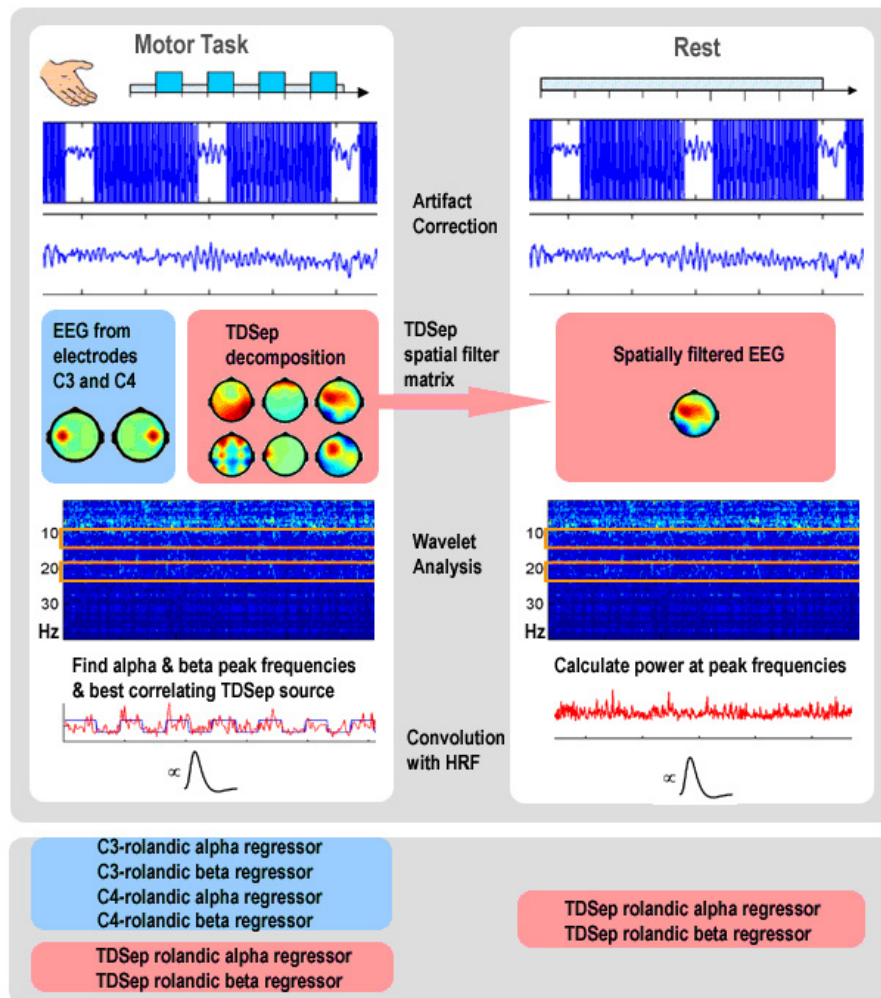


Figure 29: Schematic of the estimation of the regressors of the rolandic rhythms

6.4.1 Identification of rolandic alpha and beta rhythms

Three features were used to identify rolandic rhythms: (i) frequency, (ii) suppression during motor task, and (iii) location:

Rolandic alpha rhythm has a known peak frequency around 10 Hz and rolandic beta rhythm around 20 Hz [Tiihonen, et al., 1989].

During finger movements, rolandic rhythms are known to be desynchronized [Arroyo, et al., 1993; Jasper and Penfield, 1949]. Hence, for identification of rolandic alpha and beta rhythms we performed frequency analysis of the EEG-recordings and searched for components, which were suppressed during hand movements.

Rolandic rhythms are known to occur most prominently in pericentral regions.

6.4.2 Left and Right rolandic alpha and beta rhythms during motor-task

(Blue Analysis in Figure 29)

The EEG of the channels C3 (left central electrode) and C4 (right central electrode) channels obtained in experiment 2 (motor-task) were decomposed into the time-frequency domain using wavelet analysis to obtain power time courses for all frequencies. For each subject, a two-sample t-test (task vs. rest condition) was calculated for the following eight frequency bands: delta (1.5-6 Hz), theta (6-8 Hz), alpha-1 (8-10 Hz), alpha-2 (10-12 Hz), beta-1 (12-18 Hz), beta-2 (18-21 Hz), beta-3 (21-30 Hz) and gamma (30-60 Hz). In the alpha and beta range the respective bands which correlated best with on/off periods of hand movement (over all subjects) were identified (alpha-2 and beta-2) and further referred to as rolandic alpha band and rolandic beta band, respectively.

Since it is known that each subject has its own specific rolandic frequency components [Pfurtscheller and Lopes da Silva, 1999], it is necessary to select the respective frequency for each individual separately. Hence, within the previously determined rolandic alpha and beta bands, individual peak frequencies were determined for each subject and operationally defined as ‘C3 (C4) rolandic alpha rhythm’ and ‘C3 (C4) rolandic beta rhythm’, respectively. For correlation with fMRI, power time courses of individual rolandic rhythms were convolved with the canonical hemodynamic response function provided by SPM2 and were down-sampled to the temporal resolution of the fMRI data $TR = 2.5$ s.

6.4.3 Blind source separation

In a parallel approach, it was attempted to separate the rolandic rhythms from other overlapping spatial patterns of EEG signatures. Besides the frequency range (see above), a further criterion of identification was reactivity to the motor task. We used a blind source separation algorithm (Red Analysis during ‘Motor Task’ in Figure 29), namely TDSep (temporal decorrelation source separation, see chapter 3.2.3 for details).

After TDSep transformation of EEG signals, all resulting sources were wavelet analyzed to obtain power time courses for all frequencies. As described above a two-sample t-test (task vs. rest condition) was calculated for determination of individual peak frequencies within the previously determined rolandic alpha and beta bands. TDSep sources with highest t-values at individual peak frequencies were used as operational definitions of rolandic alpha

rhythm ('TDSep rolandic alpha rhythm') and rolandic beta rhythm ('TDSep rolandic beta rhythm'), respectively. Power time courses of both rolandic rhythms were then convolved with the HRF and down-sampled to the temporal resolution of the fMRI data as described above.

Under the assumption that rolandic rhythms are spatially stationary TDSEP filter deduced in the "bimanual movement" experiment (each TDSEP source has one respective spatial filter matrix) was applied to the resting state EEG data of the first experiment (Red Analysis during 'Rest' in Figure 29) to obtain resting state rolandic alpha and beta rhythm sources and to calculate the respective power time courses. Power time courses of both rolandic rhythms during rest were convolved with the hemodynamic response function and down-sampled to the temporal resolution of the resting fMRI data (TR = 2.2 s) for further fMR analysis.

Finally, for differential analysis, we operationally defined the posterior alpha rhythm ('TDSEP posterior alpha') as the average (8 to 12 Hz) power of the TDSEP source whose alpha (8 to 12 Hz) power maximally correlated with the alpha power derived from electrode position O2 (not illustrated in Figure 29).

6.4.4 Overview of EEG-rhythms used for fMRI cross-correlation

Thus, three types of EEG-rhythms (for each case – bimanual movement task and rest condition) were derived from EEG-recordings during simultaneous fMRI and used for subsequent cross-correlation analysis:

'C3 (C4) rolandic alpha rhythm' and 'C3 (C4) rolandic beta rhythm' during motor-task (the power of the respective rhythms at electrodes C3 and C4, respectively (blue workflow in Figure 29)

'TDSEP rolandic alpha rhythm' and 'TDSEP rolandic beta rhythm' during motor-task and rest condition (the power of the respective rhythms in EEG-sources identified with a TDSEP filter) (red workflow in Figure 29)

The 'classical' posterior alpha rhythm' during motor-task and rest condition (the power of the respective rhythm identified with a TDSEP filter).

6.5 Analysis of fMRI Data

SPM 2 was used for fMRI data analysis. Functional MR images were realigned, normalized to the MNI standard brain, smoothed with double voxel size and high-pass filtered (512 s). Serial correlations were estimated using an autoregressive model to subsequently correct for non-sphericity during inference [Friston, et al., 1995b].

6.5.1 Bimanual movement task

Fifteen of sixteen data sets were used for fMRI analysis (the data set of one subject was excluded due to technical failure). Due to the presumable inverse covariance between the rhythms' power and the motor task, the BOLD variance cannot be ascribed unambiguously to one particular regressor. This means that simply putting all three regressors in one model will make results ambiguous [Andrade, et al., 1999]. Here, two different modeling approaches were employed:

a) Eight linear correlation (fixed effects) models were estimated, each including one of the following regressors (1) motor-task protocol, (2) C3 rolandic alpha rhythm, (3) C4 rolandic alpha rhythm, (4) C3 rolandic beta rhythm, (5) C4 rolandic beta rhythm, (6) TDSEP rolandic alpha rhythm, (7) TDSEP rolandic beta rhythm, (8) TDSEP posterior alpha rhythm. Additionally the respective first derivatives and realignment parameters were included in each model. Group effects were computed by a random effects analysis (one-sample t-test) which allows for assignment of the observed effects to the general population.

b) One model was calculated including motor-task protocol, orthogonalized TDSEP rolandic alpha rhythm, orthogonalized TDSEP rolandic beta rhythm and realignment parameters. The orthogonalization algorithm removed (1) signal components of the rolandic rhythms, which were correlated to the motor task and (2) signal components of the rolandic beta rhythm which were correlated to the rolandic alpha rhythm. Group effects were computed by a random effects analysis (one-sample t-test).

6.5.2 Rest condition

Fifteen data sets of sixteen subjects (the data set of one subject was excluded due to technical failure) were included in the combined EEG-fMRI analysis. Seven separate models were estimated by using the (1) C3 rolandic alpha rhythm regressor, (2) C4 rolandic alpha rhythm regressor, (3) TDSEP rolandic alpha rhythm regressor, (4) TDSEP rolandic beta rhythm regressor and (5) the posterior alpha rhythm regressors, its respective

first derivative and realignment parameters. Group effects were computed in a random effects analysis (one sample t-test) to allow for inferences from the observed effects and for applying them to the general population. Significance threshold was set to $p \leq 0.01$, uncorrected and voxel extent threshold was set to 5 voxel.

6.6 Results

Subjects underwent two subsequent experiments with simultaneous EEG-fMRI recording. In the first experiment subjects were lying quietly not performing any specific task, in the second experiment they performed a selfpaced (about one per second) effortless bimanual hand-opening-closing task in a block design to modulate rolandic rhythms [Pfurtscheller and Berghold, 1989]. Results are reported in the order of analysis starting with the motor task (experiment 2) since the analysis of the ‘rest data’ (experiment 1) is based on information obtained from experiment 2.

6.6.1 Results - Motor-task

In all fifteen subjects a clear modulation of the 10- and 20-Hz rolandic rhythms during bilateral hand movement versus rest was detected (see Figure 30 for example of modulation in one subject). As expected, both rhythms were suppressed during hand movement and reappeared during rest. This approach, however, implies that the three parameters ‘motor task’, ‘rolandic alpha rhythm’, and ‘rolandic beta rhythm’ are highly intercorrelated. Specifically, the power of the two rolandic rhythms is most likely inversely correlated to the motor task. Due to this presumable inverse covariance between the rhythms’ power and the motor paradigm, the BOLD signal variance, which correlates with the paradigm, is also inversely correlated with rolandic rhythms. As a consequence, voxels which are ‘activated’ during hand movement will tend to be ‘deactivated’ during periods of high ‘rhythm activity’. Thus, the BOLD variance in the motor-task experiment cannot be ascribed unambiguously to one particular regressor. Simply putting all three regressors in one model will make results ambiguous [Andrade, et al., 1999].

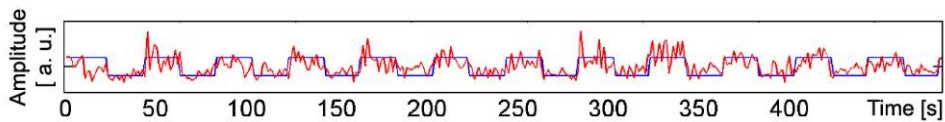


Figure 30: Modulation of the rolandic alpha rhythm during bimanual hand movement. The subject moved both hands every 20 s for 20 s (red). The blue line indicates the timing of the hand movement task (positive state codes rest, negative state codes hand movement).

Here, as a first step, one separate model for each regressor was calculated, thus testing whether each regressor correlates with the BOLD signal irrespective of the others. In this type of analysis, differences between the respective functional maps can indicate characteristics of the respective regressor. For example, in addition to movement-induced modulations of rolandic rhythms, there are also spontaneous fluctuations. These fluctuations slightly differ between the hemispheres [Niedermeyer and Koshino, 1975]. While it is not entirely clear whether such fluctuations represent the same phenomena as the movement-correlated events, they offer a continuous ‘additional signal’ which goes beyond the mere on-off dichotomy of the motor-task. The EEG-recordings at C3 versus C4 positions, respectively, pick up lateralized fluctuations of rolandic rhythms.

In the following first the results will be described which were obtained by calculating separate models for each functional regressor as described under point ‘a’ in chapter 6.5.1 on page 62. Then, in paragraph 6.6.1.8, findings obtained from a single model comprising three functional regressors (task-protocol, blindly separated alpha and beta rhythms) as described under point ‘b’ in chapter 6.5.1 on page 62 are reported. All results reported in this section refer to a statistical threshold of $p \leq 0.01$, uncorrected, random effects, $N = 15$, if not stated otherwise.

6.6.1.1 *fMRI correlates of ‘C3 / C4 rolandic beta rhythm’ during motor task*

For the C3 (left central electrode position), a statistical t-map is depicted in Figure 31. Negative correlation with the BOLD signal was observed in pre- and postcentral gyrus (right: BAs 1, 2, 3, 4, 40, left BAs 1, 2, 3, 4, 6) and cerebellum bilaterally (stronger left than right), parietotemporal operculum/insula (right: BAs 13, 22, left: BAs 13, 21, 22, 29, 41, 42) bilaterally, superior/medial frontal gyrus (BA 6), left thalamus and basal ganglia. Positive correlation was found in the left precuneus.

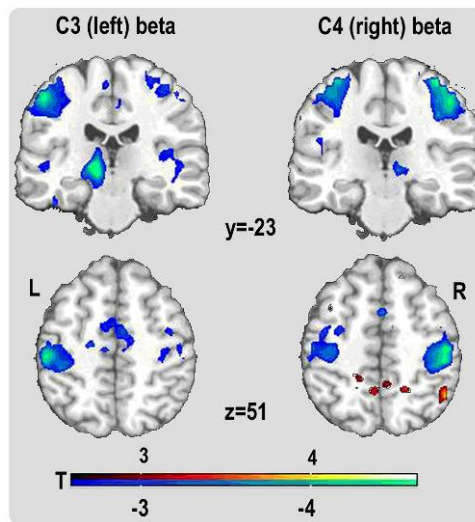


Figure 31: fMRI correlation of the rolandic beta rhythm during motor task. Negative correlations between the BOLD signal and the rolandic beta rhythm obtained from electrode positions C3 and C4 respectively (random effects analysis $N=15$, $p \leq 0.01$, uncorrected). The correlations dependent on the electrode position are lateralized (C3: left / C4: right). Colour coded t-values.

For C4 (right central electrode position), negative correlation with the BOLD signal was found in bilateral (right > left) pre- and postcentral gyrus (BAs 1, 2, 3, 4, 6, 40), bilateral cerebellum (right > left), left parietotemporal operculum, right/central superior/medial frontal gyrus (BA6), bilateral thalamus (right > left), and bilateral basal ganglia. Positive correlations were found in bilateral precuneus (left > right), posterior cingulum, paracentral lobule and Brodmann's area 6.

Thus, in general, there is an inverse correlation between the power of the rolandic beta rhythm and the BOLD signal in cortical bilateral sensorimotor structures, however, there is a clear hemispheric dominance corresponding to the side of the electrode, i.e., rolandic beta rhythm obtained from the left hemisphere ('C3 rolandic beta'), has a much stronger (inverse) correlation with the BOLD signal in the left hemisphere, and vice versa for the right side (Figure 31).

6.6.1.2 fMRI correlates of 'C3 / C4 rolandic alpha rhythm' during motor-task

Rolandic alpha rhythm at C3 showed inverse correlation to the fMRI signal in right pre- and postcentral gyrus (BAs 2, 3, 4, 40), right frontoparietal operculum and insula (BAs 13, 22, 45, 47), left parahippocampal gyrus, left caudate, right frontal pole (BA 11) and lingual

gyrus (BA 17, 18). There were no significant positive correlations at the same statistical threshold.

Rolandic alpha rhythm at electrode position C4 showed maximum inverse correlation in the right postcentral gyrus (BA 3), bilateral brain stem (right red nucleus and nucleus subthalamicus), left middle frontal gyrus (BA 10). A positive correlation was found in the left posterior cingulate gyrus (BA 31), left precuneus, left and central paracentral lobule (BA 5).

Global maxima for inverse correlations are displayed in Figure 32a. Activation maxima for 'rolandic alpha versus beta' BOLD correlates differed slightly with respect to pre- and postcentral spatial distribution.

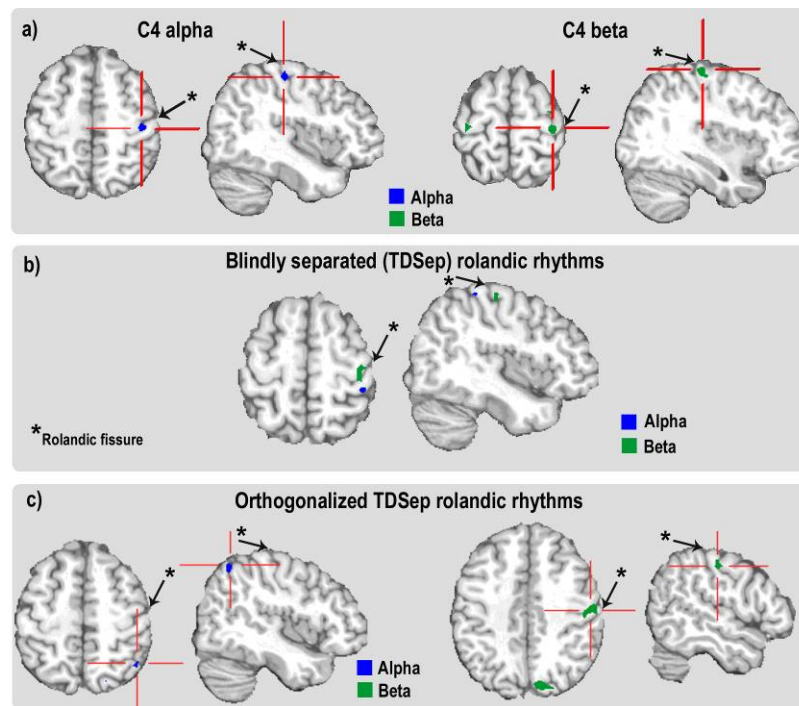


Figure 32: Motor-task condition – Maximal correlation of rolandic alpha versus beta rhythm. a) Maximal negative fMRI correlates of rolandic alpha (left) and beta (right) rhythms obtained from electrode position C4 (random effects analysis N=15). b) Maximal negative fMRI correlates of blind-source separated ‘TDSep rolandic alpha rhythm’ (blue) and ‘TDSep rolandic beta rhythm’ (green) (random effects analysis N=15). c) Maximal negative fMRI correlates of orthogonalized ‘TDSep rolandic alpha rhythm’ (blue) and ‘TDSep rolandic beta rhythm’ (green) obtained from a single-model analysis comprising the protocol and both blind-source separated rolandic rhythms (random effects analysis N=15).

6.6.1.3 Blind-source separated simulated brain rhythms

To isolate rolandic rhythms from other EEG signatures, temporal decorrelation source separation TDSep (see paragraph 3.2.3) was employed. In the following rhythms obtained by this method are referred to as ‘TDSep rolandic alpha / beta rhythm’.

Before applying the TDSep algorithm to experimental EEG-data, the algorithm was tested on simulated data. Artificial EEG-data was composed as follows (Figure 33): 21 data channels with individual random noise plus ‘posterior alpha rhythm’ consisting of a 10-Hz sinus wave with highest strength in posterior channels and ‘bilateral rolandic rhythms’, consisting of a 11-Hz and a 19-Hz sinus wave and being modulated in strength every 20 seconds. Both, posterior alpha and rolandic rhythms gradually declined in channels adjacent to the site of maximum strength. As shown in Figure 33, by means of TDSep, rolandic rhythms were reliably identified. The temporal and spatial characteristics of these rhythms were reconstructed in a far better way than by any single EEG electrode signal,

demonstrating the superiority of this method. This superiority was confirmed on the experimental data. The power of the rolandic alpha and beta rhythms, respectively, from TDSEP sources was stronger correlated with the motor task than the power of both rhythms from C3 or C4 EEG-signal, respectively. This indicates higher functional specificity of signals from TDSEP sources. Furthermore, regressors obtained from TDSEP sources explained more of the BOLD signal variance. In the following all rest-condition results refer to a Random effects group analysis (N=17) and a statistical threshold of $p < 0.01$, uncorrected, if not stated otherwise.

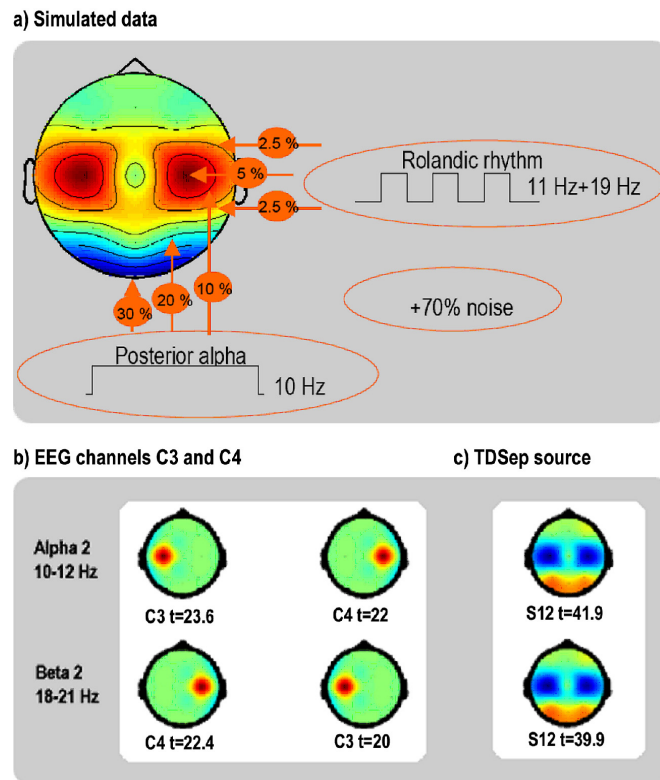


Figure 33: Temporal delayed source separation (TDSep) of simulated and real data: TDSEP algorithm for blind source separation was tested with simulated EEG data. a) The 21 simulated EEG channels consisted of individual noise, posterior alpha rhythm and block-modulated rolandic rhythms. b) Correlation analysis and subsequent t-test between alpha-2 / beta-2 band of all 21 simulated EEG channels and the modulating block-function yields C3 and C4 as best correlating channels (t-values are depicted color-coded in the scalp maps, maximum t-values are given beneath). c) By means of blind source separation using the TDSEP-algorithm, rolandic rhythms were reliably identified. Presented are the scalp maps of the best correlating TDSEP source (S12) for both frequency bands (weighting of single channels is color-coded, negative=blue, positive=red). The scalp maps and the higher t-values indicate that this method allowed a better reconstruction of the temporal and spatial characteristics of these rhythms than the single EEG-signal at positions C3 or C4.

6.6.1.4 fMRI correlates of 'TDSEP rolandic beta rhythm' during motor-task

Negative correlation was noted in bilateral pre- and postcentral gyrus (BAs 1, 2, 3, 4, 40, right: plus BA 6), left insula, transverse temporal gyrus and postcentral gyrus (BAs 13,40), bilateral thalamus and brainstem and bilateral cerebellum. Positive correlation was detected in bilateral paracentral lobule (BA 5, 3, 4, 6, 7), bilateral temporo-parietal cortex and precuneus, and bilateral dorsal prefrontal and cingulate cortex (right: BA 6, 8, 9, 32, left: BAs 6,32). These correlations become spatially more coherent at a threshold of $p \leq 0.05$ (Figure 34a).

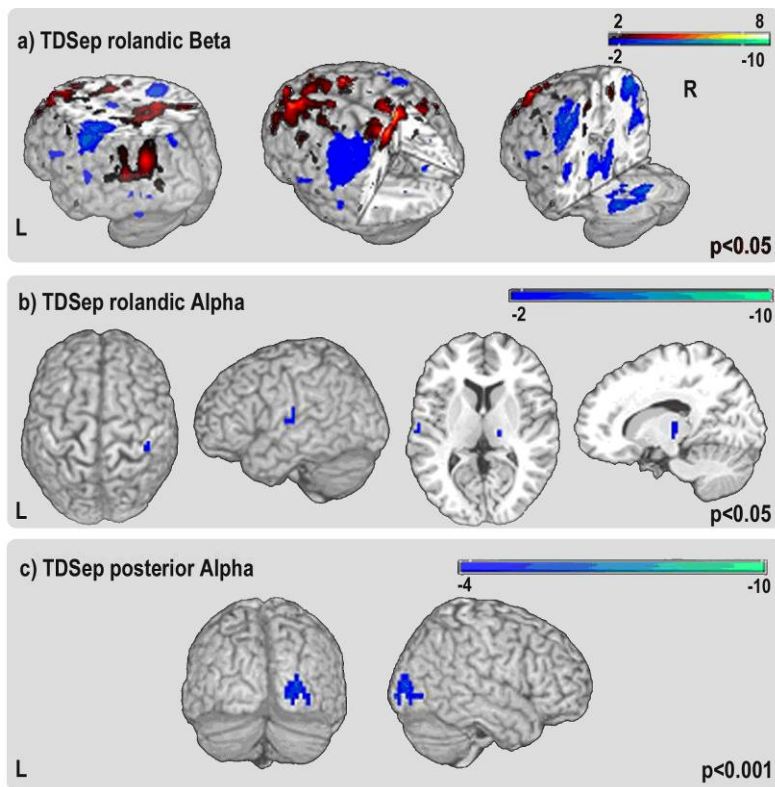


Figure 34: Motor-task condition. Correlation of the blind-source separated rolandic alpha, rolandic beta and posterior alpha rhythm with the fMRI BOLD signal. Random effects analysis $N=15$, color-coded t-values. a) Negative (blue) and positive (red) correlations between BOLD signal and ‘TDSep rolandic beta rhythm’ ($p \leq 0.05$, uncorrected). b) Negative correlations between BOLD signal and ‘TDSep rolandic alpha rhythm’ ($p \leq 0.05$, uncorrected). c) Negative correlations between BOLD signal and ‘TDSep posterior alpha rhythm’ ($p \leq 0.001$, corrected for multiple comparisons).

6.6.1.5 fMRI correlates of ‘TDSep rolandic alpha rhythm’ during motor-task

Correlation of the ‘TDSep rolandic alpha rhythm’ with the MR-BOLD signal was much less pronounced than for the ‘TDSep rolandic beta rhythm’. At a statistical threshold of $p \leq 0.05$ (uncorrected), there was negative correlation with a maximum in the left temporoparietal operculum (BA 42), and further in right postcentral gyrus (BAs 2, 40), and right thalamus (Figure 34b). Positive correlations were found in bilateral precentral gyrus/inferior frontal gyrus (BAs 4, 6), bilateral cingulate gyrus, inferior parietal gyrus (BA 24/13) and right precuneus.

Figure 32b shows global maxima of inverse correlation for ‘TDSep rolandic alpha rhythm’ and ‘TDSep rolandic beta rhythm’. The global maximum for rolandic alpha is located in the postcentral gyrus. The global maximum for rolandic beta is located in precentral gyrus.

6.6.1.6 fMRI correlates of blind-source separated posterior alpha rhythm during motor-task

Posterior (classical) alpha rhythm source (TDSep posterior-alpha) was defined as the source at which alpha power maximally correlates with EEG-alpha power derived from electrode position O2. Negative correlations between ‘TDSep posterior alpha rhythm‘ and BOLD signal were found in the right occipital cortex, Brodmann’s areas 17 and 18 ($p \leq 0.001$, corrected at cluster level, see Figure 34c).

6.6.1.7 fMRI-correlates of the bimanual motor task itself

This analysis reveals the activation of the bimanual motor task itself compared to the rest condition (Figure 35, random effects analysis, $N = 15$, $p < 0.001$, uncorrected). Activation was seen in bilateral pre- and postcentral gyrus (BAs 1, 2, 3, 4, 6, 40), medial frontal gyrus (BA 6), parietotemporal operculum (BAs 40, 41, 42) and subcortically in anteromedial cerebellum, bilateral caudal-lateral thalamus and bilateral basal ganglia. At the same significance threshold, negative correlation was detected in the bilateral paracentral lobule (BAs 5), the postero-parietal cortex and right superior frontal gyrus (BA 6). At a lower statistical threshold of $p < 0.05$, (uncorrected), additional task-related, positive correlation with the BOLD signal was found in the left lateral occipital cortex (BAs 19, 37; presumably the extrastriate body area EBA [Astafiev, et al., 2004]) and in the left sulcus calcarinus (BAs 17,18). Additional negative correlation was found in the bilateral dorsal prefrontal cortex and precuneus.

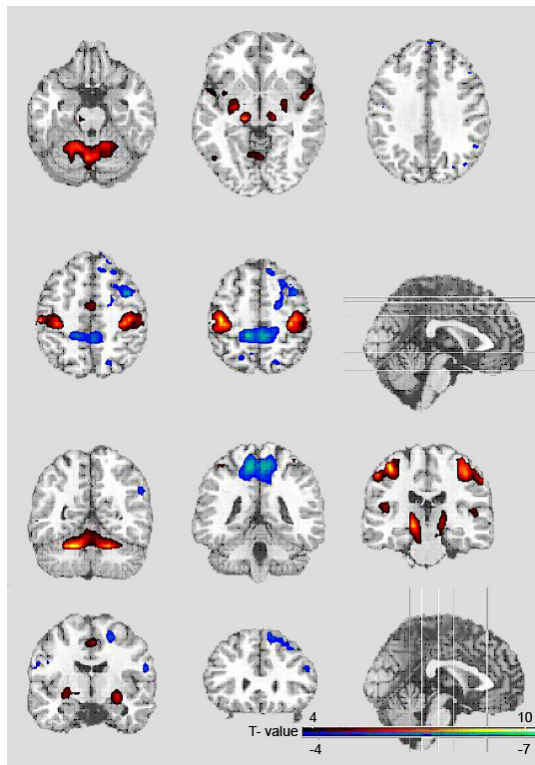


Figure 35: fMRI correlates of the bimanual movement task. Negative (blue) and positive (red) correlations between BOLD signal and motor task protocol (random effects analysis N=15) at a statistical threshold of $p \leq 0.001$, uncorrected.

6.6.1.8 fMRI correlates of protocol and orthogonalized rolandic rhythms calculated in a single model

We employed a second fMRI-data modelling approach in which the three orthogonalized functional regressors ‘task protocol’, ‘TDSep rolandic alpha’ and ‘TDSep rolandic beta’ were included in one model as described under point b) in paragraph 6.5.1 on page 62. Results for the ‘protocol’ were practically the same as described in the separate models approach given above. For the orthogonalized TDSep beta rhythm we found negative BOLD correlates in the right precentral gyrus and in the right precuneus (Figure 32c) and positive correlates in the left hippocampus/parahippocampal gyrus and in the left superior frontal gyrus. For the orthogonalized TDSep alpha regressor, there was significant negative correlation in a single cerebral area: the right inferior/posterior parietal lobule (BAs 40, 7) around the postcentral sulcus (Figure 32c) and positive correlation predominantly in the medial occipital and frontal cortex.

6.6.2 Results - Rest condition

6.6.2.1 *fMRI correlates of blind-source separated rolandic rhythms during rest*

Since blind source separation had proved to provide a better estimate of rolandic rhythms with less contamination due to volume conduction, referencing and noise we used individual spatial filters derived from experiment 1 to extract rolandic rhythms from the resting-EEG. This procedure is described in detail in paragraph 6.4. All results below refer to a statistical threshold of $p \leq 0.01$, uncorrected, random effects, $N = 15$, if not stated otherwise.

Using the power time course of the TDSEP source of the rolandic beta rhythm as regressor for the BOLD signal during the rest condition, areas of negative correlation at $p < 0.01$ were found in the right and left precentral and postcentral gyrus (BAs 2,3,4), in the bilateral middle and inferior frontal gyrus (BAs 6,8), in the bilateral middle and inferior frontal gyrus (BA 9), the right medial frontal gyrus (BAs 32,8), in the right cingulate gyrus (Figure 36a, left). Positive correlations at the same threshold were found in the bilateral cingulate gyrus (Figure 36a, right).

Using the power time course of the TDSEP source of the rolandic alpha rhythm as regressor for the BOLD signal during the rest condition negative correlations at $p < 0.05$ were found bilaterally in the inferior parietal lobule/posterior parietal cortex (BAs 40, 39), dorsal medial prefrontal cortex (BAs 8, 9) and posterior cingulate, the left premotor cortex (BAs 6, 8) and in the right orbitofrontal cortex (BAs 11, 47) and lentiform nucleus / Putamen (Figure 36b, left). Positive BOLD correlates were found in the bilateral cingulate gyrus (BAs 24, 31) and bilateral paracentral lobule Brodmann's area 5 (Figure 36b, right).

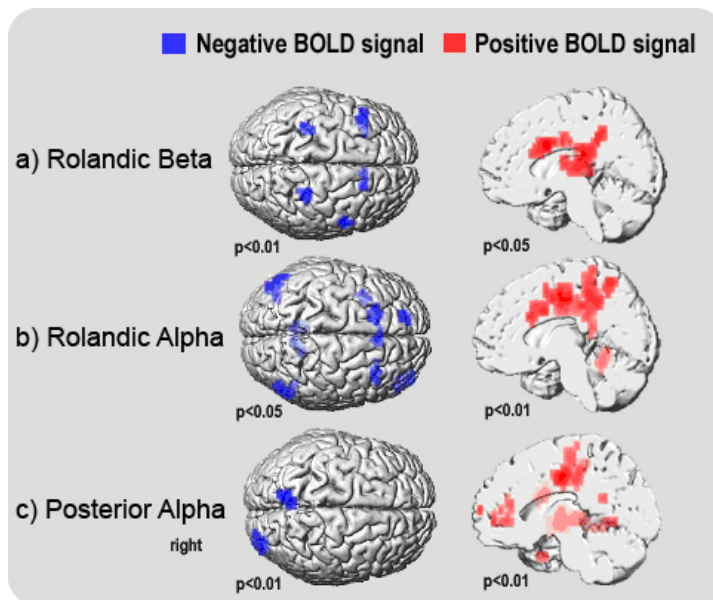


Figure 36: Rest-condition. Correlation of blind-source separated rolandic alpha, rolandic beta and classical posterior alpha rhythm with the fMRI BOLD signal. Negative (left) and positive (right) fMRI correlates (random effects analysis N=15). a) TDSep rolandic beta rhythm ($p < 0.01$, uncorrected). b) TDSep rolandic alpha rhythm ($p < 0.05$, uncorrected). c) TDSep right posterior alpha rhythm ($p < 0.01$, uncorrected)

6.6.2.2 *fMRI correlates of the blind-source separated posterior alpha rhythm during rest*

Using the power timecourse of the TDSep source for posterior alpha (obtained from correlation analysis with alpha power from electrode position O2, i.e. right occiput) as regressor, negative correlations were found in the right occipital lobe and the precuneus (Figure 36c, left) and positive correlations were found in the right anterior cingulate, bilateral cingulate gyrus (Figure 36c, right), right insula, bilateral pre- and postcentral gyrus, bilateral paracentral lobule, right middle, superior and medial frontal gyrus (BA 10), left parahippocampal gyrus, left temporal lobe Brodmann's areas 21, 22, 41, 42.

7 Discussion

In this work the methodology of simultaneous EEG-fMRI recordings was developed and applied to the research of human background rhythms. The findings of this work can be summarized as follows:

(1) EEG signal quality during fMRI scanning was shown to be sufficient by recovering visual evoked potentials (VEP) from MRI scan periods. The signal quality could be further improved by means of a specialized fMRI sequence (Paragraph 4).

(2) Human background rhythms such as posterior alpha and the subtle rolandic rhythms can be recovered from EEG recordings obtained during MRI data acquisition (Paragraph 5 and 6).

(3) fMRI correlates of these rhythms can be identified via correlation with BOLD-sensitive MR image series (Paragraph 5 and 6).

(4) In general, increased power of the examined rhythms was associated with negative BOLD signal in sensory cortical areas:

(4a) Posterior alpha rhythm correlated negatively within primary visual areas (Paragraph 5 and 6).

(4b) Rolandic rhythms correlated negatively within somatomotor areas (Paragraph 5).

(5) Rolandic alpha and beta rhythms differ with respect to their fMRI correlates under both motor-task and under rest condition. The rolandic beta rhythm is more associated with a motor-network whereas the rolandic alpha rhythm is more associated with a sensory and association network (Paragraph 6).

(6) Positive correlations: Posterior alpha rhythm during eyes closed shows BOLD correlates in thalamic structures. During eyes open condition the cingulate gyrus was associated with BOLD signal of posterior alpha and both rolandic rhythms (Paragraph 5 and 6).

In the following sections these findings shall be discussed.

7.1 Quality Insurance of the EEG-fMRI setup

Checkerboard visual stimulation was employed to investigate whether VEPs can be acquired from MRI-scan periods. VEPs elicited by a checkerboard have the advantage of

well-defined structural features. Other groups have already addressed the question whether VEPs recorded in the B₀-field of the MR-scanner are similar to those recorded outside the magnetic field of the scanner. Latencies of VEPs in inter-scan periods and outside the scanner are not significantly different [Bonmassar, et al., 1999; Kruggel, et al., 2000; Sommer, et al., 2003]. In this study we tested whether there are differences between VEPs recorded during artifact-distorted scan periods versus VEPs recorded during inter-scan periods.

As a first approximation, subtractive artifact removal was used for simultaneous VEP-fMRI measurements. No systematic differences were found between inter-scan and scan VEPs after artifact removal, neither in latency, amplitude of the main component nor in the general shape of the evoked potentials, as indicated by the high correlation coefficients between both groups of VEPs. Nevertheless, there were some minor differences between individual subjects. Given the known variability of VEPs, even without exposure to artifacts, particularly those in amplitude (Figure 17), these differences between scan and non-scan periods still lie within the range of a “natural” variance. Any systematic effects of the MRI scan were below the detection limit of this pilot study. As VEPs have relatively high amplitudes (of 20-30 μ V peak to peak), a visual paradigm was chosen as a starting point for recovering information about evoked electrical activity. These results indicate sufficient artifact correction but also suggest that the physiological processes underlying VEP generation are not significantly altered during MRI-acquisition.

7.1.1 VEP as measure of EEG signal quality

Different strategies were employed to compare evoked potentials. Visual inspection is often used as a sufficient method [Bonmassar, et al., 2002; Felblinger, et al., 1999]. For statistical evaluation the Kruskal-Wallis-test can be employed to test for differences between conditions inter-individually, [Kruggel, et al., 2000; Muri, et al., 1998]. This test is a non-parametric analogue of the parametric ANOVA. It is used for multiple comparisons between subjects; however, it has fewer assumptions about the data (no normal distribution or homogenous variances are necessary). Here, we used an intra-individual, non-parametric, rank-based test for the statistical comparison of VEPs recorded with concurrent MR acquisition versus without. As there are repeated measurements and only two conditions, a paired rank-based test for single comparison is suitable. The Wilcoxon-signed-rank test has, in the case of a normal distribution approximately 95-96 % of the

power of an analogous paired t-test [Glantz, 1997]. The application of a t-test is only robust for deviations from the normal distribution if the number of pairs exceeds 10 [Sachs, 1993]. Because in this study only five pairs were evaluated, a rank-based test was considered most appropriate. Due to the relatively high variance of this component the test power is relatively poor (Figure 17) and no inferences regarding N3 latency can be drawn. Larger subject numbers are required to increase the test power sufficiently. The results of the correlation analysis, however, support the hypothesis that the visual evoked P2-N3 complex is equivalent under both conditions. The findings of this work that artifact rejection in the above described manner produces a sufficient EEG signal quality has also been confirmed by a recent study [Sammer, et al., 2005].

7.1.2 'Stepping Stone Sequence' phase shifts

Applying 'Stepping Stone Sequence' introduced by Anami and coworkers [Anami, et al., 2003] significantly reduced remnant artifacts after artifact correction. The sequence was designed to sample EEG data points exclusively, while no fMRI induced artifact are present. It was originally designed for an EEG sampling rate of 1000 Hz. Since the amplifier used in this work recorded with a sampling rate of 5000 Hz the stepping stone criteria should only be valid for every fifth data point. Figure 23 shows that the track carrying the lowest variance after artifact reduction differs in different measurements. This might be caused by the Phase-Locked-Loop synchronisation mechanism of the EEG recording clock and the internal clock of the MR gradient system. It is therefore recommended to identify the best of the possible five tracks by comparing remnant variance.

7.1.3 Cardioballistic artifacts

In contrast to other studies, cardioballistic artifacts were of minor importance in the setup of this work. This is probably due to the tight fixation of the electrodes within the EEG-cap and was also confirmed by others [Anami, et al., 2002]. The EEG-equipment used here was highly adjusted to the MR-conditions, allowing for high quality EEG-recordings. By means of a specially adapted EEG-cap with sewed-in electrodes, artifacts associated with electrode movements were minimized. Thus, cardioballistic artifacts were reduced significantly (e. g. Figure 24). Cardioballistic artifacts have been shown to have a maximum frequency component around the 5-Hz band [Allen, et al., 1998]. In the wavelet analysis of alpha and beta rhythms we did not see any pulse related frequency component

above 7 Hz. Therefore, we did not expect significant interference of possible cardioballistic artifacts with the alpha and beta frequency band and the application of a pulse filter algorithm did not seem to be necessary. However, when signals of interest receive contribution from the lower frequency components of the EEG, such as oscillatory theta/delta activity, and long latency event related potentials (e.g. P300, N400), the use of such algorithms would be advisable.

7.1.4 Spectral analysis and implications for EEG-fMRI recordings

Considering the results of the spectral analysis, it has become clear that high frequency artifact residuals are still present to a considerable degree while using standard image acquisition sequences. Since these artifacts are not time locked to the stimulus onset (depending on experimental design), they may be overcome by sufficient averaging and possibly low pass filtering. The introduction of the ‘Stepping Stone’ sequence significantly reduced the remnant artifact and makes low pass filtering unnecessary. Studies on EEG phenomena such as studies on high frequency components of event related potentials (as the N20 of the somatosensory evoked potential) or high frequency oscillations [Baker, et al., 2003] might benefit from the correction algorithms and recording sequence established in this study.

7.2 Simultaneous EEG-fMRI measurements of spontaneous rhythms

Simultaneous EEG-fMRI measurements currently provide a unique opportunity to anatomically localize synchronized neuronal activity non-invasively. Though both methodologies have been established for some time, the combination of both has remained problematic until now. The reason is magneto-electrical interference causing mutual artifacts [Huang-Hellinger, et al., 1995; Ives, et al., 1993]. Functional-MRI-BOLD image distortions occur due to magnetic susceptibility changes, eddy currents or chemical shift artifacts caused by certain types of EEG electrodes, cream, leads, or amplifiers [Bonmassar, et al., 2001a]. Additionally there is the risk of patient harm by currents due to induced voltages and by burning due to heated electrodes [Lemieux, et al., 1997].

Using appropriate materials for EEG-recordings, combined EEG-fMRI measurements were first employed to localize sources of interictal epileptic activity [Krakow, et al., 1999; Seeck, et al., 1998; Symms, et al., 1999; Warach, et al., 1996]. In these measurements, MRI

scans were triggered by EEG-recorded epileptic spikes. Artifacts in the EEG-signal caused by high frequency pulses and MR-gradients during fMRI scans did not allow for an evaluation of the EEG during the MR-scan periods. Until recently combined EEG-fMRI measurements were only possible in the interleaved modus due to these MR-scan related artifacts. A number of studies investigating localization of event-related-potential generators used this approach [Babiloni, et al., 2002; Bonmassar, et al., 2001b; Christmann, et al., 2002; Kruggel, et al., 2001; Kruggel, et al., 2000; Thees, et al., 2003]. Continuous EEG evaluation during fMRI scans only recently became an option with the advent of adapted EEG-amplifiers and adaptive artifact filter algorithms [Allen, et al., 2000; Hoffmann, et al., 2000; Sijbers, et al., 1999]. Suitable EEG-amplifiers have to cover a high dynamic range to record low amplitude EEG and high amplitude MR-artifacts. The filter algorithms are based on estimating an artifact template in the frequency or time domain, which is subtracted from the contaminated EEG-signal. Using appropriate technical equipment and filter programs for artifact-correction, simultaneous and continuous EEG-fMRI measurements - as applied here - have been realized in some recent studies on epilepsy [Benar, et al., 2006; Benar, et al., 2002; Hamandi, et al., 2004; Hamandi, et al., 2005; Hoffmann, et al., 2000; Kobayashi, et al., 2006; Lemieux, et al., 2001; Liston, et al., 2004; Salek-Haddadi, et al., 2002], in studies investigating responses to acoustic stimuli during sleep and wakefulness [Czisch, et al., 2004; Czisch, et al., 2002] and in a study showing rapid eye movement (REM) related activations during sleep [Kaufmann, et al., 2006]. Recently other groups employed continuous studies on the posterior alpha activity [Feige, et al., 2005; Goldman, et al., 2002; Goncalves, et al., 2006; Henning, et al., 2006; Laufs, et al., 2003a; Laufs, et al., 2003b].

In this work, by applying advanced “artifact correction technology”, continuous EEG-fMRI recordings are reported, which appear superior to interleaved EEG and fMRI recordings. However, MR-artifact correction of the EEG signal is not without risk of getting an altered signal. Thus the similar finding obtained in the “interleaved study on posterior alpha rhythm”, which did not employ any artifact correction, validates the results delivered by the rather new continuous EEG-fMRI technique. On the other hand, considering the similar results obtained with both the continuous and the interleaved EEG-fMRI approach, one may question the advantage of MR-artifact correction over linear interpolation of the disturbed signal periods. Two important advantages of the continuous approach must be mentioned, however: Assuming efficient artifact correction, there is no

need to minimize the MR-scan time, thus allowing the study to cover the whole brain (in contrast to the interleaved study, where only six slices were recorded). The other theoretical advantage of continuous recording should be an improved signal to noise ratio of the EEG estimate.

Spontaneous modulation of the strength of the brain rhythm of interest is an important prerequisite for mapping it by means of fMRI. Since the rhythm power is convolved with the HRF, which acts as a low pass filter, a slow modulation of the rhythm (in the order of seconds) is required to get an efficient predictor for the fMRI-BOLD signal. Thus, the efficacy of these study designs crucially depends on the variance of the rhythm predictor. In fact, the three subjects (of both EEG-fMRI studies focusing on the posterior alpha rhythm) showing no significant negative correlations with the posterior alpha-power were the ones with the lowest variance of the alpha predictor.

7.2.1 Inverse relation between posterior alpha activity and fMRI-signal in the occipital cortex

An inverse relationship between posterior alpha activity and occipital fMRI-BOLD signal has been shown in the study focusing on the posterior alpha rhythms and in the study focusing on rolandic rhythms (Figure 25, Figure 26 and Figure 34). How do these findings correspond to the present knowledge on the localization of the posterior alpha rhythm?

In invasive studies on dogs, intracerebral electrode recordings showed alpha activity in the occipital cortex with large intracortical coherences [Lopes da Silva, et al., 1973]. Localization of the human posterior alpha rhythm by means of non-invasive EEG or magnetoencephalography (MEG) is problematic due to the impossibility of uniquely localizing sources in a conductive volume from only surface information ('the inverse problem') [Koles, 1998]. Alpha-rhythm dipole source localization limited to a single equivalent dipole applied on EEG data revealed alpha activity to be localized near the occipital midline [Henderson, et al., 1975; Michel, et al., 1992]. A two-equivalent-dipoles source model localized alpha activity symmetrically in the occipital areas [Valdes-Sosa, et al., 1992]. Using brain-electrical-source-analysis (BESA) software [Scherg, 1990; Scherg and Von Cramon, 1986], which allows for fitting multiple dipoles, alpha-sources were located in the occiput, however, with varying distance from the midline depending (beside other factors) on the strategy used in the workup of the data [Rodin and Rodin, 1995]. A calcarine origin of the posterior alpha-rhythm has been suggested as a result of MEG

studies [Chapman, et al., 1984; Williamson and Kaufman, 1989]. Another, more recent MEG study reports sources of the posterior alpha rhythm clustered mainly around the parieto-occipital sulcus and, to a lesser extent, around the calcarine sulci, with several generators [Hari, et al., 1997]. Independent component analysis applied to EEG data identified lateral occipital and central occipital components of the posterior alpha rhythm [Makeig, et al., 2002]. All these findings are based on methods which have with respect to the precision of localization. Therefore, smaller discrepancies between these and the results of this study might be ascribed to limitations in spatial precision of the mentioned methods. Nevertheless, in general, there is good agreement between the inverse correlations which was found here consistently in the studies of this work in Brodmann's areas 18 and 19 and the electrophysiologically localized bilateral occipital sources.

While the posterior alpha rhythm is a highly consistent feature in occipital brain regions, the extension of the alpha rhythm to more frontal brain regions shows pronounced inter-subject variability (Figure 26). Since the group analysis tends to "hide" such inter-subject variability, the latter is reflected in individual subject's analysis. Thus, correlations to the alpha rhythm in the occipital cortex (BAs 18, 19) were consistently noted across individual subjects and accordingly were significant in the random effects group analysis. Additional circumscribed negative correlations occurring in several subjects were located in the prefrontal cortex and the anterior cingulum. Since these areas were not consistently seen across individual subjects, in random effects group analysis, there were no corresponding significant correlations. It seems that one explanation of inter-subject variability of posterior alpha rhythm related BOLD changes could be state dependant such as attention, memory load, spontaneous cognitive processes or vigilance [Goncalves, et al., 2006; Henning, et al., 2006; McGonigle, et al., 2000; Smith, et al., 2005].

The negative correlations in the somatosensory Brodmann's areas 1, 3 and 5, which occurred in single subjects as well as in random effects group analysis, might be correlates of the rolandic alpha-rhythm, which oscillates in the same frequency range as the posterior alpha rhythm [Hari, et al., 1997]. The finding hint that rolandic rhythms could be mapped as well by means of EEG-fMRI measurements led to the study focusing on rolandic rhythms which is part of this work.

Avoiding the inverse problem, indirect functional imaging methods like PET and fMRI have been used to localize alpha activity. Correlates of the alpha rhythm have been found

in the occipital cortex in a PET study [Sadato, et al., 1998] as well as in fMRI [Feige, et al., 2005; Goldman, et al., 2002; Henning, et al., 2006; Patel, et al., 1997] and in an study by means of non-invasive near infrared spectroscopy [Moosmann, et al., 2003]. The study by Patel et al. used an eyes-open/eyes-closed paradigm to modulate alpha activity. Avoiding the covariance of two conditions – eyes-opening/eyes-closing and alpha activity - Goldman et al. reported data from an interleaved EEG-fMRI study on spontaneously fluctuating posterior alpha activity of four subjects with their eyes closed during the whole experiment. The data in this study matched their results with respect to the negative correlations between the BOLD-signal and alpha activity in the occiput. Henning and Feige found posterior alpha correlates in the occiput with eyes-opening and closing in darkness [Feige, et al., 2005; Henning, et al., 2006] or lighted environment [Feige, et al., 2005]. Contrarily another study showed a broad attentional network covarying with alpha activity [Laufs, et al., 2003a; Laufs, et al., 2003b]. Recently a study was published confirming the results of this study by showing an inverse relationship of posterior alpha activity and BOLD signal in occipital areas [Goncalves, et al., 2006]. By focusing on inter-subject variability they found as well diverse activation patterns depending on the respective brain state of different subjects which could be responsible for different findings in the studies of Laufs and colleagues.

7.2.2 There is distinct laterality of the fMRI response to right versus left rolandic rhythms:

There are strong and clearly lateralized correlations between ‘C3/C4 rolandic rhythms’ during motor-task and the BOLD signal. The lateralisation of the BOLD signal, particularly for the rolandic areas (MI, SI) clearly corresponds to the site of the EEG-electrode, i.e. there was a left hemispheric dominance in fMRI signal for C3 and right hemispheric dominance for C4, respectively. These findings indicate that spontaneous fluctuations of the rolandic rhythms, occurring in addition to the block-wise modulations by the motor task, have distinct fMRI correlates in the respective hemisphere (Figure 31).

7.2.3 During motor-task: Maximum inverse fMRI responses to rolandic alpha and beta rhythms are located in precentral and postcentral areas respectively.

Spatial differences in the sites of fMRI correlation between rolandic alpha versus beta rhythms obtained from positions C3/C4 were found. The maximum inverse correlation for

the two rhythms in primary sensorimotor areas was located more anterior for the beta rhythm as compared to the alpha rhythm (Figure 32a). In a next step, rhythms were identified by blind source separation, in order to provide less ‘contamination’ by other signal sources and therefore more specificity. The validity of this approach was supported by simulated data (Figure 33) and by stronger correlations between the power of blindly separated rolandic rhythms (as compared to the EEG-rhythms obtained from positions C3/C4) and the motor-task-function. Results were similar to those of the original EEG rolandic rhythms at positions C3/C4. Both blindly separated rolandic rhythms were associated with inverse fMRI responses in the primary sensorimotor cortex. FMRI correlate of the blindly separated rolandic alpha rhythm was located more posterior than correlates of the blindly separated beta rhythm. The maximum inverse correlation for the ‘TDSep rolandic beta rhythm’ was located in the precentral gyrus and that for the ‘TDSep rolandic alpha rhythm’ was located in the postcentral gyrus (Figure 32b). One model was calculated including three regressors: motor protocol, blindly separated rolandic alpha rhythm and blindly separated rolandic beta rhythm. After orthogonalization of the three regressors - to avoid ambiguity of the results [Andrade, et al., 1999] - fMRI responses to alpha and beta rolandic rhythms persist in pre- and postcentral areas, with the response to rolandic alpha shifting backwards to the posterior parietal cortex (Figure 32c).

These data are in agreement with previous MEG-studies in which reactive sources of rolandic beta rhythm were localized in MI and of rolandic alpha rhythm in SI [Salmelin, et al., 1995] during phasic motor activity [Salmelin and Hari, 1994b] and tactile stimulation [Cheyne, et al., 2003]. One should note that in intracortical recordings, both the rolandic alpha and beta rhythm are found in pre- and postcentral areas in man [Jasper and Andrews, 1938b] and in monkey [Rougeul, et al., 1979]. Thus, the respective association of the rolandic beta rhythm with motor cortex and the rolandic alpha with somatosensory cortex is probably not exclusive. Nevertheless, in these intracranial recordings, the maximal beta rhythm amplitude tends to be found more anterior and the alpha rhythm more posterior to the rolandic fissure. These findings are supported by our results. A recent study confirmed the findings of this work by modulating parametrically the strength of the post-movement beta rebound and showing BOLD correlates in the postcentral cortex [Parkes, et al., 2006].

7.2.4 During rest: different networks for rolandic alpha and beta rhythms with topographies similar to those reported by invasive cortical recordings.

Under 'rest' condition, maximal negative BOLD correlates of the rolandic beta rhythm are located in bilateral primary sensorimotor areas. Additionally a negatively correlating network of premotor areas (BAs 6, 8, 9) was identified. These findings are in good concordance with previous invasive animal studies which reported beta oscillations in primary sensorimotor cortex [Rougeul, et al., 1979] and the premotor area [MacKay and Mendonca, 1995a] during premovement maintenance behaviour [Brovelli, et al., 2004; Donoghue, et al., 1998; MacKay and Mendonca, 1995b; Sanes and Donoghue, 1993]. Electrocorticograms from exposed cortex in conscious resting patients revealed beta activity in the precentral gyrus and premotor areas 6-8, and to a lesser degree in the postcentral gyrus [Jasper and Penfield, 1949].

We found negative correlations of the rolandic alpha rhythm and the BOLD signal during rest predominantly in the posterior-inferior parietal cortex (BAs 39, 40) and the prefrontal cortex (BAs 8, 9) being in good concordance with findings from invasive human-electrocorticograms, which show alpha rhythmic activity (non-reactive to eyes opening/closing) predominantly in posterior parietal areas and to a lesser degree in the postcentral gyrus and frontal Brodmann's areas 8, 9, 45, 46.

These findings confirm that localized EEG signatures yield localized correlations in fMRI and that spontaneous (stimulus independent) fluctuations of rolandic rhythms can significantly influence the BOLD signal. Based on data obtained during a single experiment, the behavior of several synchronized brain networks can be assessed simultaneously.

7.2.5 Non-linear analyses

The relationship between the power of human background rhythms and hemodynamic signals as BOLD-fMRI is not necessarily linear as assumed in this study. However there is evidence that neuronal activation transfers mainly linear to the hemodynamic signal. Studies about the temporal linearity show that the relationship is linear for stimulation intervals down to 1-2 seconds [Boynton, et al., 1996; Wobst, et al., 2001]. For shorter intervals of neuronal activation changes non-linearities were observed. Since changes of

the power of spontaneous EEG rhythms can occur down to these intervals future analyses should consider the possibilities of non-linear effects.

The transformation of the amplitude of a neuronal activation to the hemodynamic signal strength is as well reported to be linear in a first approximation [Logothetis, et al., 2001]. However, animal studies demonstrated that the transfer function can be better approximated by a power [Devor, et al., 2003] or inverse sigmoid [Jones, et al., 2004] functions for a larger stimulation amplitude range.

Highly resolved optical recordings on rats have shown that the neurovascular transfer function is also non-local, i.e., the hemodynamic signal observed at a given location is a function of electrophysiological activity over a broader spatial region [Devor, et al., 2005]. These findings should be of lower impact for fMRI studies with spatial resolutions delivered by MR devices with a magnetic field strength of 1.5 T – 3 T.

Nevertheless, assuming a linear relationship between the power of human background rhythms and the fMRI BOLD response produces significant results as shown in this work. Still the statistics and differentiation of the results may be further improved by including the possibilities of non-linear coupling.

7.3 Functional Implications

For the background rhythms examined in this work different neuronal networks have been identified. The posterior alpha rhythm seems to be connected to thalamo-cortical pathways ending in visual areas. Focussing on rolandic rhythms two different neuronal networks were associated with the rolandic alpha and beta rhythms, indicating different functional significances of both rhythms for the rest as well as for the motor-task condition.

In addition to previous ‘mere’ electrophysiological studies, the simultaneous EEG-fMRI approach provides information on the metabolic/cerebral blood flow effects associated with the EEG-rhythms.

7.3.1 Where rhythms idle, cortex deactivates?

The functional role of human background rhythms is not yet clear. Posterior alpha rhythm and rolandic rhythms are frequently referred to as ‘idle rhythms’ indicating a ‘resting state’ of the respective (sensory) system [Adrian and Matthews, 1934; Pfurtscheller, 1992]. The simultaneous EEG-fMRI approach provides information about the hemodynamic state of

brain structures. With this approach, we were able to monitor hemodynamic changes associated with these rhythms. We found rhythm related decreases of the BOLD signal, indicating ‘deactivation’, in cortical areas which are known to exhibit these rhythms (for details see 7.2.1 and 7.2.3).

Decreased cortical metabolism / blood flow can be caused (1) by less excitatory drive or (2) arguably, by active inhibition. The relation between the BOLD signal and inhibition is not clear yet [Ritter and Villringer, 2002]. However, inhibition is often associated with decreased neuronal activity in downstream neuronal populations being accompanied by a BOLD signal decrease [Wenzel, et al., 2000]. EEG rhythms presumably depend on the balance between excitatory drive and inhibitory feedback as shown for instance by network modeling studies [Bartos, et al., 2002; Traub, et al., 1997]. The fMRI data in this work support the notion, that idling rhythms are an indicator of inhibited, less active cortical areas.

This finding is in line with results from transcranial-magnetic-stimulation (TMS) studies demonstrating a close correlation between motor cortex excitability and the power of rolandic rhythms: Motor responses evoked by TMS have been shown to be facilitated during event related desynchronization (ERD), i.e., during a decrease in rolandic rhythm strength up to 200 ms after somatosensory stimulation [Deletis, et al., 1992; Deuschl, et al., 1991; Hirashima and Yokota, 1997; Komori, et al., 1992; Maertens de Noordhout, et al., 1992; Rossini, et al., 1991; Terao, et al., 1995]. Reduced cortex excitability has been shown during event related synchronization (ERS) in the motor cortex i.e., an increased power of rolandic rhythms following 200 to 1000 ms after somatosensory stimulation [Chen, et al., 1999].

Positive BOLD responses, i.e. activations, were found for all three examined idling rhythms (posterior alpha, rolandic alpha and beta) in the cingulate gyrus (Figure 36) during eyes open condition and in five subjects during eyes closed condition in the study focusing on posterior alpha rhythm (see chapter 5.6). These results suggest that the cingulate gyrus plays a significant role for the generation or modulation of idling rhythms. The posterior cingulate and medial parietal cortex are known from PET studies to be activated during rest-conditions [Gusnard and Raichle, 2001]. With the feasibility of simultaneous measures of metabolism/hemodynamics and electrophysiology, these findings can be extended by the fact, that activity in this structure is correlated with the strength of idling rhythms.

7.3.2 Thalamus as generator of the posterior alpha rhythm

Electrophysiological findings suggest that neuronal networks between thalamus and the occipital cortex are responsible for synchronized posterior alpha oscillations [Creutzfeldt, 1975]. If so, one might expect correlations between local thalamic blood oxygenation and posterior alpha activity.

Indeed, in the interleaved EEG-fMRI study we found positive correlations between the BOLD-signal and posterior alpha-activity in the thalamus, but also in cerebrospinal-fluid cavities. Cardiac cycle and breathing associated vessel pulsations, cerebrospinal fluid movement, and tissue deformation are well known causes for MRI artifacts, which occur predominantly around ventricles, large vessels and cisterns [Dagli, et al., 1999; Windischberger, et al., 2002]. The cisternal BOLD signal changes reported here may be ascribed to such artifacts. By means of the advanced continuous EEG-fMRI approach we hoped to reduce these artifacts and to accentuate the thalamic signal. However, under these conditions, no positive correlations were found at all, not even in the thalamus or ventricles, given a statistical threshold of $p < 0.001$. At a lower statistical threshold of $p < 0.05$, positive correlations were found in the thalamus, the lateral ventricles (central part, temporal horn, occipital horn), in the third ventricle, and in the cisterna ambiens. Since the thalamus constitutes the lateral walls of the third ventricle and directly underlies the central part of the lateral ventricle, a possible thalamic signal cannot be unambiguously separated from ventricular artifacts. The (positive) thalamic activation pattern for the 24-28 Hz band was very similar to that for the alpha band, but was not present for the 3-6-Hz, 54-58-Hz and 34-38-Hz bands, respectively. The findings for the 24-28 Hz band might be indicative of an artificial origin of the BOLD signal in this region, but might also be ascribed to a harmonic of the alpha frequency. In conclusion, while our data provide some evidence for a thalamic activation positively associated with alpha activity, definite proof will be a matter for further validation studies e.g. by using ECG-triggered MRI-data-acquisition.

What do these results imply about the “generator” of the posterior alpha rhythm? It is known from intracerebral electrode recordings in dogs that alpha activity occurs not only in the occipital cortex but also in the thalamus, however with larger intracortical than thalamo-cortical coherences [Lopes da Silva, et al., 1973]. The lateral geniculate nucleus (constituting the caudal thalamus) was shown to have a small, although significant influence on cortico-cortical coherences; the pulvinar (posterior thalamus) has been shown

to have an even larger influence [Lopes da Silva, et al., 1980]. However, after mathematically ‘disconnecting’ thalamus through elimination of all intracortical coherences explainable by thalamic input, there was still an appreciable amount of cortico-cortical coherences. Thus, other factors than the thalamus must be responsible for the large values of intracortical coherences. A persisting reactive posterior alpha rhythm (the alpha rhythm was attenuated by forced eye-opening) in a 57-year-old man with infarction of the ventral midbrain and the dorsomedial thalamus bilaterally [Yazawa, et al., 2001] lends support to this theory. On the other hand, a study investigating the effect of thalamic arteriovenous malformations on the EEG pattern showed that lesions in the posterior thalamus result in alpha-rhythm suppression, including its total elimination [Lukashevich and Sazonova, 1996]. Interestingly, the same group found alpha-rhythm suppression to a similar extent also with lesions in the body of the caudate nucleus [Sazonova and Lukashevich, 1995]. Certainly cerebral lesions in general might lead to a radical change of the whole physiological state responsible for the generation of the alpha-rhythm and are thus unsuitable for inferring the locus of possible generators. Considering the many unsuccessful efforts to find a single generator for the posterior alpha rhythm, the assumption of a ‘diffuse and distributed’ alpha system was proposed [Basar, et al., 1997]. Recently, Hughes et al. [Hughes, et al., 2004] proposed oscillations induced by activation of the metabotropic glutamate receptor mGluR1a as a mechanism for the promotion of EEG alpha and theta by the lateral geniculate. However, it is not yet conclusively known to which degree intracortical synchronization mechanisms participate in the generation or selection of the alpha rhythm [Lopes da Silva, et al., 1997].

There are some previous results on metabolic and hemodynamic changes in the thalamus associated with alpha activity. The PET study by Sadato et al. reported positive CBF responses to posterior alpha activity in the pons and midbrain on the left, the amygdala, thalamus, basal prefrontal cortex, insula and dorsal premotor cortex on the right and the hypothalamus [Sadato, et al., 1998]. In this study the subjects had their eyes open watching a static picture and being exposed to music in 8 out of 10 PET-scans. Another PET study revealed as well corticothalamic loops by pharmacologically suppressing alpha activity by lorazepam [Schreckenberger, et al., 2004]. The interleaved EEG-fMRI study on spontaneous posterior alpha rhythm modulations by Goldman et al. revealed positive correlations between BOLD-signal and alpha-power in the thalamus and insula in four subjects [Goldman, et al., 2002], a finding similar to the results in this study. Feige et al.

report thalamic activations which are related to posterior alpha rhythm modulations induced by eye lid closure in an EEG-fMRI study [Feige, et al., 2005]. Contrary to these results, an alpha-related decrease of thalamic glucose metabolism was reported in a PET study, in which glucose metabolism was monitored during 30 minutes of an eyes-open/eyes-closed task (reversing every 3 minutes) [Lindgren, et al., 1999]. Here it remains unclear whether changes are related to the posterior alpha power or to visual stimulation, which interacts closely with alpha activity.

In conclusion, all of the mentioned indirect neuroimaging studies did not reveal a single, exclusive posterior alpha generator. As shown in this work while examining posterior alpha rhythm in eyes open condition (see paragraph 5.6 for details) the cingulate gyrus seems to play a significant role for the generation or modulation of the posterior alpha rhythm as well.

In future attempts, one should consider that the proportion of neurons involved in generation or modulation of the cortical rhythms might be relatively small [Hari, et al., 1997] and therefore be associated with only subtle metabolic and hemodynamic changes. High-field MRI systems might be an appropriate approach to address this issue. However, imaging artifacts are even more of a problem at higher fields. Reducing these artifacts by appropriate methods, as e.g. retrospective gating [Hu, et al., 1995], frequency band-rejection [Biswal, et al., 1996], inclusion of Fourier terms of the cardiac model within the general linear model in fMRI analysis [Dagli, et al., 1999] or the use of specialized fMRI sequences as described in this work will be necessary.

7.3.3 Motor-task versus rest: Different dynamics - different networks

Rolandic rhythms are suppressed during sensorimotor task and reappear after cessation of the movement [Cheyne, et al., 2003]. This data of this work here show significant inverse correlations between rolandic alpha and beta regressors and the BOLD signal in the post- and precentral gyrus respectively (Figure 32a and Figure 32b), i.e. BOLD correlates of movement related dynamics of the rolandic rhythms are strongest in these cortical structures.

Orthogonalization removes the on-off dichotomy of the motor-protocol from the rhythm-regressors, i.e. spontaneous amplitude fluctuations now become dominant features of the regressors. Whereas for the rolandic beta rhythm a maximum inverse fMRI correlate

persists in the right precentral gyrus after orthogonalization, maximum inverse fMRI correlates of the rolandic alpha rhythm shift to the more posterior parietal Brodmann's areas 7 and 40, adjacent to the postcentral sulcus (Figure 32c). These results are in concordance with results from the rest condition: Whereas the maximum inverse BOLD response for the rolandic beta rhythm was found in the primary sensorimotor cortex, maximum inverse BOLD correlates of the rolandic alpha rhythm were located in posterior parietal association areas Brodmann's areas 40 and 39 (Figure 36b, left). The topographic overlap in Brodmann's area 40 between the negative BOLD response to the orthogonalized rolandic alpha rhythm during motor task and the negative BOLD response to the rolandic alpha rhythm during rest can probably be ascribed to the fact, that orthogonalization removes motor-induced suppression periods and leaves spontaneous amplitude fluctuations which are also the dominant features during the rest condition.

The data indicate, that motor-task related modulations of the rolandic-rhythms' strength have inverse fMRI correlates in the primary motor (rolandic beta) and primary somatosensory (rolandic alpha) cortex (Figure 32a and Figure 32b) whereas spontaneous power fluctuations during rest have inverse fMRI correlates in a sensorimotor-premotor network for the rolandic beta rhythms and a prefrontal-parietal sensory-integration network for the rolandic alpha rhythm (Figure 36a and Figure 36b).

One can conclude, that (1) sensorimotor-task related modulations of cortical activity, as expressed by rolandic rhythms' strength, occur predominantly in the primary sensorimotor areas. (2) Modulations of cortical activity during rest, expressed by spontaneous fluctuations of rolandic beta and alpha rhythms, occur predominantly in a motor-premotor network (rolandic beta) and a multisensory-integration network (rolandic alpha).

7.3.4 Functional significance of rolandic rhythms

It has been proposed, that voluntary movement depends on a 'cortico-peripheral-cortical sensorimotor loop', i.e. the excitability of efferent cortical motor pathways is controlled by multisensory afferents [Favorov, et al., 1988]. This loop is assumed to be supported by oscillatory neuronal activity [MacKay and Mendonca, 1995b]. This theory implies that network oscillations facilitate processing of information in the sensorimotor system. Rhythmic activity in this loop during the wait states might prepare the human to react more quickly or forcefully to anticipated events.

The data presented here are supportive for this theory. Two networks, which are related to rolandic EEG rhythms, were identified here. One comprises predominantly motor-associated cortical areas the other includes prefrontal and parietal areas which are significant for multimodal-sensory integration and attention. Though, the structures of the identified networks do not necessarily exhibit all synchronous rhythms, the dynamics of each network follows the temporal behavior of the rolandic rhythms, indicating a close functional relation.

7.3.4.1 Motor-maintenance network related to the rolandic beta-rhythm

Rolandic beta rhythm strength during a motor task inversely correlates with the BOLD signal in the primary sensorimotor cortex, premotor and supplementary motor areas, thalamus, basal ganglia and cerebellum. During continuous rest rolandic beta rhythm strength inversely correlates with the BOLD signal in the primary sensorimotor cortex and premotor areas. Thus, during motor task and during rest, fMRI correlates the rolandic beta-rhythm can be found exclusively in structures with primary significance for motor processing. The fact, that greater rhythm power is associated with increased motor-cortex ‘deactivation’ indicates that the rolandic beta rhythm is involved in the prevention of motor activities, including preparation and execution. These results support the theory of a motor-maintenance network related to the rolandic beta-rhythm [Favorov, et al., 1988].

Positive correlations between the BOLD signal and the rolandic beta rhythm during motor-task occur in fronto-parietal areas, which are not present under continuous rest condition or after orthogonalization of the motor-task-rolandic-beta regressor. This very likely represents an expectation-network which is ‘activated’ during the rest period in anticipation for the next ‘start’ command. The posterior parietal cortex, Brodmann’s area 5, bilaterally (the global maximum in our study) has been shown previously to be activated during expectation of an event [MacKay and Crammond, 1987]. Gusnard et al. propose an involvement of these areas in self-referential mental activity that becomes attenuated during an attention demanding motor task [Gusnard, et al., 2001].

7.3.4.2 Self-monitoring network related to the rolandic alpha rhythm

The rolandic alpha rhythm during motor-task showed fMRI correlates exclusively in the somatosensory system: thalamus, SII and SI (Figure 34b). This indicates a close association between the rolandic alpha rhythm and the somatosensory system. Suppression

of the rolandic alpha rhythm during motor-execution seems to reflect increased excitatory drive paralleled by less inhibitory activity in the respective somatosensory structures.

During rest rolandic-alpha rhythm related ‘deactivations’ were found in a parietal-frontal network. Neurophysiological studies suggest that in both frontal and parietal cortex eye and hand position signals dynamically interact to built-up the cortical representation of spatial frames of reference [Rizzolatti, et al., 1998]. Parietal cortex can act as a recurrent network where gain mechanisms might select the relative contribution of directional eye and hand signals to neural activity, by weighting them in a flexible way and on the basis of task demands. Particularly, the posterior parietal cortex is viewed as an area important for sensorimotor integration and for the forming of intentions [Andersen and Buneo, 2002]. Anatomical studies [Marconi, et al., 2001] suggest, that information originating from extrastriate, parietal and frontal areas can be addressed to other parietal areas, and to premotor cortex as well, by virtue of local intraparietal and long parieto-frontal connections.

Positive fMRI correlates of the rolandic alpha rhythm during rest were found in posterior medial structures, particularly posterior cingulum, precuneus and pericentral lobule (BA 5). Besides that these areas are known to show task-independent decreases from the baseline during the performance of goal-directed action [Gusnard and Raichle, 2001], they have the highest level of glucose use in the human cerebral cortex [Harley and Bielajew, 1992]. The role of the precuneus has been suggested to be mental imagery at the retrieval stage of episodic memory [Fletcher, et al., 1995; Shallice, et al., 1994]. Thus, an increase of rolandic alpha power is paralleled by ‘deactivation’ of the externally directed self referential – attentional network and ‘activation’ of an internally directed mental-imagery network.

Synchronized alpha activity might favor the maintenance of immobility as well as the fixation of attention on a non-somatosensory target by temporarily blocking association areas.

The data of this work substantiate the hypothesis that the rolandic beta rhythm favors the maintenance of immobility (deactivation of motor-cortex) and the rolandic alpha rhythm favors the fixation of attention on a non-somatosensory target by temporarily blocking association areas (deactivation of fronto-parietal cortex).

7.3.5 Implications on the term baseline in fMRI

The results of this work show that spontaneous neuronal activity interacts with hemodynamic measures as the fMRI BOLD signal. This provides a new tool for studies in functional neuroimaging. Implications of unknown baseline fluctuations have been described [Gusnard and Raichle, 2001] and it has been shown that the use of ill-defined baseline conditions can lead to ambiguous results, e. g. reverse of the sign of activity [Stark and Squire, 2001]. Unexplained variance of neuroimaging signals as BOLD-fMRI could thus be explained by spontaneous background rhythms and should be recorded simultaneously and included in the analysis [Arthurs and Boniface, 2002]. An fMRI study in which subjects opened and closed their eyes in complete darkness showed unintuitive results, i. e. a deactivation when eyes were closed [Marx, et al., 2003]. This could be explained by an inverse Berger effect (more posterior alpha activity with eye opening) in diminishing wakefulness in darkness [Henning, et al., 2006]. Additionally, there is evidence for interactions between the neuronal background activity and the amplitude of the visual evoked response on the neuronal as well as on the metabolic level. Electrophysiological studies investigating the relationship between pre-stimulus EEG power and evoked responses indicated positive correlations in the visual cortex of humans [Brandt, et al., 1991] and cats [Arieli, et al., 1996]. Negative correlations in humans have been found between the amplitudes of motor evoked responses (MEPs) and spectral alpha content [Rossini, et al., 1991], as well as between the alpha and the beta band EEG activity and auditory evoked responses (AER) [Rahn and Basar, 1993]. In terms of metabolism it has been reported that the same stimulation induced different increments of cerebral metabolic rate of oxygen (CMRO₂) from each of two different baseline conditions, so that approximately the same final values were reached [Hyder, et al., 2002]. This suggests baseline fluctuations to be relevant in functional imaging studies. Simultaneous fMRI-EEG measurements seem an appropriate tool to address this issue.

8 Conclusion

The data provided by this thesis show that imaging of brain rhythms can be achieved by simultaneous EEG-fMRI recordings. This methodology was developed further by implementing an adapted MR sequence and the EEG-fMRI signal quality was confirmed by means of visual evoked potentials. Together with the post processing methods applied in this work, simultaneous EEG-fMRI recordings can thus provide valuable information about the neuronal basis of brain rhythms and their regional hemodynamic correlates. The data further substantiate the hypothesis that ‘idling’ rhythms indicate distinct deactivated sensory cortical areas. Increased power of all examined rhythms was associated with negative BOLD signal in sensory cortical areas, indicating less energy consumption in those areas with higher synchronicity. The posterior alpha or so-called Berger rhythm is coupled inversely to the hemodynamics in primary visual areas, whereas rolandic alpha and beta rhythm could be localized to somatomotor areas. Different networks were found for rolandic alpha and beta rhythms. The rolandic beta rhythm is more associated with a motor-network whereas the rolandic alpha rhythm is more associated with a sensory and association network which represents a fundamental characteristic of the sensorimotor system. The rolandic oscillations may bind sensorimotor areas into a functional loop during pre-movement motor maintenance behaviour [Brovelli, et al., 2004]. Furthermore thalamic and cingulate structures were shown to be possible generative or modulatory structures for the brain rhythms examined in this study.

The experimental data obtained in this work suggest that the inverse correlation of an ‘idling’ rhythm’s strength with the metabolism in ‘its cortical areas’, and the positive correlation with cingulate or thalamic areas are both general organizational principles. The notion of a default mode of the brain [Gusnard, et al., 2001] may perhaps be further subdivided into different networks with a “default mode”, each of them electrophysiologically defined by its “idle rhythm”.

9 Outlook

In this thesis the putative localization, generation and functional implications of prominent human background rhythms were characterized with simultaneous EEG-fMRI recordings. The methodological advances and physiological findings of this study outline some imminent future applications in neuroimaging research.

The results presented in this work rely on examinations of healthy humans. Alterations of background rhythms have been characterized in a broad spectrum of neuropsychiatric conditions. One such condition is hepatic encephalopathy, resulting from failure in the excretion of the toxic ammonium from the hepatic metabolism. Here, alpha and beta activities show a spatial redistribution, i. e. a frontalisation [Kullmann, et al., 2001]. The methodology developed in this work could help to diagnose and to examine any specific effects on the central nervous system associated with diseases of this type.

Similarly, research on epileptic EEG features should be undertaken, going beyond the assessment and hemodynamically guided localisation of spike-wave phenomena [Detre, 2004; Hamandi, et al., 2004; Lemieux, 2004; Salek-Haddadi, et al., 2003]. One interesting experimental paradigm would be to investigate explicitly the pattern of alterations of frequency and amplitude features preceding the onset of manifest generalized spike-wave and seizure activity. This may result in a set of stable EEG features and hemodynamic correlates predictive for onset of seizures in the respective patient. This could possibly allow for the future use of these features in a therapeutic sense, i.e. defining a threshold condition for feedback-sensitive variants of vagal nerve [Murphy and Patil, 2005] or deep brain stimulation [Garcia, et al., 2005].

A further perspective is the progression of data fusion algorithms. EEG and fMRI are supposed to be direct or indirect measures of the same underlying neuronal events. So far both measures are highly processed and at the end features of each signal are simply correlated. Integrative forward modelling could overcome shortcomings of current analysis methods, mainly the limitation with inferring causality via correlation. Hierarchical bayesian modelling was proposed to explain simultaneously measured EEG and fMRI signal in a generative forward model [Friston, 2005; Friston, et al., 2003] as well as 'Independent Component Analysis' [Calhoun, et al., 2005; Eichele, et al., 2006], and 'Parallel Factor Analysis' [Martinez-Montes, et al., 2004; Valdes-Sosa, 2004].

Extensions of the current work are naturally all other rhythms both in the lower and the higher frequency range. In a cognitive neuroscience framework these rhythms, more precisely, paradigm induced oscillations are of special interest [Fell, et al., 2003; Klimesch, 1999; Singer, 2001]. Gamma oscillations appear to be involved in binding sensory inputs and higher mental activities like perception and consciousness and are therefore of great interest to understand higher functionalities of the brain [Eckhorn, et al., 1988; Fries, et al., 2001; Gray, et al., 1989; Tallon-Baudry, et al., 2001]. Relatively newly discovered phenomena are the so-called high-frequency oscillations. High-frequency oscillations superimpose on an early component of the somatosensory evoked potential and have frequencies around 600 Hz [Baker, et al., 2003]. High-frequency oscillations are supposed to be generated directly by spike bursts instead of post-synaptic potentials as other EEG signals origin from. So far methodical limitations have restricted research on these oscillations to mere electrophysiological studies. The approach introduced here could shed light into these interesting phenomena.

One aim of EEG/ERP-fMRI research should be simply to re-assess and re-examine in detail seminal psychophysiological experiments from the last five decades [Naaanen, et al., 1978; Sokolov, 1963; Sutton, et al., 1965]. Replication studies with combined methods, principally including the traditional peripheral psychophysiological measures such as electrodermal and cardio-respiratory activity allows to empirically assess and localize many of the basic model elements and theoretical foundations of modern cognitive neuroscience and thus neuroimaging. Exemplarily, assessment of the various expressions of the principled unitary Orienting Response [Ranganath and Rainer, 2003; Sokolov, 1963] such as alpha desynchronization and N1 response decrement in habituation, learning or memory processes will firstly give topographical indexes of the mechanism components, and may enhance the ability to update these models and thus our concepts and understanding of the brain-behavior relationship.

The field of studies examining the 'traditional' event related potential components (such as N1, MMN, P300) seems to transfer from making inferences from averaged potentials towards the analysis of single events, so called single trial analysis [Quian Quiroga and Garcia, 2003; Spencer, 2005]. This is due to the fact that beyond the invariable and averaged brain response to stimulation there are spontaneous or induced brain activations that vary in time or over trials. First attempts to characterize these time-variant features were made in this and others work on spontaneous fluctuations of inherent brain signals

[Czisch, et al., 2004; Goldman, et al., 2002; Laufs, et al., 2003a; Moosmann, et al., 2003]. Systematically induced single-trial variations of stimulation events could reveal brain mechanisms associated with such processes as learning and memory. A recent study combined single-trial event related potentials with fMRI to show pattern learning processes on a milli-second time scale [Eichele, et al., 2006]. Characterisation of trial-to-trial variability in this fashion could be of high impact in patient groups where higher mental processes are altered, as for example in schizophrenic patients [Ford, et al., 1994; Javitt, et al., 1993; Javitt, et al., 1996; Shelley, et al., 1991].

10 References

- Adrian, E.D. and Matthews, B.H. (1934): The Berger rhythm: potential changes from the occipital lobes in man, *Brain* (vol. 57), pp. 355-385.
- Allen, P.J.; Josephs, O. and Turner, R. (2000): A method for removing imaging artifact from continuous EEG recorded during functional MRI, *Neuroimage* (vol. 12), No. 2, pp. 230-239.
- Allen, P.J.; Polizzi, G.; Krakow, K.; Fish, D.R. and Lemieux, L. (1998): Identification of EEG events in the MR scanner: the problem of pulse artifact and a method for its subtraction, *Neuroimage* (vol. 8), No. 3, pp. 229-239.
- Anami, K.; Mori, T.; Tanaka, F.; Kawagoe, Y.; Okamoto, J.; Yarita, M.; Ohnishi, T.; Yumoto, M.; Matsuda, H. and Saitoh, O. (2003): Stepping stone sampling for retrieving artifact-free electroencephalogram during functional magnetic resonance imaging, *Neuroimage* (vol. 19), No. 2, pp. 281-295.
- Anami, K.; Saitoh, O. and Yumoto, M. (2002): Reduction of ballistocardiogram with a vacuum head-fixating system during simultaneous fMRI and multi-channel monopolar EEG recording, *Recent Adv Hum Brain Mapp* (vol. 1232), pp. 427-431.
- Andersen, P.; Andersson, S. A. and Lomo, T. (1968): Thalamo-cortical relations during spontaneous barbiturate spindles, *Electroencephalogr Clin Neurophysiol* (vol. 24), No. 1, p. 90.
- Andersen, R. A. and Buneo, C. A. (2002): Intentional maps in posterior parietal cortex, *Annu Rev Neurosci* (vol. 25), pp. 189-220.
- Andrade, A.; Paradis, A.L.; Rouquette, S. and Poline, J.B. (1999): Ambiguous results in functional neuroimaging data analysis due to covariate correlation, *Neuroimage* (vol. 10), No. 4, pp. 483-486.
- Arieli, A.; Sterkin, A.; Grinvald, A. and Aertsen, A. (1996): Dynamics of ongoing activity: explanation of the large variability in evoked cortical responses, *Science* (vol. 273), No. 5283, pp. 1868-1871.
- Arroyo, S.; Lesser, R.P.; Gordon, B.; Uematsu, S.; Jackson, D. and Webber, R. (1993): Functional significance of the mu rhythm of human cortex: an electrophysiologic study with subdural electrodes, *Electroencephalogr Clin Neurophysiol* (vol. 87), No. 3, pp. 76-87.
- Arthurs, O. J. and Boniface, S. (2002): How well do we understand the neural origins of the fMRI BOLD signal?, *Trends Neurosci* (vol. 25), No. 1, pp. 27-31.
- Arthurs, O. J. and Boniface, S. J. (2003): What aspect of the fMRI BOLD signal best reflects the underlying electrophysiology in human somatosensory cortex?, *Clin Neurophysiol* (vol. 114), No. 7, pp. 1203-9.
- Ashburner, J. and Friston, K. J. (1999): Nonlinear spatial normalization using basis functions, *Hum Brain Mapp* (vol. 7), No. 4, pp. 254-66.
- Astafiev, S.V.; Stanley, C.M.; Shulman, G.L. and Corbetta, M. (2004): Extrastriate body area in human occipital cortex responds to the performance of motor actions, *Nat Neurosci* (vol. 7), No. 5, pp. 542-548.
- Babiloni, F.; Babiloni, C.; Carducci, F.; Del Gratta, C.; Romani, G.L.; Rossini, P.M. and Cincotti, F. (2002): Cortical source estimate of combined high resolution EEG and fMRI data related to voluntary movements, *Methods Inf Med* (vol. 41), No. 5, pp. 443-450.
- Baker, S. N.; Curio, G. and Lemon, R. N. (2003): EEG oscillations at 600 Hz are macroscopic markers for cortical spike bursts, *J Physiol* (vol. 550), No. Pt 2, pp. 529-34.
- Bartos, M.; Vida, I.; Frotscher, M.; Meyer, A.; Monyer, H.; Geiger, J.R. and Jonas, P. (2002): Fast synaptic inhibition promotes synchronized gamma oscillations in hippocampal interneuron networks, *Proc Natl Acad Sci USA* (vol. 99), No. 20, pp. 13222-13227.
- Basar, E.; Schurmann, M.; Basar-Eroglu, C. and Karakas, S. (1997): Alpha oscillations in brain functioning: an integrative theory, *Int J Psychophysiol* (vol. 26), No. 1-3, pp. 5-29.
- Becker, R.; Ritter, P.; Moosmann, M. and Villringer, A. (2005): Visual evoked potentials recovered from fMRI scan periods, *Hum Brain Mapp* (vol. 26), No. 3, pp. 221-230.
- Bell, A. J. and Sejnowski, T. J. (1995): An information-maximization approach to blind separation and blind deconvolution, *Neural Comput* (vol. 7), No. 6, pp. 1129-59.
- Benar, C. G.; Grova, C.; Kobayashi, E.; Bagshaw, A. P.; Aghakhani, Y.; Dubeau, F. and Gotman, J. (2006): EEG-fMRI of epileptic spikes: Concordance with EEG source localization and intracranial EEG, *Neuroimage* (vol. 30), No. 4, pp. 1161-70.

- Benar, C.G.; Gross, D.W.; Wang, Y.; Petre, V.; Pike, B.; Dubeau, F. and Gotman, J. (2002): The BOLD response to interictal epileptiform discharges, *Neuroimage* (vol. 17), No. 3, pp. 1182-1192.
- Berger, H. (1929): Über das Elektroenkephalogramm des Menschen, *Arch Psychiat Nervenkr* (vol. 87), pp. 527-570.
- Berger, H. (1933): Über das Elektroenkephalogramm des Menschen, *Arch Psychiat Nervenkr* (vol. 99), pp. 555-574.
- Berger, H. (1936): Über das Elektroenkephalogramm des Menschen, *Arch Psychiat Nervenkr* (vol. 104), pp. 678-689.
- Biswal, B.; DeYoe, A.E. and Hyde, J.S. (1996): Reduction of physiological fluctuations in fMRI using digital filters, *Magn Reson Med* (vol. 35), No. 1, pp. 107-113.
- Bonmassar, G.; Anami, K.; Ives, J. and Belliveau, J.W. (1999): Visual evoked potential (VEP) measured by simultaneous 64-channel EEG and 3T fMRI, *Neuroreport* (vol. 10), No. 9, pp. 1893-1897.
- Bonmassar, G.; Hadjikhani, N.; Ives, J.R.; Hinton, D. and Belliveau, J.W. (2001a): Influence of EEG electrodes on the BOLD fMRI signal, *Hum Brain Mapp* (vol. 14), No. 2, pp. 108-115.
- Bonmassar, G.; Purdon, P.L.; Jaaskelainen, I.P.; Chiappa, K.; Solo, V.; Brown, E.N. and Belliveau, J.W. (2002): Motion and ballistocardiogram artifact removal for interleaved recording of EEG and EPs during MRI, *Neuroimage* (vol. 16), No. 4, pp. 1127-1141.
- Bonmassar, G.; Schwartz, D.P.; Liu, A.K.; Kwong, K.K.; Dale, A.M. and Belliveau, J.W. (2001b): Spatiotemporal brain imaging of visual-evoked activity using interleaved EEG and fMRI recordings, *Neuroimage* (vol. 13), No. 6 Pt 1, pp. 1035-1043.
- Boynton, G. M.; Engel, S. A.; Glover, G. H. and Heeger, D. J. (1996): Linear systems analysis of functional magnetic resonance imaging in human V1, *J Neurosci* (vol. 16), No. 13, pp. 4207-21.
- Brandt, M.E.; Jansen, B.H. and Carbonari, J.P. (1991): Pre-stimulus spectral EEG patterns and the visual evoked response, *Electroencephalogr Clin Neurophysiol* (vol. 80), No. 1, pp. 16-20.
- Brechet, R. and Lecasble, R. (1965): Reactivity of mu-rhythm to flicker., *Electroencephalogr Clin Neurophysiol* (vol. 18), pp. 721-722.
- Brett, M. (1999): Thresholding with Random Field Theory: <http://imaging.mrc-cbu.cam.ac.uk/imaging/PrinciplesMultipleComparisons>.
- Brett, M.; Johnsrude, I. S. and Owen, A. M. (2002): The problem of functional localization in the human brain, *Nat Rev Neurosci* (vol. 3), No. 3, pp. 243-9.
- Brinker, G.; Bock, C.; Busch, E.; Krep, H.; Hossmann, K. A. and Hoehn-Berlage, M. (1999): Simultaneous recording of evoked potentials and T2*-weighted MR images during somatosensory stimulation of rat, *Magn Reson Med* (vol. 41), No. 3, pp. 469-73.
- Brovelli, A.; Ding, M.; Ledberg, A.; Chen, Y.; Nakamura, R. and Bressler, S.L. (2004): Beta oscillations in a large-scale sensorimotor cortical network: Directional influences revealed by Granger causality, *Proc Natl Acad Sci USA* (vol. 101), No. 26, pp. 9849-9854.
- Buxton, R. B.; Uludag, K.; Dubowitz, D. J. and Liu, T. T. (2004): Modeling the hemodynamic response to brain activation, *Neuroimage* (vol. 23 Suppl 1), pp. S220-33.
- Calhoun, V. D.; Adali, T.; Pearlson, G. and Kiehl, K. A. (2005): Neuronal chronometry of target detection: Fusion of hemodynamic and event-related potential data, *Neuroimage* (vol. 30), No. 2, pp. 544-53.
- Caton, R. (1875): The electrical currents of the brain, *British Medical Journal* (vol. 2), p. 278.
- Chapman, R.M.; Ilmoniemi, R.J.; Barbanera, S. and Romani, G.L. (1984): Selective localization of alpha brain activity with neuromagnetic measurements, *Electroencephalogr Clin Neurophysiol* (vol. 58), No. 6, pp. 569-572.
- Chawla, D.; Lumer, E.D. and Friston, K.J. (1999): The relationship between synchronization among neuronal populations and their mean activity levels, *Neural Comput* (vol. 11), No. 6, pp. 1389-1411.
- Chen, R.; Corwell, B. and Hallett, M. (1999): Modulation of motor cortex excitability by median nerve and digit stimulation, *Exp Brain Res* (vol. 129), No. 1, pp. 77-86.
- Cheyne, D.; Gaetz, W.; Garnero, L.; Lachaux, J.P.; Ducorps, A.; Schwartz, D. and Varela, F.J. (2003): Neuromagnetic imaging of cortical oscillations accompanying tactile stimulation, *Brain Res Cogn Brain Res* (vol. 17), No. 3, pp. 599-611.
- Christmann, C.; Ruf, M.; Braus, D.F. and Flor, H. (2002): Simultaneous electroencephalography and functional magnetic resonance imaging of primary and secondary somatosensory cortex in humans after electrical stimulation, *Neurosci Lett* (vol. 333), No. 1, pp. 69-73.

- Collins, D. L. (1994): 3D Model-Based Segmentation of Individual Brain Structures from Magnetic Resonance Imaging, Mc Gill University.
- Creutzfeldt, O. and Struck, G. (1962): Neurophysiology and morphology of the chronically isolated cortical islet in the cat: brain potentials and neuron activity of an isolated nerve cell population without afferent fibers, *Arch Psychiatr Nervenkr Z Gesamte Neurol Psychiatr* (vol. 203), pp. 708-31.
- Creutzfeldt, O.D. (1975): Neurophysiological Correlates of Different Functional States of the Brain, Ingvar, D.H.& Lassen, N.A., *Brain Work. The Coupling of Function, Metabolism and Blood Flow in the Brain* pp. 21-46, Munksgaard, Copenhagen, Denmark.
- Czisch, M.; Wehrle, R.; Kaufmann, C.; Wetter, T. C.; Holsboer, F.; Pollmacher, T. and Auer, D. P. (2004): Functional MRI during sleep: BOLD signal decreases and their electrophysiological correlates, *Eur J Neurosci* (vol. 20), No. 2, pp. 566-74.
- Czisch, M.; Wetter, T.C.; Kaufmann, C.; Pollmacher, T.; Holsboer, F. and Auer, D.P. (2002): Altered Processing of Acoustic Stimuli during Sleep: Reduced Auditory Activation and Visual Deactivation Detected by a Combined fMRI/EEG Study, *Neuroimage* (vol. 16), No. 1, pp. 251-258.
- Dagli, M.S.; Ingeholm, J.E. and Haxby, J.V. (1999): Localization of cardiac-induced signal change in fMRI, *Neuroimage* (vol. 9), No. 4, pp. 407-415.
- Dale, A.M.; Liu, A.K.; Fischl, B.R.; Buckner, R.L.; Belliveau, J.W.; Lewine, J.D. and Halgren, E. (2000): Dynamic statistical parametric mapping: combining fMRI and MEG for high-resolution imaging of cortical activity, *Neuron* (vol. 26), No. 1, pp. 55-67.
- Daubechies, I. (1990): The wavelet transform time-frequency localization and signal analysis, *IEEE Trans Inform Theory* (vol. 36), pp. 961-1004.
- Davidson, R.J.; Jackson, D.C. and Larson, C.L. (2000): Human electroencephalography, *Handbook of psychophysiology* pp. 27-56, Cambridge University Press, Cambridge.
- Deletis, V.; Schild, J.H.; Beric, A. and Dimitrijevic, M.R. (1992): Facilitation of motor evoked potentials by somatosensory afferent stimulation, *Electroencephalogr Clin Neurophysiol* (vol. 85), No. 5, pp. 302-310.
- Detre, J. A. (2004): fMRI: applications in epilepsy, *Epilepsia* (vol. 45 Suppl 4), pp. 26-31.
- Deuschl, G.; Michels, R.; Berardelli, A.; Schenck, E.; Inghilleri, M. and Lucking, C.H. (1991): Effects of electric and magnetic transcranial stimulation on long latency reflexes, *Exp Brain Res* (vol. 83), No. 2, pp. 403-410.
- Devor, A.; Dunn, A. K.; Andermann, M. L.; Ulbert, I.; Boas, D. A. and Dale, A. M. (2003): Coupling of total hemoglobin concentration, oxygenation, and neural activity in rat somatosensory cortex, *Neuron* (vol. 39), No. 2, pp. 353-9.
- Devor, A.; Ulbert, I.; Dunn, A. K.; Narayanan, S. N.; Jones, S. R.; Andermann, M. L.; Boas, D. A. and Dale, A. M. (2005): Coupling of the cortical hemodynamic response to cortical and thalamic neuronal activity, *Proc Natl Acad Sci U S A* (vol. 102), No. 10, pp. 3822-7.
- Donoghue, J.P.; Sanes, J.N.; Hatsopoulos, N.G. and Gaal, G. (1998): Neural discharge and local field potential oscillations in primate motor cortex during voluntary movements, *J Neurophysiol* (vol. 79), No. 1, pp. 159-173.
- Dustman, R. E.; Shearer, D. E. and Emmerson, R. Y. (1999): Life-span changes in EEG spectral amplitude, amplitude variability and mean frequency, *Clin Neurophysiol* (vol. 110), No. 8, pp. 1399-409.
- Eckhorn, R.; Bauer, R.; Jordan, W.; Brosch, M.; Kruse, W.; Munk, M. and Reitboeck, H. J. (1988): Coherent oscillations: a mechanism of feature linking in the visual cortex? Multiple electrode and correlation analyses in the cat, *Biol Cybern* (vol. 60), No. 2, pp. 121-30.
- Eichele, T.; Moosmann, M.; Calhoun, V.D.; Specht, K.; Nordby, H. and Hugdahl, K. (2006): Joint ICA of simultaneous single trial ERP-fMRI, *Neuroimage* (vol. 32 Suppl 1), p. S92.
- Faraday, M. (1832): Experimental Researches in Electricity, *Phil Trans* (vol. CXXII), pp. 125-62.
- Favorov, O.; Sakamoto, T. and Asanuma, H. (1988): Functional role of corticoperipheral loop circuits during voluntary movements in the monkey: a preferential bias theory, *J Neurosci* (vol. 8), No. 9, pp. 3266-3277.
- Feige, B.; Scheffler, K.; Esposito, F.; Di Salle, F.; Hennig, J. and Seifritz, E. (2005): Cortical and subcortical correlates of electroencephalographic alpha rhythm modulation, *J Neurophysiol* (vol. 93), No. 5, pp. 2864-72.

- Felblinger, J.; Slotboom, J.; Kreis, R.; Jung, B. and Boesch, C. (1999): Restoration of electrophysiological signals distorted by inductive effects of magnetic field gradients during MR sequences, *Magn Reson Med* (vol. 41), No. 4, pp. 715-721.
- Fell, J.; Fernandez, G.; Klaver, P.; Elger, C. E. and Fries, P. (2003): Is synchronized neuronal gamma activity relevant for selective attention?, *Brain Res Brain Res Rev* (vol. 42), No. 3, pp. 265-72.
- Fletcher, P.C.; Frith, C.D.; Baker, S.C.; Shallice, T.; Frackowiak, R.S. and Dolan, R.J. (1995): The mind's eye--precuneus activation in memory-related imagery, *Neuroimage* (vol. 2), No. 3, pp. 195-200.
- Ford, J. M.; White, P.; Lim, K. O. and Pfefferbaum, A. (1994): Schizophrenics have fewer and smaller P300s: a single-trial analysis, *Biol Psychiatry* (vol. 35), No. 2, pp. 96-103.
- Frahm, J.; Bruhn, H.; Merboldt, K.D. and Hancicke, W. (1992): Dynamic MR imaging of human brain oxygenation during rest and photic stimulation, *J Magn Reson Imaging* (vol. 2), pp. 501-505.
- Fries, P.; Reynolds, J. H.; Rorie, A. E. and Desimone, R. (2001): Modulation of oscillatory neuronal synchronization by selective visual attention, *Science* (vol. 291), No. 5508, pp. 1560-3.
- Friston, K. (2005): A theory of cortical responses, *Philos Trans R Soc Lond B Biol Sci* (vol. 360), No. 1456, pp. 815-36.
- Friston, K. J.; Frith, C. D.; Frackowiak, R. S. and Turner, R. (1995a): Characterizing dynamic brain responses with fMRI: a multivariate approach, *Neuroimage* (vol. 2), No. 2, pp. 166-72.
- Friston, K. J.; Harrison, L. and Penny, W. (2003): Dynamic causal modelling, *Neuroimage* (vol. 19), No. 4, pp. 1273-302.
- Friston, K. J.; Penny, W.; Phillips, C.; Kiebel, S.; Hinton, G. and Ashburner, J. (2002): Classical and Bayesian inference in neuroimaging: theory, *Neuroimage* (vol. 16), No. 2, pp. 465-83.
- Friston, K.J.; Holmes, A.P.; Poline, J.B.; Grasby, P.J.; Williams, S.C.; Frackowiak, R.S. and Turner, R. (1995b): Analysis of fMRI time-series revisited, *Neuroimage* (vol. 2), No. 1, pp. 45-53.
- Friston, K.J.; Holmes, A.P.; Worsley, K.J.; Poline, J.-P.; Frith, C.D. and Frackowiak, R.S. (1995c): Statistical Parametric Maps in Functional Imaging: A General Linear Approach, *Human Brain Mapping*, No. 2, pp. 189-210.
- Friston, K.J.; Worsley, K.J.; Frackowiak, R. S.; Mazziotta, J. C. and Evans, A. C. (1994): Assessing the significance of focal activations using their spatial extent, *Human Brain Mapping* (vol. 1), No. 3, pp. 210-220.
- Gabor, D. (1946): Theory of communication, *J IEE* (vol. 93), No. III, pp. 429-457.
- Garcia, L.; D'Alessandro, G.; Bioulac, B. and Hammond, C. (2005): High-frequency stimulation in Parkinson's disease: more or less?, *Trends Neurosci* (vol. 28), No. 4, pp. 209-16.
- Gastaut, H. (1952): Etude ,lectrocorticographique de la r,activit, des rythmes rolandiques., *Rev Neurol Paris* (vol. 87), pp. 176-182.
- Glantz, A. (1997): Alternatives to Analysis of Variance and the t Test Based on Ranks, Glantz, A., *Primer of Bio-Statistics*, 4th. ed., pp. 323-372, McGraw-Hill, New York.
- Goldman, R.I.; Stern, J.M.; Engel, J., Jr. and Cohen, M.S. (2002): Simultaneous EEG and fMRI of the alpha rhythm, *Neuroreport* (vol. 13), No. 18, pp. 2487-2492.
- Goncalves, S. I.; de Munck, J. C.; Pouwels, P. J.; Schoonhoven, R.; Kuijer, J. P.; Maurits, N. M.; Hoogduin, J. M.; Van Someren, E. J.; Heethaar, R. M. and Lopes da Silva, F. H. (2006): Correlating the alpha rhythm to BOLD using simultaneous EEG/fMRI: Inter-subject variability, *Neuroimage* (vol. 30), No. 1, pp. 203-13.
- Gray, C. M.; Konig, P.; Engel, A. K. and Singer, W. (1989): Oscillatory responses in cat visual cortex exhibit inter-columnar synchronization which reflects global stimulus properties, *Nature* (vol. 338), No. 6213, pp. 334-7.
- Gusnard, D.A.; Akbudak, E.; Shulman, G.L. and Raichle, M.E. (2001): Medial prefrontal cortex and self-referential mental activity: relation to a default mode of brain function, *Proc Natl Acad Sci USA* (vol. 98), No. 7, pp. 4259-4264.
- Gusnard, D.A. and Raichle, M.E. (2001): Searching for a baseline: functional imaging and the resting human brain, *Nat Rev Neurosci* (vol. 2), No. 10, pp. 685-694.
- Hamandi, K.; Salek-Haddadi, A.; Fish, D. R. and Lemieux, L. (2004): EEG/functional MRI in epilepsy: The Queen Square Experience, *J Clin Neurophysiol* (vol. 21), No. 4, pp. 241-8.

- Hamandi, K.; Salek Haddadi, A.; Liston, A.; Laufs, H.; Fish, D. R. and Lemieux, L. (2005): fMRI temporal clustering analysis in patients with frequent interictal epileptiform discharges: comparison with EEG-driven analysis, *Neuroimage* (vol. 26), No. 1, pp. 309-16.
- Hari, R.; Salmelin, R.; Makela, J.P.; Salenius, S. and Helle, M. (1997): Magnetoencephalographic cortical rhythms, *Int J Psychophysiol* (vol. 26), No. 1-3, pp. 51-62.
- Harley, C.A. and Bielajew, C.H. (1992): A comparison of glycogen phosphorylase a and cytochrome oxidase histochemical staining in rat brain, *J Comp Neurol* (vol. 322), No. 3, pp. 377-389.
- Heeger, D. J. and Ress, D. (2002): What does fMRI tell us about neuronal activity?, *Nat Rev Neurosci* (vol. 3), No. 2, pp. 142-51.
- Henderson, C.J.; Butler, S.R. and Glass, A. (1975): The localization of equivalent dipoles of EEG sources by the application of electrical field theory, *Electroencephalogr Clin Neurophysiol* (vol. 39), No. 2, pp. 117-130.
- Henning, S.; Merboldt, K. D. and Frahm, J. (2006): Task- and EEG-correlated analyses of BOLD MRI responses to eyes opening and closing, *Brain Res* (vol. 1073-1074), pp. 359-64.
- Hirashima, F. and Yokota, T. (1997): Influence of peripheral nerve stimulation on human motor cortical excitability in patients with ventrolateral thalamic lesion, *Arch Neurol* (vol. 54), No. 5, pp. 619-624.
- Hoffmann, A.; Jager, L.; Werhahn, K.J.; Jaschke, M.; Noachtar, S. and Reiser, M. (2000): Electroencephalography during functional echo-planar imaging: detection of epileptic spikes using post-processing methods, *Magn Reson Med* (vol. 44), No. 5, pp. 791-798.
- Horwitz, B. and Poeppel, D. (2002): How can EEG/MEG and fMRI/PET data be combined?, *Hum Brain Mapp* (vol. 17), No. 1, pp. 1-3.
- Hu, X.; Le, T.H.; Parrish, T. and Erhard, P. (1995): Retrospective estimation and correction of physiological fluctuation in functional MRI, *Magn Reson Med* (vol. 34), No. 2, pp. 201-212.
- Huang-Hellinger, F.R.; Breiter, H.C.; McCormack, G.M.; Cohen, M.S.; Kwong, K.K.; Savoy, R.L.; Weisskoff, R.M.; Davis, T.L.; Baker, J.R.; Belliveau, J.W. and Rosen, B.R. (1995): Simultaneous Functional Magnetic Resonance Imaging and Electrophysiological Recording, *Human Brain Mapping* (vol. 3), pp. 13-23.
- Hubbard, O.; Sunde, D. and Goldensohn, E. S. (1976): The EEG in centenarians, *Electroencephalogr Clin Neurophysiol* (vol. 40), No. 4, pp. 407-17.
- Huettel, S. A.; Song, A. W. and McCarthy, G. (2004): *Functional Magnetic Resonance Imaging*, Sinauer, Sunderland, MA.
- Hughes, S. W.; Lorincz, M.; Cope, D. W.; Blethyn, K. L.; Kekesi, K. A.; Parri, H. R.; Juhasz, G. and Crunelli, V. (2004): Synchronized oscillations at alpha and theta frequencies in the lateral geniculate nucleus, *Neuron* (vol. 42), No. 2, pp. 253-68.
- Hyder, F.; Rothman, D.L. and Shulman, R.G. (2002): From the Cover: Total neuroenergetics support localized brain activity: Implications for the interpretation of fMRI, *Proc Natl Acad Sci USA* (vol. 99), No. 16, pp. 10771-10776.
- Ives, J.R.; Warach, S.; Schmitt, F.; Edelman, R.R. and Schomer, D.L. (1993): Monitoring the patient's EEG during echo planar MRI, *Electroencephalogr Clin Neurophysiol* (vol. 87), No. 6, pp. 417-420.
- Jancke, L.; Specht, K.; Mirzazade, S.; Loose, R.; Himmelbach, M.; Lutz, K. and Shah, N.J. (1998): A parametric analysis of the 'rate effect' in the sensorimotor cortex: a functional magnetic resonance imaging analysis in human subjects, *Neurosci Lett* (vol. 252), No. 1, pp. 37-40.
- Jasper, H. and Penfield, W. (1949): Electro corticograms in man: effect of voluntary movement upon the electrical activity of the precentral gyrus., *Arch Psychiatr Z Neurol* (vol. 183), pp. 163-74.
- Jasper, H.H. and Andrews, H.L. (1938a): Normal differentiation of occipital and precentral regions in man, *Arch Neurol Psychiatry* (vol. 39), pp. 96-115.
- Jasper, H.H. and Andrews, H.L. (1938b): Normal differentiation of occipital and precentral regions in man, Jasper, H.H. and Andrews, H.L., *Electroencephalography* pp. 96-115.
- Javitt, D. C.; Doneshka, P.; Zylberman, I.; Ritter, W. and Vaughan, H. G., Jr. (1993): Impairment of early cortical processing in schizophrenia: an event-related potential confirmation study, *Biol Psychiatry* (vol. 33), No. 7, pp. 513-9.
- Javitt, D. C.; Steinschneider, M.; Schroeder, C. E. and Arezzo, J. C. (1996): Role of cortical N-methyl-D-aspartate receptors in auditory sensory memory and mismatch negativity generation: implications for schizophrenia, *Proc Natl Acad Sci U S A* (vol. 93), No. 21, pp. 11962-7.

- Jones, M.; Hewson-Stoate, N.; Martindale, J.; Redgrave, P. and Mayhew, J. (2004): Nonlinear coupling of neural activity and CBF in rodent barrel cortex, *Neuroimage* (vol. 22), No. 2, pp. 956-65.
- Josephs, O.; Turner, R. and Friston, K.J. (1997): Event-Related fMRI, *Human Brain Mapping* (vol. 5), pp. 243-248.
- Kandel, E.R.; Schwartz, J.H. and Jessell, T.M. (2000): *Principles of neural science*, McGraw-Hill Publishing Co, New York.
- Kaufmann, C.; Wehrle, R.; Wetter, T. C.; Holsboer, F.; Auer, D. P.; Pollmacher, T. and Czisch, M. (2006): Brain activation and hypothalamic functional connectivity during human non-rapid eye movement sleep: an EEG/fMRI study, *Brain* (vol. 129), No. Pt 3, pp. 655-67.
- Kilner, J. M.; Mattout, J.; Henson, R. and Friston, K. J. (2005): Hemodynamic correlates of EEG: a heuristic, *Neuroimage* (vol. 28), No. 1, pp. 280-6.
- Klimesch, W. (1999): EEG alpha and theta oscillations reflect cognitive and memory performance: a review and analysis, *Brain Res Brain Res Rev* (vol. 29), No. 2-3, pp. 169-95.
- Kobayashi, E.; Bagshaw, A. P.; Benar, C. G.; Aghakhani, Y.; Andermann, F.; Dubeau, F. and Gotman, J. (2006): Temporal and Extratemporal BOLD Responses to Temporal Lobe Interictal Spikes, *Epilepsia* (vol. 47), No. 2, pp. 343-54.
- Koles, Z.J. (1998): Trends in EEG source localization, *Electroencephalogr Clin Neurophysiol* (vol. 106), No. 2, pp. 127-137.
- Komori, T.; Watson, B.V. and Brown, W.F. (1992): Influence of peripheral afferents on cortical and spinal motoneuron excitability, *Muscle Nerve* (vol. 15), No. 1, pp. 48-51.
- Koshino, Y. and Niedermeyer, E. (1975): Enhancement of Rolandic mu-rhythm by pattern vision, *Electroencephalogr Clin Neurophysiol* (vol. 38), No. 5, pp. 535-538.
- Krakov, K.; Allen, P. J.; Lemieux, L.; Symms, M. R. and Fish, D. R. (2000): Methodology: EEG-correlated fMRI, *Adv Neurol* (vol. 83), pp. 187-201.
- Krakov, K.; Lemieux, L.; Messina, D.; Scott, C. A.; Symms, M. R.; Duncan, J. S. and Fish, D. R. (2001): Spatio-temporal imaging of focal interictal epileptiform activity using EEG-triggered functional MRI, *Epileptic Disord* (vol. 3), No. 2, pp. 67-74.
- Krakov, K.; Woermann, F.G.; Symms, M.R.; Allen, P.J.; Lemieux, L.; Barker, G.J.; Duncan, J.S. and Fish, D.R. (1999): EEG-triggered functional MRI of interictal epileptiform activity in patients with partial seizures, *Brain* (vol. 122), No. Pt 9, pp. 1679-1688.
- Kreger, K.S. and Giordano, C.R. (1992): Biopotential adaptive filtering in an MR environment, *ISMRM 11th Annual Scientific Meeting* (vol. 1), p. 661.
- Krugel, F.; Herrmann, C.S.; Wiggins, C.J. and von Cramon, D.Y. (2001): Hemodynamic and electroencephalographic responses to illusory figures: recording of the evoked potentials during functional MRI, *Neuroimage* (vol. 14), No. 6, pp. 1327-1336.
- Krugel, F.; Wiggins, C.J.; Herrmann, C.S. and von Cramon, D.Y. (2000): Recording of the event-related potentials during functional MRI at 3.0 Tesla field strength, *Magn Reson Med* (vol. 44), No. 2, pp. 277-282.
- Kubota, Y.; Sato, W.; Toichi, M.; Murai, T.; Okada, T.; Hayashi, A. and Sengoku, A. (2001): Frontal midline theta rhythm is correlated with cardiac autonomic activities during the performance of an attention demanding meditation procedure, *Brain Res Cogn Brain Res* (vol. 11), No. 2, pp. 281-7.
- Kullmann, F.; Hollerbach, S.; Lock, G.; Holstege, A.; Dierks, T. and Scholmerich, J. (2001): Brain electrical activity mapping of EEG for the diagnosis of (sub)clinical hepatic encephalopathy in chronic liver disease, *Eur J Gastroenterol Hepatol* (vol. 13), No. 5, pp. 513-22.
- Kwong, K.K.; Belliveau, J.W.; Chesler, D.A.; Goldberg, I.E.; Weisskoff, R.M.; Poncelet, B.P.; Kennedy, D.N.; Hoppel, B.E.; Cohen, M.S.; Turner, R.; Cheng, H.M.; Brady, T.J. and Rosen, B.R. (1992): Dynamic magnetic resonance imaging of human brain activity during primary sensory stimulation, *Proc Natl Acad Sci USA* (vol. 89), pp. 5675-5679.
- Laudon, M. K.; Webster, J. G.; Frayne, R. and Grist, T. M. (1998): Minimizing interference from magnetic resonance imagers during electrocardiography, *IEEE Trans Biomed Eng* (vol. 45), No. 2, pp. 160-4.
- Laufs, H.; Kleinschmidt, A.; Beyerle, A.; Eger, E.; Salek-Haddadi, A.; Preibisch, C. and Krakow, K. (2003a): EEG-correlated fMRI of human alpha activity, *Neuroimage* (vol. 19), No. 4, pp. 1463-76.
- Laufs, H.; Krakow, K.; Sterzer, P.; Eger, E.; Beyerle, A.; Salek-Haddadi, A. and Kleinschmidt, A. (2003b): Electroencephalographic signatures of attentional and cognitive default modes in spontaneous brain activity fluctuations at rest, *Proc Natl Acad Sci U S A* (vol. 100), No. 19, pp. 11053-8.

- Lazeyras, F.; Zimine, I.; Blanke, O.; Perrig, S. H. and Seeck, M. (2001): Functional MRI with simultaneous EEG recording: feasibility and application to motor and visual activation, *J Magn Reson Imaging* (vol. 13), No. 6, pp. 943-8.
- Lelord, G. (1957): Different modalities of reaction of the central and anterior rhythms at 10/sec, *Electroencephalogr Clin Neurophysiol* (vol. 9), p. 561.
- Lemieux, L. (2004): Electroencephalography-correlated functional MR imaging studies of epileptic activity, *Neuroimaging Clin N Am* (vol. 14), No. 3, pp. 487-506.
- Lemieux, L.; Allen, P.J.; Franconi, F.; Symms, M.R. and Fish, D.R. (1997): Recording of EEG during fMRI experiments: patient safety, *Magn Reson Med* (vol. 38), No. 6, pp. 943-952.
- Lemieux, L.; Salek-Haddadi, A.; Josephs, O.; Allen, P.; Toms, N.; Scott, C.; Krakow, K.; Turner, R. and Fish, D.R. (2001): Event-related fMRI with simultaneous and continuous EEG: description of the method and initial case report, *Neuroimage* (vol. 14), No. 3, pp. 780-787.
- Levin, K.H. and Lüders, H.O. (2000): *Comprehensive Clinical Neurophysiology*, WB Saunders, Philadelphia.
- Lindgren, K.A.; Larson, C.L.; Schaefer, S.M.; Abercrombie, H.C.; Ward, R.T.; Oakes, T.R.; Holden, J.E.; Perlman, S.B.; Benca, R.M. and Davidson, R.J. (1999): Thalamic metabolic rate predicts EEG alpha power in healthy control subjects but not in depressed patients, *Biol Psychiatry* (vol. 45), No. 8, pp. 943-952.
- Liston, A. D.; Salek-Haddadi, A.; Kiebel, S. J.; Hamandi, K.; Turner, R. and Lemieux, L. (2004): The MR detection of neuronal depolarization during 3-Hz spike-and-wave complexes in generalized epilepsy, *Magn Reson Imaging* (vol. 22), No. 10, pp. 1441-4.
- Llinas, R. R.; Ribary, U.; Jeanmonod, D.; Kronberg, E. and Mitra, P. P. (1999): Thalamocortical dysrhythmia: A neurological and neuropsychiatric syndrome characterized by magnetoencephalography, *Proc Natl Acad Sci U S A* (vol. 96), No. 26, pp. 15222-7.
- Logothetis, N. K. and Pfeuffer, J. (2004): On the nature of the BOLD fMRI contrast mechanism, *Magn Reson Imaging* (vol. 22), No. 10, pp. 1517-31.
- Logothetis, N.K.; Pauls, J.; Augath, M.; Trinath, T. and Oeltermann, A. (2001): Neurophysiological investigation of the basis of the fMRI signal, *Nature* (vol. 412), No. 6843, pp. 150-157.
- Lopes da Silva, F. H.; Pijn, J. P.; Velis, D. and Nijssen, P. C. (1997): Alpha rhythms: noise, dynamics and models, *Int J Psychophysiol* (vol. 26), No. 1-3, pp. 237-49.
- Lopes da Silva, F.H.; van Lierop, T.H.; Schrijer, C.F. and van Leeuwen, W.S. (1973): Organization of thalamic and cortical alpha rhythms: spectra and coherences, *Electroencephalogr Clin Neurophysiol* (vol. 35), No. 6, pp. 627-639.
- Lopes da Silva, F.H.; Vos, J.E.; Mooibroek, J. and Van Rotterdam, A. (1980): Relative contributions of intracortical and thalamo-cortical processes in the generation of alpha rhythms, revealed by partial coherence analysis, *Electroencephalogr Clin Neurophysiol* (vol. 50), No. 5-6, pp. 449-456.
- Lukashevich, I.P. and Sazonova, O.B. (1996): [The effect of lesions of different parts of the optic thalamus on the nature of the bioelectrical activity of the human brain] Vliianie porazheniia razlichnykh otdelov zritel'nogo bugra na kharakter bioelektricheskoi aktivnosti mozga cheloveka, *Zh Vyssh Nerv Deiat Im IP Pavlova* (vol. 46), No. 5, pp. 866-874.
- Luu, P.; Tucker, D. M. and Makeig, S. (2004): Frontal midline theta and the error-related negativity: neurophysiological mechanisms of action regulation, *Clin Neurophysiol* (vol. 115), No. 8, pp. 1821-35.
- MacKay, W.A. and Crammond, D.J. (1987): Neuronal correlates in posterior parietal lobe of the expectation of events, *Behav Brain Res* (vol. 24), No. 3, pp. 167-179.
- MacKay, W.A. and Mendonca, A.J. (1995a): Field potential oscillatory bursts in parietal cortex before and during reach, *Brain Research* (vol. 704), No. 2, pp. 167-174.
- MacKay, W.A. and Mendonca, A.J. (1995b): Field potential oscillatory bursts in parietal cortex before and during reach, *Brain Res* (vol. 704), No. 2, pp. 167-174.
- Maddochs, J.A.; Hodge, R.S. and Rex, J. (1951): Observations on the occurrence of precentral activities in the lower brainstem., *Electroencephalogr Clin Neurophysiol Suppl* (vol. 3), p. 370.
- Maertens de Noordhout, A.; Rothwell, J.C.; Day, B.L.; Dressler, D.; Nakashima, K.; Thompson, P.D. and Marsden, C.D. (1992): Effect of digital nerve stimuli on responses to electrical or magnetic stimulation of the human brain, *J Physiol* (vol. 447), pp. 535-548.

- Makeig, S.; Jung, T. P.; Bell, A. J.; Ghahremani, D. and Sejnowski, T. J. (1997): Blind separation of auditory event-related brain responses into independent components, *Proc Natl Acad Sci U S A* (vol. 94), No. 20, pp. 10979-84.
- Makeig, S.; Westerfield, M.; Jung, T.P.; Enghoff, S.; Townsend, J.; Courchesne, E. and Sejnowski, T.J. (2002): Dynamic brain sources of visual evoked responses, *Science* (vol. 295), No. 5555, pp. 690-694.
- Manganotti, P.; Gerloff, C.; Toro, C.; Katsuta, H.; Sadato, N.; Zhuang, P.; Leocani, L. and Hallett, M. (1998): Task-related coherence and task-related spectral power changes during sequential finger movements, *Electroencephalogr Clin Neurophysiol* (vol. 109), No. 1, pp. 50-62.
- Mansfield, P. and Grannell, P.K. (1973): NMR 'diffraction' in solids?, *J Phys C* (vol. 6), pp. 442-426.
- Manshanden, I.; De Munck, J. C.; Simon, N. R. and Lopes da Silva, F. H. (2002): Source localization of MEG sleep spindles and the relation to sources of alpha band rhythms, *Clin Neurophysiol* (vol. 113), No. 12, pp. 1937-47.
- Marconi, B.; Genovesio, A.; Battaglia-Mayer, A.; Ferraina, S.; Squatrito, S.; Molinari, M.; Lacquaniti, F. and Caminiti, R. (2001): Eye-hand coordination during reaching. I. Anatomical relationships between parietal and frontal cortex, *Cereb Cortex* (vol. 11), No. 6, pp. 513-527.
- Martinez-Montes, E.; Valdes-Sosa, P. A.; Miwakeichi, F.; Goldman, R. I. and Cohen, M. S. (2004): Concurrent EEG/fMRI analysis by multiway Partial Least Squares, *Neuroimage* (vol. 22), No. 3, pp. 1023-34.
- Marx, E.; Stephan, T.; Nolte, A.; Deutschlander, A.; Seelos, K.C.; Dieterich, M. and Brandt, T. (2003): Eye closure in darkness animates sensory systems, *Neuroimage* (vol. 19), No. 3, pp. 924-934.
- McGonigle, D. J.; Howseman, A. M.; Athwal, B. S.; Friston, K. J.; Frackowiak, R. S. and Holmes, A. P. (2000): Variability in fMRI: an examination of intersession differences, *Neuroimage* (vol. 11), No. 6 Pt 1, pp. 708-34.
- Michel, C.M.; Lehmann, D.; Henggeler, B. and Brandeis, D. (1992): Localization of the sources of EEG delta, theta, alpha and beta frequency bands using the FFT dipole approximation, *Electroencephalogr Clin Neurophysiol* (vol. 82), No. 1, pp. 38-44.
- Moosmann, M.; Ritter, P.; Krastel, I.; Brink, A.; Thees, S.; Blankenburg, F.; Taskin, B.; Obrig, H. and Villringer, A. (2003): Correlates of alpha rhythm in functional magnetic resonance imaging and near infrared spectroscopy, *Neuroimage* (vol. 20), No. 1, pp. 145-158.
- Muri, R.M.; Felblinger, J.; Rosler, K.M.; Jung, B.; Hess, C.W. and Boesch, C. (1998): Recording of electrical brain activity in a magnetic resonance environment: distorting effects of the static magnetic field, *Magn Reson Med* (vol. 39), No. 1, pp. 18-22.
- Murphy, J. V. and Patil, A. A. (2005): Improving the lives of patients with medically refractory epilepsy by electrical stimulation of the nervous system, *Expert Rev Med Devices* (vol. 2), No. 2, pp. 175-89.
- Naatanen, R.; Gaillard, A. W. and Mantysalo, S. (1978): Early selective-attention effect on evoked potential reinterpreted, *Acta Psychol* (vol. 42), No. 4, pp. 313-29.
- Ngai, A. C.; Jolley, M. A.; D'Ambrosio, R.; Meno, J. R. and Winn, H. R. (1999): Frequency-dependent changes in cerebral blood flow and evoked potentials during somatosensory stimulation in the rat, *Brain Res* (vol. 837), No. 1-2, pp. 221-8.
- Niazy, R. K.; Beckmann, C. F.; Iannetti, G. D.; Brady, J. M. and Smith, S. M. (2005): Removal of FMRI environment artifacts from EEG data using optimal basis sets, *Neuroimage* (vol. 28), No. 3, pp. 720-37.
- Niedermeyer, E. (1997): Alpha rhythms as physiological and abnormal phenomena, *Int J Psychophysiol* (vol. 26), No. 1-3, pp. 31-49.
- Niedermeyer, E. and Koshino, Y. (1975): My-Rhythmus: Vorkommen und klinische Bedeutung, *EEG EMG Z Elektroenzephalogr Elektromyogr Verwandte Geb* (vol. 6), pp. 69-78.
- Nunez, P. L. and Silberstein, R. B. (2000): On the relationship of synaptic activity to macroscopic measurements: does co-registration of EEG with fMRI make sense?, *Brain Topogr* (vol. 13), No. 2, pp. 79-96.
- Ogawa, S.; Lee, T. M.; Stepnoski, R.; Chen, W.; Zhu, X. H. and Ugurbil, K. (2000): An approach to probe some neural systems interaction by functional MRI at neural time scale down to milliseconds, *Proc Natl Acad Sci U S A* (vol. 97), No. 20, pp. 11026-31.

- Ogawa, S.; Tank, D.W.; Menon, R.S.; Ellermann, J.M.; Kim, S.G.; Merkle, H. and Ugurbil, K. (1992): Intrinsic signal changes accompanying sensory stimulation: functional brain mapping with magnetic resonance imaging, *Proc Natl Acad Sci USA* (vol. 89), pp. 5951-5955.
- Ohmoto, T.; Mimura, Y.; Baba, Y.; Miyamoto, T.; Matsumoto, Y.; Nishimoto, A. and Matsumoto, K. (1978): Thalamic control of spontaneous alpha-rhythm and evoked responses, *Appl Neurophysiol* (vol. 41), No. 1-4, pp. 188-92.
- Onton, J.; Delorme, A. and Makeig, S. (2005): Frontal midline EEG dynamics during working memory, *Neuroimage* (vol. 27), No. 2, pp. 341-56.
- Parkes, L. M.; Bastiaansen, M. C. and Norris, D. G. (2006): Combining EEG and fMRI to investigate the post-movement beta rebound, *Neuroimage* (vol. 29), No. 3, pp. 685-96.
- Patel, P.; L, Al-Dayeh and M, Singh (1997): Localization of Alpha-Activity by Simultaneous fMRI and EEG Measurements, *Proceedings of the International Society for Magnetic Resonance in Medicine* (vol. 3), p. 1653.
- Perneger, T. V. (1998): What's wrong with Bonferroni adjustments, *BMJ* (vol. 316), No. 7139, pp. 1236-8.
- Petsche, H. and Sterc, J. (1968): The significance of the cortex for the travelling phenomenon of brain waves, *Electroencephalogr Clin Neurophysiol* (vol. 25), No. 1, pp. 11-22.
- Pfurtscheller, G. (1981): Central beta rhythm during sensorimotor activities in man, *Electroencephalogr Clin Neurophysiol* (vol. 51), No. 3, pp. 253-264.
- Pfurtscheller, G. (1992): Event-related synchronization (ERS): an electrophysiological correlate of cortical areas at rest, *Electroencephalogr Clin Neurophysiol* (vol. 83), No. 1, pp. 62-69.
- Pfurtscheller, G. and Berghold, A. (1989): Patterns of cortical activation during planning of voluntary movement, *Electroencephalogr Clin Neurophysiol* (vol. 72), No. 3, pp. 250-258.
- Pfurtscheller, G. and Lopes da Silva, F.H. (1999): Event-related EEG/MEG synchronization and desynchronization: basic principles (vol. 110), No. 11, pp. 1842-1857.
- Pfurtscheller, G.; Zalaudek, K. and Neuper, C. (1998): Event-related beta synchronization after wrist, finger and thumb movement, *Electroencephalogr Clin Neurophysiol* (vol. 109), No. 2, pp. 154-60.
- Phillips, C.; Rugg, M.D. and Friston, K.J. (2002): Anatomically informed basis functions for EEG source localization: combining functional and anatomical constraints, *Neuroimage* (vol. 16), No. 3 Pt 1, pp. 678-695.
- Purves, D.; Augustine, G.J.; Fitzpatrick, D.; Katz, L.C.; LaMantia, A.-S.; McNamara, J.O. and Williams, S.M. (2001): *Neuroscience*, second. ed., Sinauer, Sunderland.
- Quian Quiroga, R. and Garcia, H. (2003): Single-trial event-related potentials with wavelet denoising, *Clin Neurophysiol* (vol. 114), No. 2, pp. 376-90.
- Rahn, E. and Basar, E. (1993): Prestimulus EEG-activity strongly influences the auditory evoked vertex response: a new method for selective averaging, *Int J Neurosci* (vol. 69), No. 1-4, pp. 207-220.
- Raichle, M.E.; MacLeod, A.M.; Snyder, A.Z.; Powers, W.J.; Gusnard, D.A. and Shulman, G.L. (2001): A default mode of brain function, *Proc Natl Acad Sci USA* (vol. 98), No. 2, pp. 676-682.
- Ranganath, C. and Rainer, G. (2003): Neural mechanisms for detecting and remembering novel events, *Nat Rev Neurosci* (vol. 4), No. 3, pp. 193-202.
- Ritter, P. and Villringer, A. (2002): Inhibition and functional magnetic resonance imaging, Tomita, M.; Kanno, I. and Hamel, E., *Brain Activation and CBF Control* first. ed., pp. 213-222, Elsevier.
- Rizzolatti, G.; Luppino, G. and Matelli, M. (1998): The organization of the cortical motor system: new concepts, *Electroencephalogr Clin Neurophysiol* (vol. 106), No. 4, pp. 283-296.
- Rodin, E.A. and Rodin, M.J. (1995): Dipole sources of the human alpha rhythm, *Brain Topogr* (vol. 7), No. 3, pp. 201-208.
- Rossini, P.M.; Desiato, M.T.; Lavaroni, F. and Caramia, M.D. (1991): Brain excitability and electroencephalographic activation: non-invasive evaluation in healthy humans via transcranial magnetic stimulation, *Brain Res* (vol. 567), No. 1, pp. 111-119.
- Rougeul, A.; Bouyer, J.J.; Dedet, L. and Debray, O. (1979): Fast somato-parietal rhythms during combined focal attention and immobility in baboon and squirrel monkey, *Electroencephalogr Clin Neurophysiol* (vol. 46), No. 3, pp. 310-319.
- Sachs, L. (1993): t-Test und Welch-Test für den Vergleich zweier Mittelwerte unabh.,ngiger Stichproben, Sachs, L., *Statistische Methoden*, 7. ed., pp. 74-79, Springer-Verlag, Berlin.

- Sadato, N.; Nakamura, S.; Oohashi, T.; Nishina, E.; Fuwamoto, Y.; Waki, A. and Yonekura, Y. (1998): Neural networks for generation and suppression of alpha rhythm: a PET study, *Neuroreport* (vol. 9), No. 5, pp. 893-897.
- Salek-Haddadi, A.; Friston, K. J.; Lemieux, L. and Fish, D. R. (2003): Studying spontaneous EEG activity with fMRI, *Brain Res Brain Res Rev* (vol. 43), No. 1, pp. 110-33.
- Salek-Haddadi, A.; Merschhemke, M.; Lemieux, L. and Fish, D.R. (2002): Simultaneous EEG-Correlated Ictal fMRI, *Neuroimage* (vol. 16), No. 1, pp. 32-40.
- Salenius, S.; Schnitzler, A.; Salmelin, R.; Jousmaki, V. and Hari, R. (1997): Modulation of human cortical rolandic rhythms during natural sensorimotor tasks, *Neuroimage* (vol. 5), No. 3, pp. 221-8.
- Salmelin, R.; Hamalainen, M.; Kajola, M. and Hari, R. (1995): Functional segregation of movement-related rhythmic activity in the human brain, *Neuroimage* (vol. 2), No. 4, pp. 237-243.
- Salmelin, R. and Hari, R. (1994a): Characterization of spontaneous MEG rhythms in healthy adults (vol. 91), No. 4, pp. 237-248.
- Salmelin, R. and Hari, R. (1994b): Spatiotemporal characteristics of sensorimotor neuromagnetic rhythms related to thumb movement, *Neuroscience* (vol. 60), No. 2, pp. 537-50.
- Sammer, G.; Blecker, C.; Gebhardt, H.; Kirsch, P.; Stark, R. and Vaitl, D. (2005): Acquisition of typical EEG waveforms during fMRI: SSVEP, LRP, and frontal theta, *Neuroimage* (vol. 24), No. 4, pp. 1012-24.
- Sanes, J.N. and Donoghue, J.P. (1993): Oscillations in local field potentials of the primate motor cortex during voluntary movement, *Proc Natl Acad Sci USA* (vol. 90), No. 10, pp. 4470-4474.
- Sazonova, O.B. and Lukashovich, I.P. (1995): The EEG characteristics in a lesion of different sections of the human caudate nucleus, *Zh Vyssh Nerv Deiat Im IP Pavlova* (vol. 45), No. 5, pp. 886-893.
- Scarff, C. J.; Reynolds, A.; Goodyear, B. G.; Ponton, C. W.; Dort, J. C. and Eggermont, J. J. (2004): Simultaneous 3-T fMRI and high-density recording of human auditory evoked potentials, *Neuroimage* (vol. 23), No. 3, pp. 1129-42.
- Scheffe, H. (1959): *The Analysis of Variance*, Wiley, New York.
- Scherg, M. (1990): Fundamentals of dipole source potential analysis, Grandori, F.; Hoke, M. and Romani, G.L., *Auditory evoked magnetic fields and electrical potentials* pp. 40-69, Karger, Basel.
- Scherg, M. and Von Cramon, D. (1986): Evoked dipole source potentials of the human auditory cortex, *Electroencephalogr Clin Neurophysiol* (vol. 65), No. 5, pp. 344-360.
- Schoppenhorst, M.; Brauer, F.; Freund, G. and Kubicki, S. (1980): The significance of coherence estimates in determining central alpha and mu activities, *Electroencephalogr Clin Neurophysiol* (vol. 48), No. 1, pp. 25-33.
- Schreckenberger, M.; Lange-Asschenfeld, C.; Lochmann, M.; Mann, K.; Siessmeier, T.; Buchholz, H. G.; Bartenstein, P. and Grunder, G. (2004): The thalamus as the generator and modulator of EEG alpha rhythm: a combined PET/EEG study with lorazepam challenge in humans, *Neuroimage* (vol. 22), No. 2, pp. 637-44.
- Schutz, E. and Muller, H. W. (1951): Über ein neues Zeichen zentral nervöser Erregbarkeitssteigerung im Elektroenzephalogramm, *Klin Wochenschr* (vol. 29), No. 1-2, pp. 22-3.
- Seeck, M.; Lazeyras, F.; Michel, C.M.; Blanke, O.; Gericke, C.A.; Ives, J.; Delavelle, J.; Golay, X.; Haenggeli, C.A.; de Tribolet, N. and Landis, T. (1998): Non-invasive epileptic focus localization using EEG-triggered functional MRI and electromagnetic tomography, *Electroencephalogr Clin Neurophysiol* (vol. 106), No. 6, pp. 508-512.
- Shallice, T.; Fletcher, P.; Frith, C.D.; Grasby, P.; Frackowiak, R.S. and Dolan, R.J. (1994): Brain regions associated with acquisition and retrieval of verbal episodic memory, *Nature* (vol. 368), No. 6472, pp. 633-635.
- Shelley, A. M.; Ward, P. B.; Catts, S. V.; Michie, P. T.; Andrews, S. and McConaghy, N. (1991): Mismatch negativity: an index of a preattentive processing deficit in schizophrenia, *Biol Psychiatry* (vol. 30), No. 10, pp. 1059-62.
- Sijbers, J.; Michiels, I.; Verhoye, M.; Van Audekerke, J.; Van der Linden A. and Van Dyck, D. (1999): Restoration of MR-induced artifacts in simultaneously recorded MR/EEG data, *Magn Reson Imaging* (vol. 17), No. 9, pp. 1383-1391.
- Singer, W. (2001): Consciousness and the binding problem, *Ann N Y Acad Sci* (vol. 929), pp. 123-46.
- Smith, S. M.; Beckmann, C. F.; Ramnani, N.; Woolrich, M. W.; Bannister, P. R.; Jenkinson, M.; Matthews, P. M. and McGonigle, D. J. (2005): Variability in fMRI: a re-examination of inter-session differences, *Hum Brain Mapp* (vol. 24), No. 3, pp. 248-57.

- Sokolov, E. N. (1963): Perception and the Conditioned Reflex, Pergamon Press, Oxford.
- Sommer, M.; Meinhardt, J. and Volz, H.P. (2003): Combined measurement of event-related potentials (ERPs) and fMRI, *Acta Neurobiol Exp* (vol. 63), No. 1, pp. 49-53.
- Spencer, K. M. (2005): Averaging, Detection, and Classification of single-trial ERPs, Handy, T.C., *Event Related Potentials. A Methods Handbook* pp. 209-228, The MIT Press, Cambridge.
- Stark, C. E. and Squire, L. R. (2001): When zero is not zero: the problem of ambiguous baseline conditions in fMRI, *Proc Natl Acad Sci U S A* (vol. 98), No. 22, pp. 12760-6.
- Sutton, S.; Braren, M.; Zubin, J. and John, E. R. (1965): Evoked-potential correlates of stimulus uncertainty, *Science* (vol. 150), No. 700, pp. 1187-8.
- Symms, M.R.; Allen, P.J.; Woermann, F.G.; Polizzi, G.; Krakow, K.; Barker, G.J.; Fish, D.R. and Duncan, J.S. (1999): Reproducible localization of interictal epileptiform discharges using EEG-triggered fMRI, *Phys Med Biol* (vol. 44), No. 7, pp. 161-168.
- Tallon-Baudry, C.; Bertrand, O. and Fischer, C. (2001): Oscillatory synchrony between human extrastriate areas during visual short-term memory maintenance, *J Neurosci* (vol. 21), No. 20, p. RC177.
- Tanaka, E. and Iinuma, T. A. (1975): Correction functions for optimizing the reconstructed image in transverse section scan, *Phys Med Biol* (vol. 20), No. 3, pp. 789-98.
- Terao, Y.; Sakurai, Y.; Sakuta, M.; Ishii, K. and Sugishita, M. (1993): FDG-PET in an amnesic and hypersomnic patient with bilateral paramedian thalamic infarction, *Rinsho Shinkeigaku* (vol. 33), No. 9, pp. 951-6.
- Terao, Y.; Ugawa, Y.; Uesaka, Y.; Hanajima, R.; Gemba-Shimizu, K.; Ohki, Y. and Kanazawa, I. (1995): Input-output organization in the hand area of the human motor cortex, *Electroencephalogr Clin Neurophysiol* (vol. 97), No. 6, pp. 375-381.
- Thees, S.; Blankenburg, F.; Taskin, B.; Curio, G. and Villringer, A. (2003): Dipole Source Localisation and fMRI of Simultaneously Recorded Data Applied to Somatosensory Categorisation., *Neuroimage* (vol. 13), No. 3, pp. 707-19.
- Tiihonen, J.; Kajola, M. and Hari, R. (1989): Magnetic mu rhythm in man, *Neuroscience* (vol. 32), No. 3, pp. 793-800.
- Torrence, C. and Compo, G.P. (1998): A practical guide to wavelet analysis., *Bull Am Meteorol Soc* (vol. 79), No. 1, pp. 61-78.
- Toumskoy, E. V. and Maiorchik, V. E. (1969): Concerning the role of thalamic structures in the genesis and regulation of alpha rhythm, *Electroencephalogr Clin Neurophysiol* (vol. 26), No. 5, p. 550.
- Traub, R.D.; Jefferys, J.G. and Whittington, M.A. (1997): Simulation of gamma rhythms in networks of interneurons and pyramidal cells, *J Comput Neurosci* (vol. 4), No. 2, pp. 141-150.
- Valdes-Sosa, P. A. (2004): Spatio-temporal autoregressive models defined over brain manifolds, *Neuroinformatics* (vol. 2), No. 2, pp. 239-50.
- Valdes-Sosa, P.; Bosch, J.; Grave, R.; Hernandez, J.; Riera, J.; Pascual, R. and Biscay, R. (1992): Frequency domain models of the EEG, *Brain Topogr* (vol. 4), No. 4, pp. 309-319.
- Villringer, A. and Dirnagl, U. (1995): Coupling of brain activity and cerebral blood flow: basis of functional neuroimaging, *Cerebrovasc Brain Metab Rev* (vol. 7), No. 3, pp. 240-276.
- Walter, W.G. (1936): The location of cerebral tumors by electroencephalography, *Lancet* (vol. 2), pp. 305-308.
- Warach, S.; Ives, J.R.; Schlaug, G.; Patel, M.R.; Darby, D.G.; Thangaraj, V.; Edelman, R.R. and Schomer, D.L. (1996): EEG-triggered echo-planar functional MRI in epilepsy, *Neurology* (vol. 47), No. 1, pp. 89-93.
- Wenzel, R.; Wobst, P.; Heekeren, H.H.; Kwong, K.K.; Brandt, S.A.; Kohl, M.; Obrig, H.; Dirnagl, U. and Villringer, A. (2000): Saccadic suppression induces focal hypooxygenation in the occipital cortex., *J Cereb Blood Flow Metab* (vol. 7), No. 0271-678X, pp. 1103-1110.
- Williamson, S.J. and Kaufman, L. (1989): Advances in neuromagnetic instrumentation and studies of spontaneous brain activity, *Brain Topogr* (vol. 2), No. 1-2, pp. 129-139.
- Windischberger, C.; Langenberger, H.; Sycha, T.; Tschernko, E.M.; Fuchsjager-Mayerl, G.; Schmetterer, L. and Moser, E. (2002): On the origin of respiratory artifacts in BOLD-EPI of the human brain, *Magn Reson Imaging* (vol. 20), No. 8, pp. 575-582.

- Wobst, P.; Wenzel, R.; Kohl, M.; Obrig, H. and Villringer, A. (2001): Linear Aspects of Changes in Deoxygenated Hemoglobin Concentration and Cytochrome Oxidase Oxidation during Brain Activation., *Neuroimage* (vol. 13), No. 3, pp. 520-530.
- Worsley, K. J.; Evans, A. C.; Marrett, S. and Neelin, P. (1992): A three-dimensional statistical analysis for CBF activation studies in human brain, *J Cereb Blood Flow Metab* (vol. 12), No. 6, pp. 900-18.
- Worsley, K.J. ; Marrett, S. ; Neelin, P ; Vandal, A. C. ; Friston, K. J. and Evans, A. C. (1996): A unified statistical approach for determining significant signals in images of cerebral activation, *Human Brain Mapping* (vol. 4), No. 1, pp. 58-73.
- Yazawa, S.; Kawasaki, S.; Kanemaru, A.; Kuratsuwa, Y.; Yabuoshi, R. and Ohi, T. (2001): Bilateral paramedian thalamo-midbrain infarction showing electroencephalographic alpha activity, *Intern Med* (vol. 40), No. 5, pp. 443-448.
- Zschocke, S. and Hansen, H.C. (2002): *Klinische Elektroenzephalographie*, 2nd. ed., Springer, Berlin.

11 Curriculum Vitae

October 1993 - December 1999

Study for a **Masters degree ('Diplom') in Physics** at the University Heidelberg, Germany.

March 1997 - August 1997

Exchange student at the University of Uppsala, Sweden.

June 1998 - Juli 1999

Masters thesis ('Diplomarbeit') at the Deutsches Krebsforschungszentrum in Heidelberg.
Supervisor: Prof. J. Debus

March 2000 – April 2005

Research Assistant at the Berlin Neuroimaging Center and the Charité, University Medicine Berlin.

Since June 2003

Studies for a **PhD in Biology (Neurobiology)** at the Faculty of Biology, Humboldt University Berlin, Supervisors: Prof. A.V.M. Herz and Prof. A. Villringer

Since August 2005

Research assistant at the Department of Biological and Medical Psychology, University of Bergen, Norway.

12 Publications in Peer Reviewed Journals

- Eichele T, Specht K, Moosmann M, Jongsma M, Quiroga RQ, Nordby H, Hugdahl K. "Assessing the spatio-temporal evolution of neuronal activation with single-trial ERP-fMRI." *PNAS*. 2005 Dec 6; 102(49).
- Ruben J, Krause T, Taskin B, Blankenburg F, Moosmann M, Villringer A. "Subarea-specific Suppressive Interaction in the BOLD Responses to Simultaneous Finger Stimulation in Human Primary Somatosensory Cortex: Evidence for Increasing Rostral-to-caudal Convergence." *Cereb Cortex*. 2005 Jun;16(6):819-26.
- Becker R, Ritter P, Moosmann M, Villringer A. "Visual evoked potentials recovered from fMRI scan periods." *Hum Brain Mapp*. 2005 Nov;26(3):221-30.
- Moosmann M, Ritter P, Krastel I, Brink A, Thees S, Blankenburg F, Taskin B, Obrig H, Villringer A. "Correlates of alpha rhythm in functional magnetic resonance imaging and near infrared spectroscopy." *Neuroimage*. 2003 Sep;20(1):145-58.
- Blankenburg F, Taskin B, Ruben J, Moosmann M, Ritter P, Curio G, Villringer A. "Imperceptible stimuli and sensory processing impediment." *Science*. 2003 Mar 21;299(5614):1864
- Krause T, Kurth R, Ruben J, Schwiemann J, Villringer K, Deuchert M, Moosmann M, Brandt S, Wolf K, Curio G, Villringer A. "Representational overlap of adjacent fingers in multiple areas of human primary somatosensory cortex depends on electrical stimulus intensity: an fMRI study." *Brain Res*. 2001 Apr 27;899(1-2):36-46.